BLACK CARBON AND FINE AEROSOL PARTICLES CHARACTERIZATION AT DIFFERENT ENVIRONMENTAL CONDITIONS IN THE SOUTHEAST OF THE IBERIAN PENINSULA

Juan Andrés Casquero Vera

UNIVERSIDAD DE GRANADA

PH.D. DISSERTATION

UNIVERSIDAD DE GRANADA

Programa de Doctorado en Física
y Ciencias del Espacio

BLACK CARBON AND FINE AEROSOL PARTICLES CHARACTERIZATION AT DIFFERENT ENVIRONMENTAL CONDITIONS IN THE SOUTHEAST OF THE IBERIAN PENINSULA

IISTA
Instituto Interuniversitario de Investigación
del Sistema Tierra en Andalucía

Juan Andrés Casquero Vera

Unidad de
Excelencia
UGR

Grupo de Física de la Atmósfera

Editor: Universidad de Granada. Tesis Doctorales
Autor: Juan Andrés Casquero Vera
ISBN: 978-84-1306-929-6
URI: http://hdl.handle.net/10481/69643

A mi familia

To my family

“If you want to go fast, go alone;
if you want to go far, go together”

/Agradecimientos

En primer lugar, quiero dar las gracias a mis directores de tesis: el Catedrático Lucas Alados y el Profesor Hassan Lyamani. Lucas Alados, catedrático en mayúsculas, no por sus sexenios o quinquenios, sino por su confianza, paciencia, devoción, trabajo incansable y, por supuesto, por su conocimiento. Gracias por haber confiado en mí y acogerme en tu grupo, este que, sin duda, sin ti no sería lo que es hoy. En segundo lugar, y no menos por ello, Profesor Hassan Lyamani, catedrático en la sombra, en la sombra porque no se le reconoce sexenio o quinquenio alguno, pero que sin duda cualquiera de los que hemos tenido la suerte de trabajar contigo, sabemos que deberías serlo desde hace tiempo. Podría decir muchas cosas de mi amigo Hassan, porque entiendes de todo (y si no lo sabes, lo buscas y haces una tesis sobre el tema), porque eres capaz de mantener unidas cargas del mismo signo, pero sobre todo porque ayudas a cuestionar cada afirmación con esas "*discusiones"* a la inglesa. Gracias por hacerme pensar de forma crítica, por enseñarme a leer y escribir en este mundo, por todas nuestras discusiones y, en general, por todo nuestro trabajo, codo con codo, sin "clasismos".

"*Si quieres llegar rápido, ve solo; pero si quieres llegar lejos, ve acompañado*", una frase que ha dado muchos cafés y muchos "vamos a fumar", por eso quiero agradecer a los que han hecho que este duro camino haya sido posible, pero, sobre todo, haya sido más agradable. Gracias por vuestra ayuda, por todos vuestros consejos, ¡por todo! Por todo, porque realmente no puedo quedarme con

algo de vosotros, sería quedarme corto sin duda, así que, gracias a mis “pichas”: Dani el inteligente, Jose el picha larga y Rober el nieto de Isabel la Católica.

No puedo olvidarme de dar las gracias al resto del Grupo de Física de la Atmósfera (GFAT), y es que, como diría uno que yo me sé, una mano no aplaude sola. Gracias a Paco Pepe, por su amabilidad, por toda su ayuda, por todos esos “vamos a fumar” donde se aprende más que con cualquier “peiper”, por estar siempre apoyando, gracias. Gracias a todo el grupo de aerosol in-situ, a los nuevos fichajes estrella, Fernando y Andrea, y en especial a Gloria. Gloria, que desde que llegué para quedarme con el “marrón” que ella dejaba, me enseñó lo que era el in-situ y que, junto con Hassan, me enseñó a “andar” en esto. Y por supuesto, agradecer a todos con los que disfruto trabajando, pero sobre todo con los que disfruto tomando una cerveza, con esos con los que puedes “discutir” abiertamente sobre ciencia, con los que se pueden construir trabajos, con esos que saben millones pero que además saben algo muy importante, escuchar, gracias Andresito, Pablo, María José. El GFAT es enorme: los que están, los que se fueron, los nuevos, los que nos visitaron, sois tantos que no puedo nombraros a todos, pero quiero agradeceros a TODOS vuestra acogida y que me hayáis enseñado un poco más, en lo profesional y en lo personal.

I switch to English to thank Prof. Tuukka Petäjä for giving me the opportunity to join his group for a few months and showing me the NPF world. I am greatly acknowledged for his help and kindness, especially during my escape during COVID-19. I would like to thank also the whole INAR group, they kindly hosted me during my first stay in Helsinki and made me repeat 2 years later. Por último, esta tesis ha conllevado un esfuerzo importante en campañas de medidas. Quiero agradecer a todos los que han hecho posible que salieran adelante. Sin olvidar las campañas de intercomparación de la REDMAAS, donde tanto he aprendido sobre SMPSs, pero sobre todo donde tanto hemos reído.

En época en la que solo se mira a la "excelencia investigadora", quiero recordar que la investigación se hace en grupo, y como parte del grupo hay que incluir el trabajo del personal técnico, de secretaría, de conserjería, de limpieza, de informática y un largo etcétera que hacen que la investigación sea posible. Gracias a todos los que han hecho posible esta tesis, en especial al personal del CEAMA, del departamento de Física Aplicada y de la Universidad de Granada.

Finalmente, quiero agradecer a mis amigos, a mi familia elegida, y a mi familia, la de sangre, que siempre me han acompañado y apoyado. En especial a Álvaro, por aceptar mi propuesta y hacer que este trabajo al menos quede bonito. Pero sobre todo quiero agradecérselo a los que me lo han dado todo, a mis padres. Papá, cada día compartíamos el parte meteorológico granadino y sanroqueño, sin embargo, hoy no puedo compartirlos contigo, como tampoco puedo compartir el que sé que sería un día muy feliz para ti. Sé lo orgullosos que siempre habéis estado, tanto tú como mamá, por cada una de mis metas, y sé que hoy vas a ser el que más orgulloso va a estar, porque solo tú sabes el esfuerzo que estos meses ha supuesto acabar esta tesis. Pero más orgulloso me siento yo de ser lo que soy y de saber lo que sé gracias a vosotros, a vuestra educación, a vuestros valores, a vuestro sacrificio. Siempre hacías las cosas porque te salían, de ahí tus "no tienes nada que agradecerme", pero todo este trabajo y esfuerzo está dedicado a vosotros, papá y mamá.

"Vuela tan alto como puedas
sin olvidar de dónde vienes"

/Contents

/Abstract

This PhD dissertation focuses on the characterization of fine atmospheric aerosol particles emission sources (their strength, spatial and temporal variability) at different environments by means of ground-based in-situ techniques. To this end, the aerosol microphysical and optical properties obtained by state-of-the-art instrumentation in multiple experimental campaigns performed at different environments (*urban*, *suburban* and *remote high-altitude*) in the southeast of the Iberian Peninsula have been analyzed and discussed.

In order to take insight about the sources of fine atmospheric aerosol, their diurnal, weekly, seasonal and spatial variability in the Granada urban area, the aerosol number flux and concentration of fine particles obtained by eddy covariance technique are examined during the period from Nov/2016 to Apr/2018. The results show that the majority of aerosol number flux values are positive, suggesting that the urban site acts as a net source of aerosol particles to the atmosphere at different time scales. Concerning aerosol emissions sources, road traffic is identified as the main source in Granada urban area in all seasons. During winter, domestic heating and agricultural waste burning emissions are additional aerosol sources, while during spring and summer new particle formation processes contribute significantly to ultrafine aerosol particles. Wind sector analysis shows that the impact of domestic heating emissions from the urban area, especially at night, is much stronger than the impact of agricultural waste burning emissions from the suburban sector.

With the aim to disentangle the contribution of the different aerosol sources to the total aerosol number concentration at sites influenced by biomass burning emissions, a new approach based on the Rodriguez and Cuevas (2007) and Sandradewi et al. (2008) methods has been developed. This new approach has been used to determine the contributions of both vehicle and biomass burning primary emissions and secondary aerosol to the size-segregated particle number concentrations at urban and suburban sites. This method has been applied to simultaneous measurements of aerosol number size distribution in the 12–600 nm size range and black carbon (BC) concentration obtained at both sites during winter season, when the study area is usually influenced by biomass burning emissions from domestic heating and agricultural waste burning. The results show that (1) secondary aerosol is the main contributor to the particle number concentration in all size ranges at both sites, (2) primary vehicle exhaust is the main source of primary particles with contributions >70% in all size ranges at both sites and (3) primary biomass burning particles contribute significantly to the primary particles concentrations in the 25–100 and 100–600 nm size ranges at the suburban (24% and 28%, respectively) and urban (13% and 20%, respectively) sites. In addition, new particle formation (NPF) events have been found to be an important aerosol source during summer noon hours but, on average, these events do not implicate a considerable contribution to urban particles.

Despite this low contribution of NPF events to the total particle number concentration in Granada urban area, these events are of great importance for the production of cloud condensation nuclei (CCN), affecting clouds formation. Therefore, the characterization of NPF vertical distribution is of special interest. To this end, a detailed investigation of the NPF characteristics and the different factors that promote/inhibit NPF processes has been performed at two contrastive sites: urban and high-altitude remote sites. For this, simultaneous measurements of aerosol size distributions (4-500 nm) measured at both sites have been used. The

analysis shows that, with NPF event frequency >70% at both sites, nucleation mode particles highly contribute to the total aerosol number concentration in summer (47 % and 48 % at mountain and urban sites, respectively). At the high-altitude remote site, NPF events have been found to be associated with the transport of gaseous precursors from lower altitudes by orographic buoyant upward flows. Nevertheless, NPF events at the high-altitude remote site have been always observed from the smallest measured sizes of the aerosol size distribution (4 nm), implying that NPF takes place in or in the vicinity of the high-altitude remote station rather than being transported from lower altitudes. Although NPF events at the mountain site seem to be connected with those occurring at the urban site, growth rates (GRs) at mountain site are higher than those at the urban site. The analysis of sulfuric acid (H_2SO_4) shows that the concentrations of H_2SO_4 can explain a minimal contribution of the observed GRs at both sites (< 1 % and < 10 % for the 7–25 and 4–7 nm size ranges, respectively), indicating that other condensing vapours are responsible for the majority of particle growth, as well as the differing growth rates between the two sites. The results also show that the condensation sink (CS) does not play a relevant role in NPF processes at both sites and points to the availability of volatile organic compounds (VOCs) as one of the main factors controlling the NPF events at the urban and high-altitude remote sites investigated.

/Resumen

Esta tesis doctoral se centra en la caracterización de las fuentes de emisión de las partículas finas del aerosol atmosférico (su intensidad y su variabilidad espacio-temporal) en diferentes ambientes utilizando técnicas de medida in-situ desde superficie. Para ello, se han analizado las medidas de propiedades microfísicas y ópticas del aerosol obtenidas en diferentes campañas experimentales llevadas a cabo en diferentes ambientes (urbano, suburbano y remoto de alta montaña) en el sureste de la Península Ibérica.

Para conocer las fuentes de las partículas finas del aerosol atmosférico y su variabilidad diurna, semanal, estacional y espacial en el área urbana de Granada, se ha analizado la concentración numérica de partículas y su correspondiente flujo vertical, ambas obtenidas mediante la técnica *eddy covariance* durante el período de Nov/2016 a Abr/2018. Los resultados muestran que la mayoría de los valores de flujo son positivos, indicando que el entorno urbano actúa como una fuente neta de partículas de aerosoles a diferentes escalas temporales. Respecto a las fuentes de emisión de partículas, el tráfico rodado ha sido identificado como la principal fuente de partículas en el entorno urbano de Granada durante todas las estaciones del año. Durante el invierno, los sistemas de calefacción doméstica y la quema de residuos de biomasa suponen una fuente adicional de partículas, mientras que el proceso de formación de nuevas partículas contribuye significativamente a las concentraciones de partículas ultrafinas durante la primavera y el verano. El análisis por sectores de

viento muestra que el impacto de las emisiones de los sistemas de calefacción doméstica del área urbana es mucho más fuerte respecto al impacto de las emisiones de quema de residuos agrícolas del sector suburbano (especialmente por la noche).

Un nuevo método basado en Rodriguez y Cuevas (2007) y Sandradewi et al. (2008) ha sido desarrollado con el objetivo de conocer las contribuciones de las diferentes fuentes de aerosol a las concentraciones numéricas totales de partículas en áreas influenciadas por emisiones de quema de biomasa. Este nuevo método se ha utilizado para determinar las contribuciones tanto de las emisiones primarias de los vehículos y de la quema de biomasa como del aerosol secundario a las concentraciones del número de partículas segregadas por tamaño en entornos urbanos y suburbanos. En este sentido, este método se ha aplicado a las mediciones simultáneas de la distribución de tamaño de aerosoles en el rango de tamaño de 12 a 600 nm y la concentración de carbono negro (BC) obtenidas en ambos sitios durante el invierno, cuando ambos sitios suelen estar influenciados por las emisiones de la quema de biomasa procedentes de los sistemas de calefacción doméstica y la quema de residuos agrícolas. Los resultados muestran que (1) el aerosol secundario es el principal contribuyente a la concentración del número de partículas en todos los rangos de tamaño en ambos sitios, (2) el tráfico es la principal fuente de partículas primarias con contribuciones >70% en todos los rangos de tamaño en ambos sitios y (3) la quema de biomasa contribuye significativamente a las concentraciones de partículas primarias en los rangos de tamaño 25-100 y 100-600 nm en los sitios suburbanos (24% y 28%, respectivamente) y urbanos (13% y 20%, respectivamente). Además, se ha encontrado que los eventos de formación de nuevas partículas (NPF, por sus siglas en inglés) son una fuente importante de aerosoles durante las horas centrales del día en verano, pero, en promedio, estos eventos no implican una contribución considerable a las partículas urbanas.

A pesar de la baja contribución de los eventos de NPF a la concentración total de número de partículas en la zona urbana, estos eventos son de gran importancia para la producción de núcleos de condensación de nubes, afectando a la formación de estas. Por lo tanto, la caracterización de la distribución vertical de los eventos de NPF es de especial interés. Para ello, se ha llevado a cabo una investigación detallada de las características de los eventos de NPF y de los diferentes factores que promueven/inhiben los procesos de NPF en dos ambientes distintos: urbano y remoto en alta montaña. Para ello, se han utilizado mediciones simultáneas de las distribuciones de tamaño de los aerosoles (4-500 nm) medidas en ambos sitios. El análisis muestra que, con una frecuencia de eventos NPF >70% en ambos sitios, las partículas del modo de nucleación contribuyen en gran medida a la concentración numérica total de aerosoles en verano (47% y 48% en la estación de alta montaña y urbana, respectivamente). En la estación de alta montaña, se ha encontrado que los eventos de NPF están asociados al transporte de precursores gaseosos desde altitudes más bajas gracias al transporte ascendente debido a la orografía del terreno. Sin embargo, los eventos de NPF en la estación de alta montaña siempre se han observado a partir de los tamaños más pequeños medidos de la distribución de tamaño de aerosoles (4 nm), lo que implica que los eventos de NPF tienen lugar en la estación de alta montaña (o en sus proximidades), en lugar de ser transportados desde altitudes inferiores. Aunque los eventos de NPF en la estación de montaña parecen estar conectados con los que ocurren en el sitio urbano, las tasas de crecimiento (GR, por sus siglas en inglés) en la estación de montaña son más altas que las de la estación urbana. El análisis del ácido sulfúrico (H_2SO_4) muestra que las concentraciones de H_2SO_4 pueden explicar una contribución mínima a las tasas de crecimiento observadas en ambos sitios (< 1 % y < 10 % para los rangos de tamaño de 7-25 y 4-7 nm, respectivamente), indicando que otros vapores de condensación son los responsables de la mayor parte del crecimiento de las

partículas, así como de las diferentes tasas de crecimiento entre los dos ambientes. Los resultados también muestran que el sumidero de condensación (CS) no juega un papel relevante en los procesos de NPF en ambos sitios y apunta a la disponibilidad de compuestos orgánicos volátiles como uno de los principales factores que controlan los eventos de NPF en los ambientes urbanos y remotos investigados.

1 /Introduction

The atmospheric aerosol is defined as the suspension of solid and/or liquid particles, excluding clouds, in the atmospheric air (Horvath, 2000). These particles are either emitted directly to the atmosphere or produced in the atmosphere from precursor gases, and can be from both natural and anthropogenic origin (Seinfeld and Pandis, 2016). Due to their numerous sources and formation mechanisms, aerosol particles are highly variable in chemical composition and size (ranging from a few nanometers up to tenths of micrometers). Aerosol particles are trace constituents of the atmosphere, however they play an important role in atmospheric chemistry and physics, being of environmental, climate, and public health interest.

Atmospheric aerosols, particularly ultrafine particles (particles with diameters smaller than 100 nm), can easily be inhaled and deposited in nasal, tracheobronchial and alveolar regions, which poses a health risk (e.g., Cassee et al., 2019). In fact, in each breath we can inhale approximately 500 cm^3 of air and considering that an urban atmosphere like Granada, Spain, can have ~10.000 aerosol particles in 1 cm^{-3} of air (Casquero-Vera et al., 2021), each breath results in millions of respired particles. So, exposure to aerosol particles has been estimated to be one of the largest risk factors causing premature deaths globally (WHO, 2013). However, despite a large number of toxicological and epidemiological studies, there is little consistency between the findings and, currently, there is no consensus on which aerosol sources have greatest potential to affect health (WHO, 2013). In this sense, the last review of the evidence of health effects associated with exposure to

aerosol particles from five common emission sources (traffic, coal-fired power stations, diesel exhaust, domestic wood combustion heaters, and crustal dust), reported by Hime et al. (2018), concluded that the current knowledge does not allow precise quantification or definitive ranking of the health effects of aerosol particles from different sources, emphasizing the importance of further measurements and investigation of aerosol particles and their emission sources.

Besides their health effects, aerosol particles affect climate directly by scattering or absorbing incoming solar radiation, and indirectly by acting as cloud condensation nuclei (CCN) and modifying cloud properties (IPCC, 2013). Overall, aerosol particles are estimated to have a cooling effect on the climate, and thus they can partly counteract the global warming caused by greenhouse gases (IPCC, 2013). Although the uncertainties associated with the aerosol direct effect have been reduced in the last years, there is large uncertainties in determining the magnitude of the indirect climate effects of aerosol particles. A better understanding of the spatial and temporal variability of aerosol sources and sinks and their strengths as well as their formation and transformation processes in the atmosphere is of critical importance in order to better understand and quantify their radiative effects on climate.

Aerosol sources emission strength presents large spatial and temporal variability and the contribution of the different aerosol sources to the atmospheric particle concentrations is highly uncertain (IPCC, 2013). In this sense, aerosol particle flux measurements can provide important quantitative information about the characteristics of aerosol sources and sinks (e.g., Deventer et al., 2013; Järvi et al., 2009). The eddy covariance technique (EC) allows a direct and accurate measure of aerosol fluxes and thus can be used to determine aerosol sources and sinks, providing important information about their spatial variability (Mårtensson et al., 2006). Although cities are an important source of aerosol particles, EC flux measurements in urban areas are still scarce and most of previous studies have been

based on short-term measurement campaigns (e.g., Dorsey et al., 2002; Mårtensson et al., 2006; Martin et al., 2009; Schmidt and Klemm, 2008). Furthermore, most of these studies were conducted in central and northern European cities, with only a handful studies in southern Europe where the anthropogenic activities and the meteorological conditions are different to those in central and north of Europe (Conte et al., 2018, 2021; Contini et al., 2012; Donateo et al., 2019). Therefore, since urban particle fluxes depend largely on the characteristics of the site, more particle flux data from different cities (especially in southern Europe) are needed to fully understand the role of urban areas as net source of particles.

The aerosol sources are many and diverse and these sources determine the aerosol particles physical properties (size, density, shape...) and chemical composition. Aerosol sources can directly emit particles (primary aerosol) or can emit gases that favor the formation of new particles through gas-to-particle conversion processes (secondary aerosol). The formation of new atmospheric aerosol particles (also called nucleation), and their subsequent growth, commonly known as New Particle Formation (NPF) events, is an important process of secondary particles formation that has been estimated to account for approximately 50% of the total aerosol particle number concentration. During NPF events, particles can grow rapidly and reach sizes where they can act as CCNs and form cloud droplets (Kerminen et al., 2018; Rejano et al., 2021). In this sense, due to the role of NPF in the production of CCN, it is of special interest to characterize NPF in the free troposphere (FT) and its vertical distribution (Carnerero et al., 2018). In addition to its climate impact, NPF has been also increasingly investigated in urban areas due to its substantial contribution to the existing primary UFP, together resulting in high particle number concentrations (e.g., Brines et al., 2015; Németh et al., 2018, among others). However, despite the importance of this process, current knowledge about NPF processes in different environments remains poor.

Frequency, intensity and duration of NPF events are highly variable, making NPF prediction a current challenge of large interest. In addition, this high variability makes NPF contribution to the total particle number concentrations extremely dependent on location and environment where these events occur (Kerminen et al., 2018; Nieminen et al., 2018). It is known that various factors favour the occurrence of NPF events such as the availability of precursor gases, concentration of pre-existing aerosol, meteorological variables and solar radiation (Dada et al., 2017), however the vapours involved in the NPF process is still poorly understood. Sulfuric acid (H_2SO_4) has been commonly considered as one of the main precursors for aerosol nucleation and growth due to its low vapour pressure. However, H_2SO_4 alone is not sufficient to explain the observed NPF under various ambient conditions (Kulmala et al., 2004; Kulmala and Kerminen, 2008; Zhang et al., 2012) and recent studies have shown the vital roles of ammonia (NH_3), amines or highly oxygenated molecules (HOMs) in enhancing nucleation and promoting the initial growth of newly formed particles in the atmosphere (e.g., Kulmala et al., 2013; Schobesberger et al., 2013; Tröstl et al., 2016; Ehn et al., 2014). Thus, more efforts and studies in different environments with a distinct mixture of anthropogenic and natural precursor gases emissions and meteorological conditions are still needed for improving the current understanding of the new particle formation processes.

Among primary aerosols, black carbon (BC) is a primary product of incomplete combustion of carbonaceous fuels that has received increased attention during the past decades. This attention is because BC was found to have high correlation with health effects (e.g., Janssen et al., 2011; 2012) and because it is an important contributor to climate warming (e.g., Bond et al., 2013). In this sense, BC is very effective absorbing solar light which heats its surroundings. Furthermore, BC influences cloud formation which can impacts regional circulation and rainfall patterns (Cherian et al., 2017 and references therein). When deposited on ice and

snow, BC particles reduce surface albedo and heat the surface (Beres et al., 2020). For all these reasons, BC is considered as one of the most important climate forcing agents (Shindell et al., 2012).

In urban areas, BC is mainly originated from diesel engines (Hamilton and Mansfield, 1991; Pakkanen et al., 2000) but, besides traffic emissions, biomass burning and domestic heating (based on fossil or biomass fuels) constitute other important sources of BC. In this sense, EEA (2019) estimated that for EU-28, 28% and 48% of the anthropogenic BC emissions are from road transport and residential (biomass and coal) burning sources, respectively. Several studies have shown that improved technologies for new vehicles and increasingly stringent control measures on vehicle emissions have induced a downward trend in ambient BC mass concentrations during the last decade (e.g., Lyamani et al., 2011; Singh et al., 2018). However, emissions from residential combustion and open-air biomass burning are still not regulated in most European countries, and especially residential wood burning has become a common popular alternative energy source since the last years (Titos et al., 2017). Therefore, there is great interest in identifying and quantifying the contribution of BC sources for the development of effective control measures.

In this context, the methodology presented by Sandradewi et al. (2008), based on the analysis of the spectral aerosol absorption coefficient measurements, allows the quantification of biomass burning and traffic contributions to ambient BC mass concentrations in near real-time. Sandradewi et al. (2008) method has been demonstrated to be an useful approach to identify and quantify BC sources. However, BC is just a small fraction of the total aerosol population and the aerosol sources are many and varied. Since aerosol sources determine the effect of aerosol particles on both human health and climate, several approaches have been used to quantify the contribution of different sources to the ambient particulate mass concentrations in ambient air. Most of the aerosol source apportionment studies used

receptor models, such as Positive Matrix Factorization (PMF) or Chemical Mass Balance (CMB), which use online or offline aerosol chemical composition measurements (e.g., Alves et al., 2011; Minguillón et al., 2015; Tao et al., 2017; Titos et al., 2014). Observational studies source contribution to particle mass concentration have been widely conducted (e.g., Amato et al., 2016; Minguillón et al., 2015). However, since UFPs mainly control ambient particle concentrations in terms of number and coarser particles control particle concentrations in terms of mass, the sources contributions will differ in terms of number and mass concentrations. In this sense, observational studies of the contribution of primary and secondary aerosol particle sources to the total aerosol particle number concentrations are still rather limited (Cai et al., 2020; Rivas et al., 2020).

In the last years, different methods have been proposed to estimate the contribution of particles from primary and secondary sources to ultrafine particle number concentrations (e.g., Beddows et al., 2015; Beddows et al., 2009; Cai et al., 2020; Rodríguez and Cuevas, 2007). For instance, Rodríguez and Cuevas (2007) used the relationship between BC and particle number concentration for quantifying the sources and processes contributing to ultrafine particle concentrations in urban ambient air marginally or not influenced by biomass burning emissions. These authors have devised this method to distinguish between primary and secondary particles in urban areas mainly influenced by traffic emissions, assuming that BC originates only from traffic activities. In this sense, the method of Rodríguez and Cuevas (2007) does not allow to distinguish the sources of primary particles in urban areas where in addition to traffic there are other additional sources of BC. As mentioned above, biomass burning has been also recognized as an important source of BC, even in urban areas (Kalogridis et al., 2018; Titos et al., 2017) and hence this source may also have a significant contribution to urban aerosol.

1.1 /Objectives and outline

The research activities developed in this thesis have the main objective of advancing in the understanding of aerosol sources, their strength, spatial and temporal variability, with special focus on the issues that are still open and are a source of uncertainty in the atmospheric and climate studies. For this purpose, the study was carried out at contrasting environments: urban, suburban and high-altitude remote, and approached from different points of view. The first one is the characterization of the main aerosol local and regional sources affecting these three contrastive environments in the study area. The second one is to characterize the events of new particles formation at different environments with special focus on the role of precursor gases in the NPF processes.

The thesis dissertation is organized in several chapters, as indicated in the following outline:

Chapter 2 is devoted to the basic concepts behind the aerosol science needed to follow this thesis, including aerosol impact on climate and health, their properties, sources, and formation and transport processes.

Chapter 3 presents a detailed description of the experimental stations, together with a short description of the main instrumentation employed, including scanning mobility particle sizer spectrometers, multi-wavelength absorption photometer and eddy covariance system.

Chapter 4 presents the results of the detailed analysis of total aerosol number concentrations and fluxes measured using the eddy covariance technique at the top of a tower at a height of 50 m a.g.l. in the Granada urban area during the period Nov/2016 – Apr/2018. The main aim of this chapter is to identify the main sources contributing to the total aerosol number concentrations and their location in the study area.

Chapter 5 shows the results on the quantification of the contribution of different sources and processes to sub-micrometric particle concentrations in ambient air at an urban and suburban sites influenced by biomass burning emissions. This chapter presents a new approach to determine the contribution of both vehicle and biomass burning primary emissions and secondary aerosol to the size-segregated particle number concentrations.

Chapter 6 is devoted to the study of the frequency of occurrence, characteristics and factors that promote/inhibit NPF processes at two contrastive sites: urban and high-altitude remote sites. To this end, aerosol size distributions (4-500 nm) measured simultaneously at both sites during a summer campaign are analyzed and the role of precursor gases and their contribution to the formation and growth of aerosol particles at these two different environments are explored.

Finally, Chapter 7 presents a summary of the main conclusions of this thesis together with an outline of future research.

2 /Fundamentals

2.1 /Atmospheric aerosol

The atmosphere is the gaseous layer that surrounds the Earth that is mainly composed by gases but also by clouds and atmospheric aerosol particles. In this sense, atmospheric aerosol, defined as the suspension of solid and/or liquid particles (Horvath, 2000), is an atmospheric component that presents high spatial and temporal variability. Although atmospheric aerosols are a trace component of the atmosphere, they play an important role in climate and health. Several studies have shown an increase in health risk due to high aerosol concentrations, since particles can enter the human respiratory and even to the cardiovascular system (Cassee et al., 2019 and references therein). The health effects are mainly linked to particle size, as this parameter determines the region of the respiratory system in which the particle would deposit (Gómez-Moreno et al., 2011).

In addition, aerosol particles affect climate by influencing the radiative budget of the Earth. Atmospheric aerosol particles produce a radiative forcing (aerosol radiative forcing) by changing the incoming and outgoing radiation in the Earth-atmosphere system. The estimated net radiative forcing of aerosols is -0.9 (-1.9 to -0.1) W/m^2 (medium confidence), that results from a negative forcing from most aerosols and a positive contribution from black carbon aerosol (IPCC, 2013). However, aerosols still contribute to the largest uncertainty of the total radiative

forcing estimate, even though this uncertainty has been considerably reduced in the last years due to the increase in the knowledge of the aerosol properties.

The above-mentioned influence of atmospheric aerosols on the radiative budget is caused by two different mechanisms: (1) the interaction of aerosol with the solar and terrestrial radiation (direct effect of aerosol on climate or ARI) and (2) the interaction of aerosol particles with clouds (indirect effect or ACI) (Figure 2.1). The direct effect of aerosol on the Earth's energy budget (ARI) is the mechanism by which aerosol particles scatter and absorb shortwave and longwave radiation, altering the radiative balance of the Earth-atmosphere system (IPCC, 2013). The aerosol radiative forcing produced by the ARI may be positive or negative mainly depending on the absorptive capacity of aerosols. On the other hand, the indirect effect is the mechanism by which aerosol particles change cloud properties, potentially affecting precipitation and the radiative impact of clouds (IPCC, 2013). The ACI is associated to the modifications of cloud properties due to the role of aerosols acting as cloud condensation nuclei (CCN) or ice forming nuclei (IN). The increase in aerosol particle number concentrations may increase the ambient concentration of CCN/IN and therefore affects cloud properties. An increase of CCN concentrations can lead to more cloud droplets so that, for fixed cloud liquid water content, the cloud droplet size will decrease. This effect leads to brighter clouds, changing the cloud albedo. Furthermore, aerosol particles may produce an effect on the cloud (1) liquid water content, (2) height and (3) lifetime (IPCC, 2013). These aerosol effects can (1) suppress drizzle and (2-3) increase the amount of solar radiation reflected from clouds.

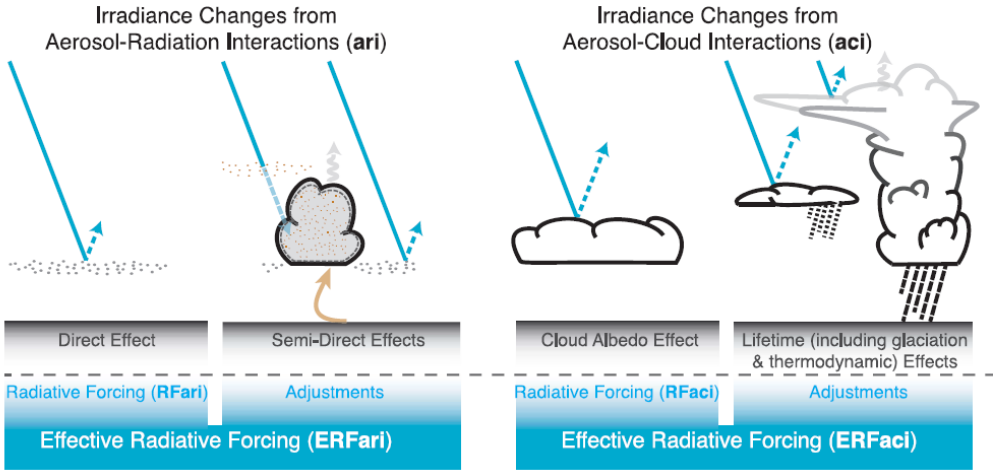

Figure 2.1 - Schematic of the aerosol-radiation and aerosol-cloud interactions. The blue arrows depict solar radiation, the grey arrows terrestrial radiation and the brown arrow symbolizes the importance of couplings between the surface and the cloud layer for rapid adjustments. (Source: IPCC, 2013).

2.2 /Aerosol sources

Depending on their sources, aerosols can be split into natural and anthropogenic, and can also be divided into primary and secondary depending on their origin. Primary aerosols are those emitted directly to the atmosphere in the particulate phase, whereas secondary particles are produced in the atmosphere by complex formation pathways via gas-to-particle conversion. The natural and anthropogenic aerosol sources are many and varied, and these sources determine the physical characteristics of aerosols (size, density, shape...) and their chemical composition.

In terms of emission sources, natural aerosol emissions are much larger (~12000 Tg/yr) than those from anthropogenic origin (~300 Tg/yr) (Gieré and Querol, 2010). Main primary natural aerosol particles include sea salt from the oceans, volcanic ash, pollen, smoke from fires and mineral dust. Mineral dust is mainly produced by wind erosion of soil in arid and semi-arid regions (e.g., Sahara

Desert) and is injected into the atmosphere under favourable weather conditions. Mineral dust is one of the major aerosols of the atmosphere that can be transported over thousands of kilometres and therefore it has a global climate effect (e.g., Ansmann et al., 2003; Benavent-Oltra et al., 2019; Cazorla et al., 2017). On the other hand, the sources of secondary natural aerosol are mainly volcanoes and the biosphere. Volcanoes emit large amount of sulfur dioxide that is considered one of the new particle formation precursors through its oxidation to sulfuric acid (e.g., Rose et al., 2019). The biosphere is considered an important source of secondary particles through dimethyl sulfide (DMS) and volatile organic compounds (VOCs) emissions that are able to form new particles by photo oxidation and the subsequent gas-to-particle conversion of the reaction products (e.g., Ehn et al., 2014).

Despite the global emissions in terms of mass concentration are dominated by natural sources, they are mainly related to contributions from the coarse particles, while the emissions from anthropogenic sources are mainly dominated by fine particles. In this sense, organic aerosol and black carbon from incomplete combustion processes or biomass burning are considered the main anthropogenic primary particles. In urban areas, traffic is the main source of organic and black carbon particles, but biomass burning has also been identified as an important source of carbonaceous particles in Europe during winter time (e.g., Titos et al., 2017), contributing for up to 80% of fine aerosol mass (Denby et al., 2010). In addition, dust emissions also have a significant component of primary anthropogenic aerosol, mainly originating from agricultural and industrial practices and road traffic due to resuspension. Secondary aerosol sources of anthropogenic origin include domestic heating systems (based on coal or wood combustion), industrial plants, traffic emissions and agricultural activities. These sources emit SO_2, NO_x, ammonia, VOCs and other tracer gases that favours the formation of secondary aerosol through new particle formation.

2.3 /Aerosol size distribution

Varying over five orders of magnitude, the size of aerosol particles is highly variable ranging from a few nanometers to several hundreds of micrometers. In general, the aerosol size distribution is characterized by different size modes, which are specific concerning their sources and transformation processes. Figure 2.2 shows a schematic of the aerosol size distribution together with an overview of the relevant processes affecting the different aerosol modes.

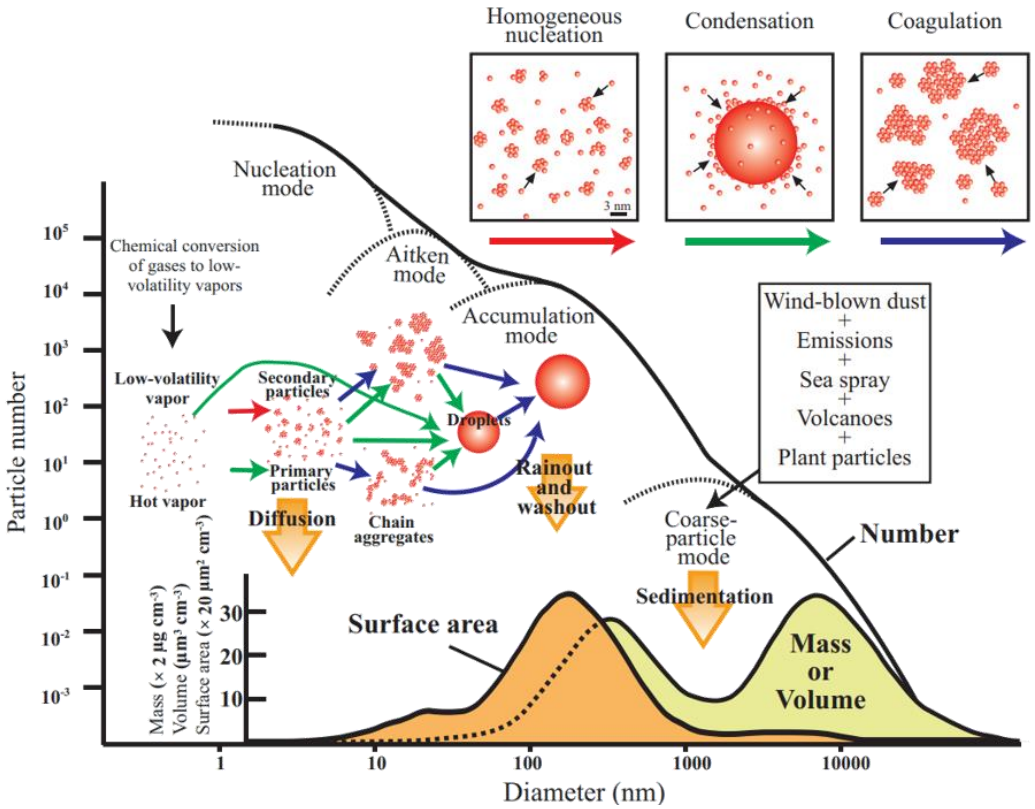

Figure 2.2 – Schematic of the number, mass, volume and surface aerosol size distribution in an idealized atmospheric sample, together with illustrations of their formation mechanisms (Figure taken from Buseck and Adachi, 2008)

The aerosol size distribution in the atmosphere is generally divided into four different aerosol modes (Nucleation, Aitken, Accumulation and Coarse) (Seinfeld and Pandis, 2016). These four aerosol modes are related with the different aerosol

sources and formation, transformation and removal processes that the particles in those modes undergo in the atmosphere. These modes are usually grouped in the so-called *ultrafine mode* for particles below 100 nm (Nucleation and Aitken modes) or *fine mode* for particles below 1 µm (Nucleation, Aitken and Accumulation modes).

Nucleation mode: contains the smallest particles with diameters smaller than a few tens of nanometres (usually ~3 and 25 nm are considered the lower and upper limits, respectively, of the nucleation mode). These particles are by far the largest in terms of aerosol particles number concentrations, however, their volume, surface or mass concentrations are small relative to the other size groups. Particles in this size range are mainly formed by (1) nucleation processes that occur at ambient temperatures and involve the nucleation of relatively nonvolatile products of photochemically initiated gas-phase reactions and (2) rapid cooling of hot and supersaturated gases from manufacturing facilities, vehicle exhaust, and biomass burning.

Aitken mode: named after the person who first recognized the importance of these particles (Dr. John Aitken), Aitken mode particles are usually considered as those in the diameter range from 25 to 100 nm. Particles in this size range includes a mixture of soot particles emitted in combustion processes and coagulated nucleation mode particles (Seinfield and Pandis, 2016). In urban areas, EURO standards vehicles highly contribute to the emission of primary particles in this size fraction (Rodríguez and Cuevas, 2007).

Accumulation mode: comprises the largest fine particles with diameters between 100 nm and 1 µm. The accumulation mode particles are mainly generated from biomass and fuel combustion processes and coagulation and growth of Aitken mode aerosols by multicomponent condensation of vapours onto the existing particles. This mode comprises particles characterized by low removal efficiency,

being rainout (e.g., forming cloud droplets) or washout (collision with rain droplets) the main removal mechanisms of these particles.

Coarse mode: contains particles with diameters larger than 1 µm. Particles in this size range are mostly primary particles generated by mechanical processes such as resuspended mineral dust, marine and volcanoes aerosol, tires and brake abrasion or biogenic emissions (e.g., pollen). The more important removal process of the coarse mode is gravitational settling (sedimentation) due to their larger size and mass. Therefore, this mode is usually characterized by short residence times in the atmosphere.

The aforementioned aerosol size ranges are described for ideal spherical particles. However, the majority of aerosol types have non-spherical shape and thus, the term *equivalent diameter* is commonly used on atmospheric sciences to define the diameter of particles as function of a determined physical property of the particles. Because of this, the measurement of aerosol diameter is done by different techniques depending on the physical property used to estimate the particle size. For example, the Aerodynamic Particle Sizer (APS) uses the aerosol time-of-flight to determine the *aerodynamic particle diameter*, the Optical Particle Counters (OPCs) provide the *optical particle diameter* by measuring their optical properties and the Scanning Mobility Particle Sizer (SMPS) provides the *Stokes or mobility particle diameter* measuring the mobility of charged particles in an electric field. All these diameters are affected, at least, by the shape and density of particles. For example, non-spherical particles have smaller electrical mobility than the spherical particles. However, density and shape of particles are usually difficult to estimate and therefore the aforementioned instruments consider spherical particles and predefined particle densities (usually 1 $g \cdot cm^{-3}$). From now on, if not stated otherwise, the term *particle diameter* refers to a diameter of a spherical particle.

2.4 /New particle formation events

The formation of new atmospheric aerosol particles, and their subsequent growth, commonly known as New Particle Formation (NPF) events, has a substantial contribution to aerosol particle number concentration, especially to the aerosol number concentrations in the Nucleation mode. Their subsequent growth to larger sizes, first to a few nm in particle diameter, then to nucleation and Aitken mode particles, and possibly up to sizes at which these particles may act as CCN (Kerminen et al., 2018; Rejano et al., 2021), makes this process an important contributor to the CCN budget in the global atmosphere (Merikanto et al., 2009).

2.4.1 State-of-the-art on new particle formation process

Nucleation is traditionally defined as the formation of a molecular cluster of a critical size (~1.5 nm) at which the cluster more likely grows than evaporates. Thus, nucleation is the critical process on the new particle formation events. The first evidence of atmospheric new particle formation was reported in the 19th century by Dr. John Aitken (Aitken, 1897). Since then, NPF has been observed to be a frequent phenomenon around the world (Kulmala et al., 2004). While there are many theories to describe the process of nucleation, there are still significant gaps in the knowledge of new particle formation (Kerminen et al., 2018). In this sense, Kulmala et al. (2013) described NPF events as a three-step process (Figure 2.3): (1) chemical reactions in the gas phase producing low-volatility vapour(s) and clusters in the mobility diameter range from 1.1 to 1.3 nm, (2) cluster stabilization or nucleation in the mobility range from 1.1-1.3 to 1.5-1.9 nm, (3) faster condensational growth of nucleated particles to larger sizes due to organic vapours that occurs above 1.5-1.9 nm.

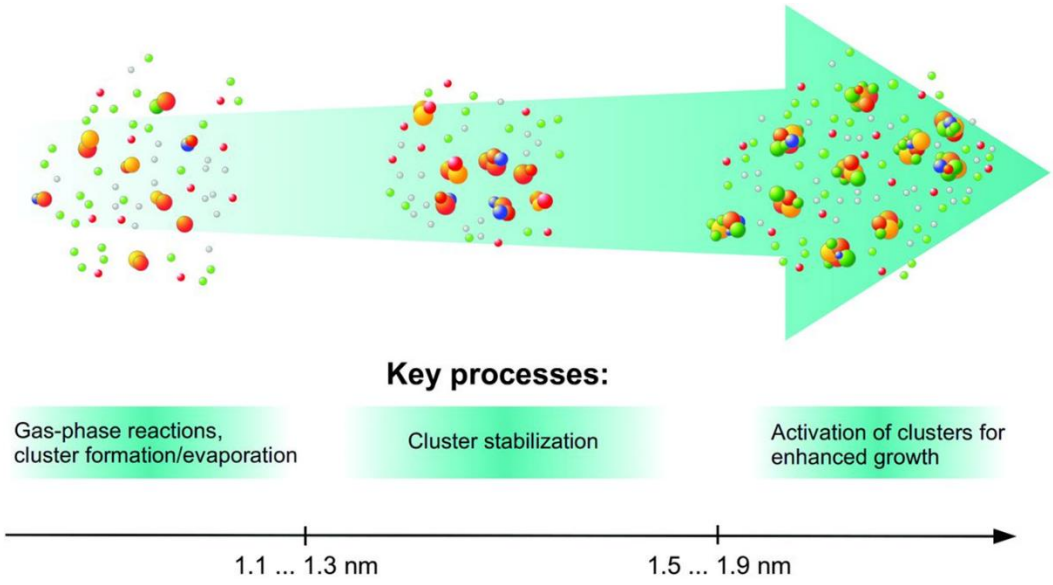

Figure 2.3 - Schematic description of main size regimes of atmospheric neutral clusters. (Figure adapted from Kulmala et al., 2013)

The progress in measurement methods and theoretical understanding, together with their application in laboratory and field conditions, brought to revise the traditional NPF view by Kulmala et al. (2014) by adding two more steps to this process: (1) a first step similar to the traditional first step, but with some new oxidation pathways; (2) clustering; (3) nucleation or barrierless nucleation; (4) the activation of clusters with a second group of vapours; and (5) a final step similar to the traditional final step, but now with multicomponent condensation.

Despite this advancement in theoretical knowledge of NPF steps, large discrepancies have been found between the expected and observed properties of NPF under atmospheric conditions (Chu et al., 2019; Kulmala et al., 2017; Nieminen et al., 2018). These discrepancies are mainly related with the poor knowledge of the molecules involved in the process to form stable clusters. In this sense, sulfuric acid (H_2SO_4) has been commonly considered as one of the main precursors for aerosol nucleation and growth due to its low vapour pressure. However, H_2SO_4 alone (binary nucleation of sulfuric acid with ambient water vapor) is not sufficient to

explain the observed NPF under various ambient conditions (Kulmala et al., 2004; Kulmala and Kerminen, 2008; Zhang et al., 2012). The introduction of bases like ammonia and amines to stabilize the sulfuric acid by an acid-base ternary nucleation has been indicated by cluster models, laboratory experiments and field observations as a favourable mechanism in the atmospheric boundary layer (e.g., Bianchi et al., 2017, 2014; Kurtén et al., 2007). Additionally, the oxidation of volatile organic compounds (VOCs) produces oxidized organic species, called HOMs (highly oxidized organic molecules) which seem to be essential for atmospheric new particle formation (e.g., Bianchi et al., 2019; Ehn et al., 2014).

It is also important to mention the role of ions in the process of new particle formation. Small air ions are formed mainly when ionizing radiation like radioactive radon and gamma or cosmic rays impact an air molecule (N_2, O_2), but also high winds or thunderstorms, or even engines and exhaust tube can form ions (e.g., Hirsikko et al., 2007; Lähde et al., 2009). For a long time, an important role of ions has been recognized in atmospheric particle formation due to their ability to stabilize small clusters and form neutral clusters by ion–ion recombination (e.g., Arnold, 1982). A charge can also provide a stabilizing effect for the nucleating cluster and enhance the formation of new particles by ion-induced NPF (Rose et al., 2018 and references therein). However, field measurements suggest that the contribution of ion-mediated processes to particle formation is only minor, less than 10%, in the boundary layer (e.g., Manninen et al., 2010), and slightly higher at mountain sites (Boulon et al., 2011; Rose et al., 2015). In this sense, studies have shown that ions may be more important at the clustering stage (e.g., Rose et al., 2018) but neutral pathways would dominate the nucleation stage, particularly beyond 2 nm diameters.

Finally, new particle formation is a competition of chemistry, enhanced or truncated by the environmental conditions that, when favorable, push forward to the survival of the smallest clusters to sizes of ~2 nm and beyond. Since extremely small

clusters have very short lifetimes due to collisions with larger particles, they experience "a grow or die dilemma" before forming new particles (Kulmala et al., 2017). In this sense, NPF event could be defined as a competition between new particle formation growth and scavenging by pre-existing aerosol particles, or even as a competition between chemistry and favorable atmospheric conditions for large clusters (>2 nm) survival. Therefore, as it has been observed in the boundary layer, lower pre-existing aerosol surface area favors particle formation (e.g., Kerminen et al., 2018 and references therein). Furthermore, in addition to the role of different atmospheric constituents, meteorological conditions play a key role on the formation and growth of new particles in the atmosphere. Solar radiation has been observed to be an important factor for atmospheric particle formation in numerous studies (e.g., Dada et al., 2017 and references therein), reflecting the significance of photochemical oxidation processes producing low-volatile vapours. Relative humidity has been also observed to favour particle formation by H_2SO_4-water nucleation.

2.4.2 New particle formation events characterization

From the observational point of view, atmospheric NPF and subsequent particle growth are seen as an emergence of new aerosol particles into the lower end of the measured particle number size spectrum, followed by the growth of these particles into larger sizes. If this event take place regionally (over a minimum distance of a few tens of km) a contour plot of measured particle number size distribution as a function of time will show the so-called *banana plots*, reminding to a banana shape (Figure 2.4 shows an example). However, if the NPF event does not take place in a regional scale, the measurements in a fixed location only capture a limited part of this process, usually called *local events*. For a proper analysis of NPF, Dal Maso et al. (2005) proposed a methodology to identify NPF event, non-event and undefined days, and furthermore to categorize NPF events in sub-classes based on the amount and accuracy of information that could be derived to characterize the NPF event.

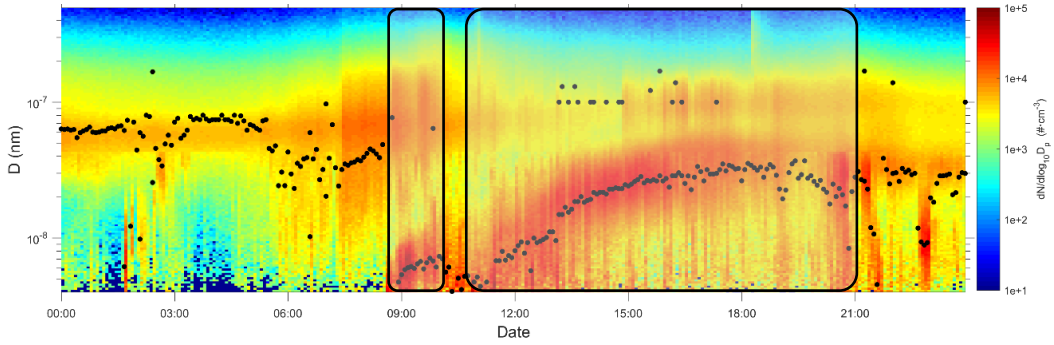

Figure 2.4 - An example illustrating a case where a local (9:00 UTC) and regional (11:00 UTC) event take place at Granada urban area. (Figure adapted from Casquero-Vera et al., 2020 supplement)

When estimating the importance of NPF in different environments, one needs to know the occurrence frequency and how strong events are when taking place. In this sense, since one regional NPF event per day is usually observed, the event frequency is usually calculated as the fraction of days having NPF events. On the other hand, the strength of an event is characterized by its duration, the rate at which new particles are formed or the growth rate of newly formed particles into larger sizes. In this sense, the two most important quantities to describe NPF events strength are the particle *formation rate* and the *growth rate*. The growth rate (GR) determines how fast particles growth ($nm \cdot h^{-1}$ as widely used unit) is a key quantity when determining the fraction of freshly formed particles able to survive to climatically relevant sizes before being lost due to coagulation, and there are different methodologies to estimate this quantity (Kontkanen, 2016). On the other hand, the particle formation rate (also commonly called nucleation rate) is defined as the flux of growing nanoparticles through a certain particle size (ΔD_p) and is denoted as J_{D_p} ($cm^{-3} \cdot s^{-1}$ as widely used unit). This quantity can be calculated considering the formation of neutral, charged particles or total (considering neutral and charged particles). In addition, as mentioned above, there is a key role of atmospheric parameters or constituents that favors or inhibit the formation of new particles. In this sense, preexisting particles are a sink of newly formed particles via

coagulation (*coagulation sink; CoagS*) and condensation (*condensation sink; CS*). Newly formed particles can coagulate with another newly formed particles or with preexisting particles and also low volatile gases can be lost by condensation on preexisting particles. These quantities are commonly used to characterize pre-existing aerosol loading that would affect the formation and growth of new particles. As mentioned above, different methodologies are used to estimate all these parameters depending on the instrumentation available. The methodology used in this thesis for the retrieval of new particle formation relevant parameters will be presented in Section 6.1.

2.5 /Aerosol optical properties

The direct effect of aerosol on the Earth's energy budget is the mechanism by which aerosol particles scatter and absorb shortwave and longwave radiation, altering the radiative balance of the Earth-atmosphere system (IPCC, 2013). In this sense, a beam of light passing through a layer of aerosol is attenuated due to scattering and absorption of radiation by particles and gas molecules. The processes of absorption, scattering and extinction are briefly described below:

- Absorption is the process in which the incident radiative energy becomes part of the internal energy of the particles or gases that interact with the radiation.
- Scattering is the process in which the incident electromagnetic wave, that transport the energy, is dispersed in all directions at the same wavelength as a result of the interaction of the particles and gases with this electromagnetic wave.

- Extinction describes the attenuation of light due to the combination of scattering and absorption processes during the light propagation though the aerosolized and/or gaseous medium.

Considering a monochromatic light beam ($I_{0\lambda}$) entering a homogeneous medium, there is an attenuation of the radiance (I_{λ}) after crossing a distance *x* in the direction of its propagation. The attenuated radiance after passing through the medium is derived from the Beer-Bouger-Lambert law:

$$I_{\lambda} = I_{0\lambda}\, e^{\sigma_{ext}(\lambda)x} = I_{0\lambda}\, e^{ATN(\lambda)} \qquad \text{Eq. (2.1)}$$

where $ATN(\lambda)$ is the attenuation and $\sigma_{ext}(\lambda)$ is the extinction coefficient for radiation of wavelength λ. The extinction coefficient is the sum of the scattering coefficient $\sigma_s(\lambda)$ and the absorption coefficient $\sigma_a(\lambda)$:

$$\sigma_{ext}(\lambda) = \sigma_s(\lambda) + \sigma_a(\lambda) \qquad \text{Eq. (2.2)}$$

Thus, the attenuation of the radiance after crossing a homogeneous medium is due to scattering and absorption. In the case of atmospheric air, the extinction, scattering and absorption are caused by air molecules and aerosol particles. In consequence, the extinction, scattering and absorption coefficients are the sum of those produced by gases and particles. In this sense, σ_{sp} and σ_{ap} refer to the scattering and absorption produced only by particles.

When the radiation interacts with particles, both processes (scattering and absorption) occur simultaneously and the relative importance of the scattering and absorption processes is characterized by the single scattering albedo (ω_0):

$$\omega_0(\lambda) = \frac{\sigma_{sp}(\lambda)}{\sigma_{sp}(\lambda) + \sigma_{ap}(\lambda)} \qquad \text{Eq. (2.3)}$$

Primarily, aerosol single scattering albedo defines the direct climate impact of aerosol (Liou, 1980; Miller and Tegen, 1998). In this sense, strong absorbing

particles exhibit ω_0 values ~0.2, that would favour the warming of the atmosphere by the aerosol direct effect. By contrast, purely scattering particles exhibit ω_0 values ~1 that would favour the cooling of the atmosphere. The single scattering albedo mainly depends on the aerosol types and aerosol aging processes. Consequently, the absorption of solar radiation by aerosols mainly results from (1) carbonaceous particles (elemental and organic carbon), especially black carbon (or soot) that is mainly originated from biomass burning and fuel combustion, and absorbs light strongly in the whole visible spectrum, and (2) mineral dust that absorb light mostly in the ultraviolet range.

Aerosol absorption and scattering coefficients (and therefore particles extinction and ω_0) depend on the light wavelength and this dependence is characterized by the aerosol scattering Ångström exponent (α_{sp}) and aerosol absorption Ångström exponent (α_{ap}):

$$\alpha_{sp}(\lambda_1, \lambda_2) = -\frac{\log[\sigma_{sp}(\lambda_1)/\sigma_{sp}(\lambda_2)]}{\log(\lambda_1/\lambda_2)} \quad \text{Eq. (2.4)}$$

$$\alpha_{ap}(\lambda_1, \lambda_2) = -\frac{\log[\sigma_{ap}(\lambda_1)/\sigma_{ap}(\lambda_2)]}{\log(\lambda_1/\lambda_2)} \quad \text{Eq. (2.5)}$$

The wavelength dependence of scattering and absorption coefficients provides qualitative information about the sources, size or shape of aerosol particles. In this sense, α_{sp} increases with decreasing particle size and for the visible spectrum takes values around 2 when the scattering process is dominated by fine particles, while it is close to 0 when the scattering process is dominated by coarse particles (Seinfeld and Pandis, 2016). By contrast, the chemical composition of aerosol material mainly determines the wavelength dependence of aerosol absorption coefficient. In this sense, α_{ap} is assumed to be a specific property of each aerosol

species. For example, black carbon aerosols have α_{ap} around 1.0, and mineral dust or other organic aerosols have higher α_{ap} values (e.g., Fialho et al., 2005; Kirchstetter et al., 2004). Mineral dust can present Fe oxidation states (as hematite, Fe_2O_3) with large absorptive properties, especially in the ultraviolet range compared to larger wavelengths (Liu et al., 2018). Wood smoke is also known to contain abundant organic materials (e.g., polycyclic aromatic hydrocarbons or humic-like substances) that strongly enhance the absorption of light in the ultraviolet and blue spectral range compared to that in the near-infrared range. Thus, the α_{ap} of an aerosol sample close to 1 is considered to be BC-rich aerosol from fossil fuel combustion, and larger α_{ap} values (>1.5) indicate aerosols from biomass/biofuel burning or mineral dust (Russell et al., 2010). In this sense, the α_{ap} is commonly used to determining the source of BC by the so-called Aethalometer model, which assumes that BC has two sources: traffic or biomass burning (Sandradewi et al., 2008).

2.6 /Planetary boundary layer dynamic

The planetary boundary layer (PBL) is the part of the troposphere that is directly influenced by the presence of the Earth's surface, and responds to surface forcings with a time scale of about an hour or less (Stull, 1998). Under an ideal scenario, shortly after sunrise, the positive net radiative flux causes the rising of ground surface temperature and, consequently, air masses located at low heights get warmer favouring convective processes. These processes lead to air lifting and consequent heating of atmospheric layers at a certain altitude over the surface inside the troposphere. In this sense, the height of the PBL is an important variable that characterizes the PBL structure and provides information on the vertical extent of mixing within this layer as well as the vertical dispersion and convective transport.

Thus, the height of this layer is relevant in different atmospheric fields such as air quality, pollutant dispersion, weather forecasting and meteorological modeling (Moreira et al., 2020).

The PBL is characterized by the permanent surface-atmosphere interaction and by its turbulent nature that makes atmospheric properties to be mixed and thus vertically homogeneous. The turbulence is a transport mechanism of gases, particles, temperature or momentum in the PBL. The turbulent structures in the PBL are called *eddies* that are either caused by mechanical processes (wind shear, surface roughness or friction) or by thermal processes (e.g., buoyancy produced by surface heating) that is the most dominant source for mixing when is present (Oke, 1992). In the PBL, the size of these eddies varies from 10^{-3} to 10^{3} m and their frequency is associated to their size.

The eddy covariance technique is a widely used method to measure the exchanges of heat, mass and momentum between a flat horizontally homogeneous surface and the overlying atmosphere. In order to determine the surface atmosphere exchange of a specific scalar, simultaneous measurements of the scalar of interest (such as total particle number concentration) and vertical wind velocity are measured by eddy covariance system. It is worth to mention that this technique assumes that the magnitude of the studied scalar only varies by the transport or emission/sink processes. From eddy covariance measurements, the vertical turbulent flux (F) crossing the measurement plane over a horizontally homogeneous area is determined as the covariance between fluctuations of the vertical wind speed (w) and a scalar (such as concentration of aerosol particles, N) as follow:

$$F = \overline{w'N'} \qquad \text{Eq. (2.6)}$$

where the overline denotes the temporal mean and primes denote the turbulent deviations from the mean. Using Reynolds decomposition, the fluctuations of the vertical wind speed (w') and particle number concentrations (N') are given by:

$$N' = N - \bar{N} \quad \text{and} \quad w' = w - \bar{w} \qquad \text{Eq. (2.7)}$$

where *N* and *w* the actual values of particle number concentration and wind velocity, and $\bar{N}$ and $\bar{w}$ are the mean values of this variables.

It is important to note that the vertical flux quantify the net transport exchange that results from both sinks and sources of particles at the surface, under the assumption that the measurements are made within an inertial layer (constant flux layer). More details on eddy covariance technique (fundaments, measurements or data analysis) can be found in Aubinet et al. (2012).

3 /Experimental sites and instrumentation

3.1 /Experimental sites

The data used in this thesis were obtained at the Andalusian Global ObseRvatory of the Atmosphere (AGORA). This observatory is located in the Granada area, in southeastern Spain, and includes several experimental sites operated by the Atmospheric Physics Group (GFAT). AGORA combines complementary stations with different atmospheric conditions with the main research activities focused on the study of the Earth's surface – atmosphere interactions. High-degree of expertise, many facilities and the combination of remote sensing and in-situ techniques provide an ideal environment for a wide range of aerosol research from urban to remote conditions.

The climate in the Granada area is typically Mediterranean-continental, with cold winters, dry and hot summers and large diurnal temperature variability. The Granada metropolitan area, with a population of approximately 0.53 million inhabitants, is situated in a valley surrounded by mountains of elevation up to 3479 m a.s.l. (Sierra Nevada mountain range). Granada city is the largest city in the metropolitan area that represents half of the metropolitan area population. Due to its location in the valley, Granada metropolitan area has a well-characterized mountain-valley wind regime with up-valley winds from NW and W during day, and down-valley winds from SE and E during night and early morning (Ortiz-Amezcua, 2019). Due to its geographical location, Granada can be influenced by long-range transport

of anthropogenic pollution from Europe and by natural dust from North Africa (Lyamani et al., 2006, 2010; Mandija et al., 2016, 2017; Valenzuela et al., 2012a, 2012b) but it is mainly influenced by local anthropogenic emissions. The main local aerosol source is road traffic as there are no large industries in Granada metropolitan area (Lyamani et al., 2011; Titos et al., 2014). In winter, domestic heating (based on fuel oil combustion and biomass burning) and agricultural wastes burning represent additional local sources of aerosols in Granada metropolitan area (Titos et al., 2017). However, despite Granada metropolitan area is a medium-size non-industrialized area, it is one of the Spanish areas that suffers serious pollution problems (Casquero-Vera et al., 2019). The meteorological conditions together with the orography of the city favor episodes with high atmospheric stability which lead to heavy pollution episodes, especially in winter (Lyamani et al., 2012).

This thesis has been mostly developed using in-situ instruments located in three stations that are part of the AGORA observatory and that are within 25 km distance range between them (Figure 3.1). These three stations are briefly described below:

- The UGR urban station is located at the Andalusian Institute for Earth System Research (IISTA-CEAMA) in Granada city (37.16º N, 3.61º W, 680 m a.s.l.). The station is situated in the southern part of the city and is about 500 m away from the principal highway that surrounds the western sector of the city and about the same distance from Camino de Ronda; that is one of the main busy roads of the city. The measurement site is surrounded by several surface types, including residential, commercial and road areas in the wind direction between 0º N and 225º S, and agricultural and suburbs areas as well as the principal highway of the city in the wind direction between 225º S and 360º N (Figure 3.1). The site combines long-term monitoring of (1) aerosol in-situ measurements for the characterization of aerosol particles at ground level (chemical, microphysical and optical properties), with (2) the

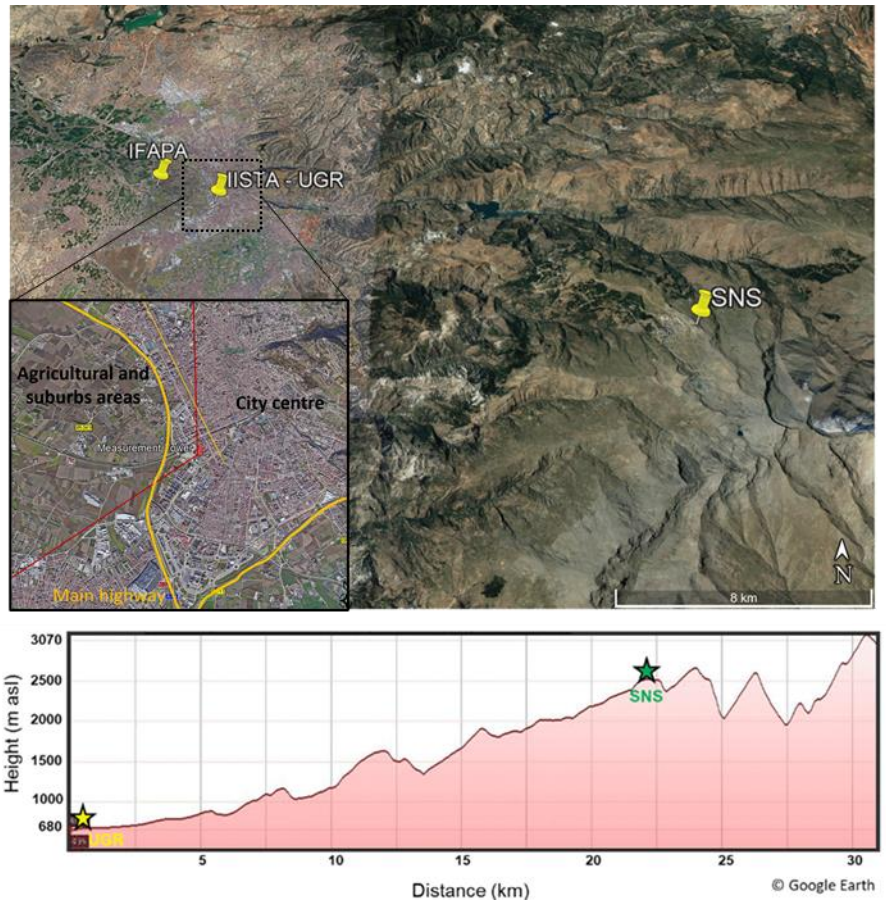

Figure 3.1 - Map showing the location of UGR urban, IFAPA suburban and SNS high-altitude remote sites (top) and topographic profile between UGR and SNS sites (bottom). Zoom on the urban area is also shown (Figure 4.1 for detailed information).

measurement of vertical distribution of atmospheric aerosol based on active and passive remote sensing, as well as (3) the monitoring of atmospheric and solar radiation at several spectral ranges. In addition, long-term monitoring of aerosol number fluxes and concentrations are performed at UGR station by using eddy covariance system installed in a tower of 50 m height that is located in the Interactive Science Museum at 100 m from the IISTA-CEAMA building. The in-situ measurements at UGR station are performed in the frame of ACTRIS (Aerosol, Cloud and Trace Gases Research Infrastructure; Pandolfi et al., 2018) and is also included in the SARGAN

(in-Situ AeRosol GAW Network; Rose et al., 2021) and NFAN networks (NOAA Federated Aerosol Network; Andrews et al., 2019).

- The SNS high-altitude remote station (37.10º N, 3.39º W, 2500 m a.s.l.) is located in the northern slope of the Sierra Nevada mountain range, ~5 km north-west of the Veleta summit (3398 m a.s.l.) and ~20 km south-east of the Granada city (Figure 3.1). Due to its location with respect to the valley, prevalent wind directions are mainly from westerly and southerly directions. Atmospheric conditions at SNS can be considered as representative of south-western European free troposphere. It is influenced by long range transport of dust from the African continent, biomass burning and local/regional pollution from the Granada metropolitan area. The latter occurs frequently at midday, especially during summer season, when the PBL height is above the SNS site.

- The IFAPA suburban station is located in the Granada metropolitan area, located in the Andalusian Institute of Agricultural and Fisheries Research and Training (IFAPA) in a suburban area ~3 km away from the UGR urban station and ~2 km away from the nearest highway (Figure 3.1). This site is surrounded by agricultural land (La Vega de Granada), where open burning of agricultural waste is the most extended waste removal technique, mainly occurring from late autumn to early spring. In addition, this site is strongly affected by local emissions from Granada urban area, the highway and the metropolitan area itself (mainly road traffic and domestic heating during winter).

Measurements included in this thesis were carried out in the frame of three measurement campaigns performed in the AGORA observatory (Table 3.1). A brief description is included below:

AGORA fluxes: Measurements at the UGR tower were conducted from November 2016 to May 2018 in the framework of work-package (WP) 12 of ACTRIS. During this campaign continuous measurements of tower-based particle flux measurements were conducted together with vertical remote sensing measurements (at the IISTA-CEAMA building) in order to compare in-situ and remote sensing particle fluxes. In this thesis the focus is kept on the tower-based aerosol fluxes.

SLOPE II: Measurements at SNS high-altitude remote site were conducted in the framework of the SLOPE II campaign (Sierra Nevada Lidar AerOsol Profiling Experiment II). The SLOPE II campaign was developed along summer 2017 (May-September) combining measurements at two different altitude sites (UGR and SNS station) with the aim to evaluate the impact of emissions from Granada metropolitan area on aerosol concentration and chemical composition over Sierra Nevada remote station. The measurements of SLOPE II campaign used in this thesis were obtained during an intensive measurement period 23/June – 24/July at UGR and SNS sites.

AMICUS: Finally, measurements at IFAPA suburban site were conducted in the framework of the AMICUS (Aerosol MIcrophysical and Chemical properties at Urban atmoSphere) winter campaign from 18 December 2015 to 01 April 2016. This campaign was conducted in the Granada metropolitan area and was designed to investigate aerosol sources and their spatial distribution in urban and suburban areas, with special emphasis on biomass burning and traffic sources impact on the study area. For that, concurrent measurements of aerosol physical and chemical properties were performed using multiple techniques in four monitoring sites situated in the Granada metropolitan area. Two of the sites (San Juan de Dios Monastery and Alhambra palace) were aimed at evaluating the impact of black carbon on monumental heritage (Patrón et al., 2017). The two other sites (IFAPA and UGR) were selected to investigate the impact of biomass burning and traffic emissions in

the urban and nearby suburban and rural areas of Granada. This thesis focuses in these latter two sites from the AMICUS campaign.

Table 3.1 – Measurement campaigns periods and sites of concurrent measurements presented in this thesis.

Campaign	Period	Concurrent measurement sites
AGORA fluxes	01/11/2016 - 01/05/2018	UGR remote sensing and tower-based fluxes
AMICUS	18/12/2015 - 01/04/2016	UGR and IFAPA
SLOPE II	23/06/2017 - 24/07/2017	UGR and SNS

3.2 /Instrumentation and experimental data

3.2.1 Scanning Mobility Particle Sizer: SMPS

Scanning Mobility Particle Sizer (SMPS) spectrometer is a real time mobility diameter size-selective particle counting instrument that provides particle number size distributions of fine mode aerosol. This instrument consists of a differential mobility analyzer (DMA) connected to a condensation particle counter (CPC). In addition, ambient air is pumped through a bipolar charger or neutralizer, which could be a radioactive (Kr^{85}, Ni^{63}, Am^{241} or Po^{210}) or an X-Ray source. Following neutralization, aerosols enter the DMA, where they are classified according to their electrical mobility (Figure 3.2). The mobility analyzer consists of two cylindrical electrodes made of polished stainless steel and insulated from each other. If the geometry and size of the DMA and its operational parameters such as sheath flow and sample flow are known, one can calculate and adjust the voltage between the electrodes needed to let the fraction of charged particles with the target electrical mobility pass through the DMA. The electrical mobility is dependent upon the size of the particle and, thus it can provide a continuous aerosol size distribution changing continuously the voltage applied in the DMA. The selected particles exit the DMA and reach the CPC, where the number concentration is determined for

each specific particle size. Since particles below approximately 100 nm cannot be detected optically, small particles need magnification to a size which can be detected optically in the CPC. Thus, in a regular butanol-based conductive cooling CPC, the aerosol flow is slightly heated and then saturated with butanol vapour. Then, in a cooling section or condenser, the butanol vapour becomes supersaturated and condenses onto the particles, forming droplets of approximately 10 µm that are led through a focusing nozzle and then counted individually by a laser optic.

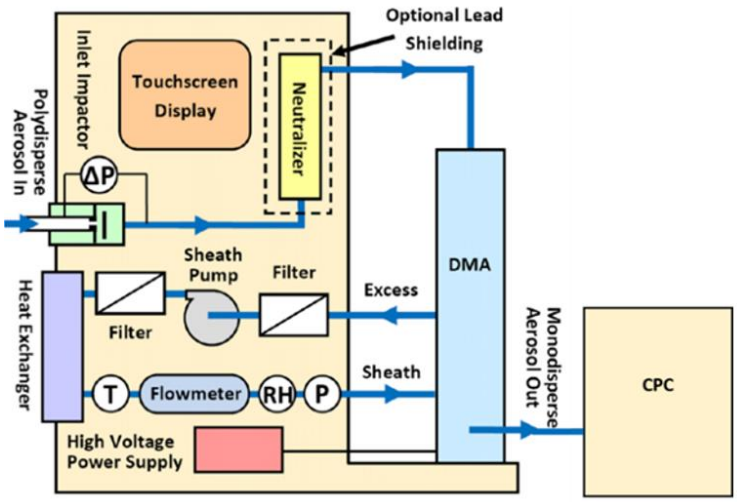

Figure 3.2 – Schematic representation of the TSI 3938 Scanning Mobility Particle Sizer. (Figure adapted from TSI manual, 2016)

The combination of different DMAs and CPCs allows the measurement of aerosol size distribution at different size ranges. There are different DMAs and CPCs that optimize the measurement of particles at different size ranges. For example, a long-DMA can detect particles in the size range of ~10 nm to 1000 nm and a nano-DMA can measure particles from 3 nm to 150 nm. In addition, particles detection in these size ranges also depends on the CPC design since not all CPCs are able to measure from 3 nm. In this sense, mainly the CPC temperature difference between saturator and condenser can be optimized to measure total particle concentration from a determined low cut particle size diameter.

In the frame of this thesis, two combination of DMAs and CPCs were used to measure the aerosol size distribution from 4 or 10 nm. In order to measure the size distribution in the 4-500 nm size range, two SMPS systems measuring simultaneously are necessary. The first one equipped with a nano-DMA (TSI model 3085) and a CPC model 3775 (TSI) to measure the aerosol size distribution in the 4-120 nm size range. The second one equipped with a long-DMA (TSI model 3081) and a CPC model 3772 (TSI) to measure the aerosol size distribution in the 10-500 nm size range.

SMPS data have been processed by AIM software (version 10.2.0, TSI, Inc). AIM software was also used to apply internal diffusion losses and multiple charges corrections. First, internal diffusion losses are produced by the particles Brownian movement. In this sense, each instrument section has an effective diffusion length depending on their geometry. Secondly, the DMA classify the particles by their electrical mobility that is a diameter dependent magnitude. However, same diameter particles have a probability to have -6, -5…+5, +6 electrical charges. This probability for each electrical charge and diameter was predicted theoretically by Fuchs (1963) and it was confirmed by Wiedensohler (1988). The correct application of the internal diffusion losses and multiple charges corrections applied by AIM software (version 10.2.0, TSI, Inc) have been validated by inter-comparisons workshops (TROPOS, Leipzig, Germany). The SMPS (including CPC) instruments used in this thesis participated in ACTRIS inter-comparisons workshops (TROPOS, Leipzig, Germany), which assures the high quality of the data used in this work. Furthermore, the quality of the SMPS measurements were checked routinely for flow rates, relative humidity (RH) and 203 nm Poly Styrene Latex particles (PSL) calibration. In addition to quality checks, SMPSs systems were intercompared before and after each campaign to ensure the comparability of the data at different stations. Following calibration procedures, uncertainty in the measured particle size distribution is within 10% and 20% for the size range 20–200 nm and 200–800 nm, respectively (Wiedensohler et al., 2018).

3.2.2 Multiwavelength absorption photometer

The multiwavelength absorption photometer provides real time absorption coefficient at several wavelengths. This photometer is based on collecting the particles sample on a filter and measuring the attenuation coefficient through the sample to derive the absorption coefficient (σ_{ap}) at several wavelengths (λ). The optical attenuation is derived from the Beer-Bouger-Lambert law (Eq. 2.1):

$$ATN(\lambda) = \ln(I_\lambda / I_{0\lambda}) = \ln(1/Tr_\lambda) \qquad \text{Eq. (3.1)}$$

where Tr_λ is the transmission for wavelength λ. The intensity (I_λ) through the filter decreases gradually as the filter get loaded with particles, compared to the intensity of the unloaded filter ($I_{0\lambda}$), increasing gradually the attenuation (ATN) and decreasing the transmission (Tr_λ). To obtain the attenuation coefficient, the change on the optical attenuation in a certain time fraction need to be scaled by the measurement spot area and the flow passing through the filter as follows:

$$\sigma_{ATN}(\lambda) = \frac{S \cdot \Delta ATN(\lambda)}{F \cdot \Delta t} \qquad \text{Eq. (3.2)}$$

where σ_{ATN} is the attenuation coefficient, *S* is the spot area and *F* is the flow passing through the filter. The attenuation coefficient does not take into account the interaction of the laser beam with the filter material or the scattering of the light due to light-aerosol interaction. Thus, those effects need to be considered to derive the aerosol absorption coefficient, typically derived as follow:

$$\sigma_{ap}(\lambda) = \frac{\sigma_{ATN}(\lambda) - f(\lambda) \cdot \sigma_{sp}(\lambda)}{C_0 \cdot R_\lambda(ATN)} \qquad \text{Eq. (3.3)}$$

where C_0 accounts for the multiple scattering of the light beam due to the filter material, that mainly depends on the filter used. This factor is usually considered wavelength independent, however, it has been recently reported a wavelength dependence by Yus-Díez et al. (2021) for certain aerosol types such as Saharan dust.

R accounts for the loading effect of the filter that varies with the amount of aerosol deposited on the filter, and therefore depending on the *ATN*. The loading with scattering aerosol leads to two different artifacts: the aerosol particles scatter light in all directions, leading firstly to an increase of backscattered light and consequently to an apparent greater reflectance of the filter, and secondly to an increased light optical path and consequently to a higher probability of encountering an embedded absorbing particle, inducing apparent absorption, which is considered by reducing a fraction (*f*) of σ_{sp}. This apparent absorption produced by particles scattering usually ranges from 0-10% of the scattering coefficient (Collaud Coen et al., 2010) and it is not possible to correct without any σ_{sp} measurements and usually are not considered since instrument and inlet losses should be accounted at both instruments. In this thesis, scattering coefficient correction is not applied to absorption coefficient and it is derived as following:

$$\sigma_{ap}(\lambda) = \frac{\sigma_{ATN}(\lambda)}{C_0 \cdot R_\lambda(ATN)} \qquad \text{Eq. (3.4)}$$

In the frame of this thesis, multiwavelength absorption photometers (also called aethalometers) model AE-33 manufactured by Magee Scientific (Figure 3.3; Drinovec et al., 2015) were used to measure the aerosol absorption coefficient at seven wavelengths (370, 470, 520, 590, 660, 880 and 950 nm). Two wavelength-independent C_0 provided by the manufacturer are used, 1.57 for the TFE-coated glass fiber tape M8020 (used until 2017) and 1.39 for the M8060 filter tape (used from 2017). Otherwise, R accounts for the loading effect of the filter that varies with the amount of aerosol deposited on the filter, and therefore depending on the *ATN*. The reduction of data at increasing loadings is well described by a linear function of attenuation ($R = 1 - k \cdot ATN$), but its magnitude cannot be predicted and mainly depends on the aerosol chemical composition. However, it is possible to eliminate the 'loading effect' of k by making two simultaneous identical

measurements σ_{ap1} and σ_{ap2} at different degrees of loading ATN_1 and ATN_2. It means two measurements at two different spots at different aerosol flow rates. The aethalometers used in this thesis, called "dual-spot" aethalometer (Drinovec et al., 2015), solves partially the effect of loading with the measurement of two attenuations in two spots with different aerosol loads.

Figure 3.3 – Multi-wavelength absorption photometer model AE-33 (Aerosol d.o.o.).

Finally, usually the target quantity is the black carbon mass concentration ($\mu g \cdot cm^{-3}$) which is usually called equivalent black carbon. This quantity is derived using σ_{ap} and the mass absorption cross section (*MAC*) by following the equation:

$$BC(\lambda) = \frac{\sigma_{ap}(\lambda)}{MAC(\lambda)} \qquad \text{Eq. (3.5)}$$

The *MAC* values provided by the manufacturer (Drinovec et al., 2015) were used in this thesis. It is also worth to mention that, if not stated otherwise, the BC used in the following sections is the BC calculated from the aerosol absorption coefficient at 880 nm wavelength and the *MAC* value of 7.77 $m^2 \cdot g^{-1}$.

3.2.3 Eddy covariance system and data processing

Aerosol flux measurements were made at a tower installed at UGR station that is located at 100 m from the IISTA-CEAMA building. Instruments for the measurement of turbulent aerosol fluxes were mounted on the top of the tower at a height of 50 m above ground level (Figure 3.4). The tower height is 2.5 times the

average height of the surrounding buildings (approximately 20 m) and hence eddy covariance setup should be in the inertial sublayer (depth usually defined between 2 to 5 times the mean building heigh). Therefore, the aerosol flux measurements presented in this thesis can be considered to be representative of the local scale (Grimmond and Oke, 1999). In order to minimize any possible disturbances from the tower itself and avoid flow distortion, the measurements were taken at 10 m above the upmost level of the tower (Figure 3.4). The measurement flux system consists of an ultrasonic anemometer (Model 81000, R.M.Young, USA) to measure the three wind components and sonic temperature, and an ultrafine condensation particle counter (UCPC, model 3776, TSI Incorporated, USA) for measurements of particle number concentrations in the diameter range 2.5 nm - 3μm. Sonic anemometer was mounted at 50 m height and the sampling inlet for UCPC was situated 25 cm below the sonic anemometer center. The air was sampled on the turbulent regime through a 10 m main stainless steel tube of 4 mm inner diameter and at a flow rate of 16 l/min. The side air flow to UCPC was drawn through a 1.0 m long tube (with 2 mm inner diameter) from the main tube at a flow rate of 1.5 l/min. Both anemometer and UCPC data were acquired at frequency of 10 Hz.

The 30-min particle number fluxes (F_N) were calculated from these raw data as the covariance of instantaneous fluctuations of the vertical wind component and particle number concentrations following Aubinet et al. (1999) guidelines. Data was processed with EddyPro 6.2.0 software (Li-Cor, Inc., USA). Before the calculation of particle number fluxes, vertical wind component and particle number concentrations raw data were, firstly, de-spiked following Vickers and Mahrt (1997) method to remove large spikes in vertical wind speed or aerosol concentration and, secondly, linearly de-trended to eliminate the presence of a possible trend in the 30-min time series. In addition, a two-dimensional coordinate rotation was applied to eliminate errors due to sensor tilt relative to the ground. Then, time lag between the

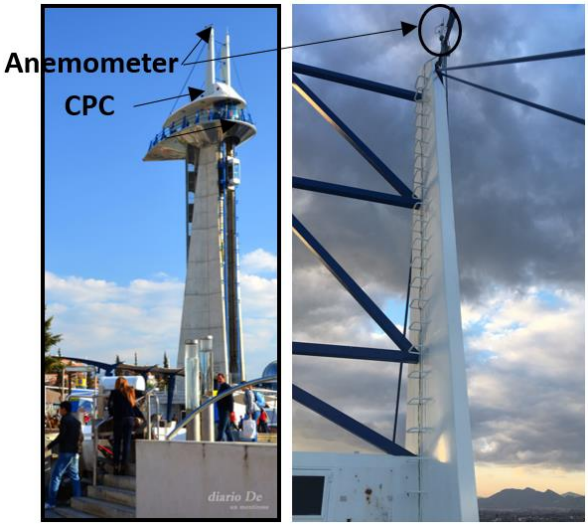

Figure 3.4 – Measurement tower and location of the instrumentation.

concentration and wind measurements induced by the sampling lines was corrected by maximizing the covariance. Finally, low frequency attenuation was corrected following Moncrieff et al. (2004) method and high frequency attenuation was corrected with Horst (1997) method using UCPC time constant of τ=0.8 provided by the manufacturer. This resulted in an average (± standard deviation) frequency attenuation corrections of aerosol flux of 7 ± 5 %. In order to ensure the quality of flux data, a stationarity test proposed by Mauder and Foken (2004) was applied. In this test the 30-min mean flux values should not deviate more than 60% from the average of fluxes from six sub periods of 5-min from the same 30-min period. Removing aerosol flux data by non-stationary test and bad data we obtained 16 393 high quality data, which represent 62% of the 26 380 original raw data. It is important to note that this data coverage is relatively high compared to other studies. Seasonal data coverage was also relatively high with data coverage higher than 60% in each season. Data coverage during day and night time was also high representing 50% and 85% of the original data, respectively. For the following analysis, only these quality assured data are used.

3.2.4 Additional experimental data

To obtain information on planetary boundary layer dynamic, vertical wind speed profiles measured by Doppler lidar system Stream Line at UGR site has been used. This instrument is operating in continuous and automatic mode since May 2016 at UGR. The mixing layer height in stable and unstable cases is estimated from the 1-hour variance of the vertical wind speed profile using variance threshold method (e.g., de Arruda Moreira et al., 2018) with variance threshold value of 0.16 m^2/s^2. This threshold value was confirmed with Doppler lidar measurements and mathematical modeling by Large Eddy Simulations (Lenschow et al., 2012). More detailed information about the retrieval method of mixing layer height using vertical wind speed profiles is given by de Arruda Moreira et al. (2018).

During SLOPE II campaign, additional instrumentation was deployed at SNS and UGR sites. In this sense, UV-B (280-320 nm) data were obtained by UVB-1 (Yankee Environmental Sytems) pyranometers, wind speed and direction were measured with RM-Young 05102 anemometers and temperature and humidity with Rotronic HygroClip 2 (HC2) probes. Particle number size distribution in the aerodynamic diameter range of 0.5–20 μm was measured with an Aerodynamic Particle Sizer (APS; TSI model 3321). Aerosol 24-h PM_{10} samples were collected on quartz fiber filters by means of high-volume sampler with a flow rate of 30 $m^3\ h^{-1}$. The filters were conditioned and treated pre- and post-sampling and major elements (Al, Ca, K, Mg, Fe, Ti, Mn, P, Na) were determined by inductively coupled plasma mass spectrometry (ICP-MS) at Institute of Environmental Assessment and Water Research (IDAEA-CSIC, Barcelona, Spain) following the procedure of Querol et al. (2001). Detection limit and accuracy were estimated in 0.02 ng m^{-3} and 3% (Pandolfi et al., 2011). The concentrations of TiO_2 and Fe_2O_3 were indirectly determined on the basis of empirical factors (TiO_2 = Ti·0.6 and Fe_2O_3 = Fe·0.7).

In addition, during SLOPE II campaign, at SNS station, concentrations of trace gases (CO, NO, NO_2, NO_x, SO_2 and O_3) were monitored, following the European AQ directives requirements, by a mobile cabin of the University of Évora. Pollutant gases (CO, NO, NO_2, NO_x, SO_2 and O_3) data from Ciudad Deportiva air quality station has been also used. This station is an urban background station located at ~3 km from UGR station. These data are provided by the Junta de Andalucía (http://www.juntadeandalucia.es/medioambiente), following the requirements of the European AQ directives. Finally, ambient air samples were collected at both sites (SNS and UGR) on TENAX, C18 and DNPH cartridges with a maximum 12-h time resolution by low-volume pumps. Volatile organic compounds retained on solid-phase filters are then chemically analyzed using gas chromatography or liquid chromatography coupled to mass spectroscopy techniques (Borrás, 2013).

Finally, during the AMICUS winter campaign an Aerosol Chemical Speciation Monitor (ACSM, Aerodyne Research Inc.) was deployed by IDAEA-CSIC (Institute of Environmental Assessment and Water Research) to measure non-refractory submicron aerosol species (organic aerosols (OA), nitrate, sulfate, ammonium and chloride) in real time (Ng et al., 2011) at UGR urban station. The instrument was operated with a time resolution of approximately 20 min. Source apportionment of organic aerosol was done in order to estimate biomass burning and hydro-carbon like OA contributions. Further details on the ACSM operation principle and OA source apportionment method can be found in Minguillón et al., (2015).

4 /Aerosol number fluxes and concentrations in Granada urban area

This chapter is adapted from "***Aerosol number fluxes and concentrations over a southern European urban area***" by J. A. Casquero-Vera, H. Lyamani, G. Titos, G. de A. Moreira, J. A. Benavent-Oltra, M. Conte, D. Contini, L. Järvi, F. J. Olmo-Reyes and L. Alados-Arboledas. Under review in Atmospheric Environment.

In this chapter, the total aerosol number concentrations and fluxes collected at the top of a tower at a height of 50 m a.g.l. in the Granada urban area during the period Nov/2016 – Apr/2018 is analyzed in detail. The main goal of this study is to identify the sources contributing to the total aerosol number concentrations and their location in the study area. To this end, the eddy covariance technique was used to examine the diurnal, weekly, seasonal, and spatial variability of total aerosol number flux and concentration. The data obtained with the eddy covariance system described in Section 3.2.3 are used in this section.

4.1 /Footprint analysis

As described in Section 3.1, the measurement site is surrounded by several surface types, including residential, commercial and road areas in the wind direction between 0º N and 225º S (urban sector), and agricultural and suburbs areas as well as the principal highway of the city in the wind direction between 225º S and 360º N (suburban sector) (Figure 4.1). The surrounding area of the tower is flat within a

radius of about 6 km and the surrounding buildings are quite uniform with mean height of 20 m. Thus, for the calculation of the flux footprint (i.e., source area of the measured flux) we used the footprint model proposed by (Kljun et al., 2004) assuming displacement height and roughness length of 13 m and 2 m, respectively, for wind direction between 0º N and 225º S and of 3.33 m and 0.5 m, respectively, for wind direction between 225º S and 360º N (Grimmond and Oke, 1999). In this sense, the flux footprint (source area) accounting for 90% of the measured aerosol flux extends from approximately 650 m to 1500 m around the tower, covering the different land cover types in the area of study (Figure 4.1). It is important to note that the contours showed in Figure 4.1 represent the average relative contributions of different land areas over the entire measurement period and that the measured individual 30-min aerosol fluxes may originate from areas outside these contours.

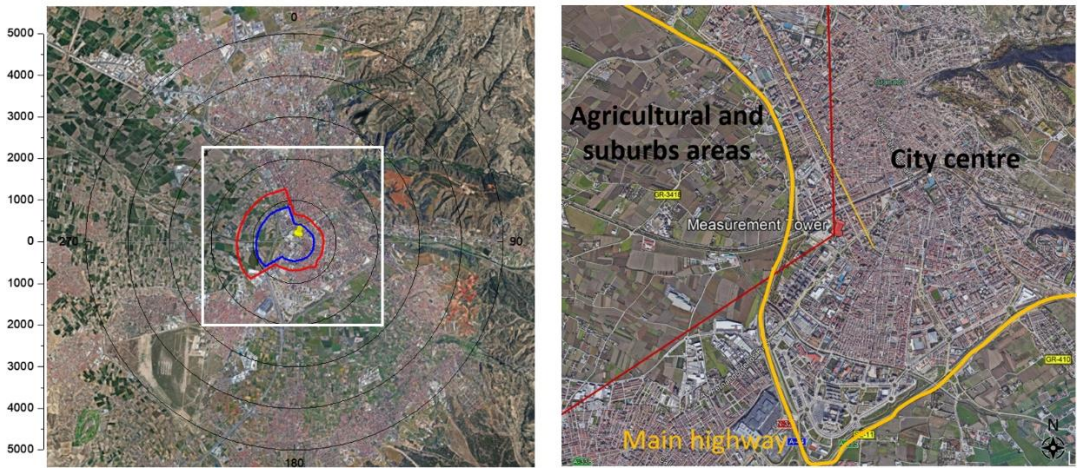

Figure 4.1 – (Left) Location of the tower in Granada area; contours show the average flux footprint (source area) accounting for 90% (red) and 70% (blue) of the measured aerosol flux for the entire measurement period. (Right) Zoom on the white square area that shows the measurement tower location and its surroundings separated in two sectors: urban (0-225º) and suburban (225-360º) sectors. The main highway surrounding the urban area and one of the main city streets are marked with yellow lines.

4.2 /Seasonal variation of aerosol number concentrations and fluxes

Statistical summary of aerosol number concentrations and fluxes measured at Granada urban site for each season and whole period between November 2016 and April 2018 is displayed in Table 4.1. Winter corresponds to the months from December to February, spring from March to May, summer from June to August and autumn from September to November. Both aerosol number concentration and flux were highly variable due to the large temporal variability in (1) emissions strength and sources, (2) meteorological conditions and (3) atmospheric boundary layer dynamics. For the analyzed period, the median aerosol number concentration was 7800 cm^{-3}, and the 1^{st} and 3^{rd} quartiles were 5000 cm^{-3} and 12 200 cm^{-3}, respectively. The median value of aerosol number flux during the whole period was 150×10^6 m^{-2} s^{-1}, and the 1^{st} and 3^{rd} quartiles were 40×10^6 m^{-2} s^{-1} and 300×10^6 m^{-2} s^{-1}, respectively. Thus, as expected, Granada area acted as a net source of particles to the atmosphere during the analyzed period. Downward negative fluxes were observed in only 12% of the analyzed data, showing that the study area behaved as a net sink of particles only occasionally.

These occasional downward fluxes were observed throughout the analyzed period and most of them were recorded during night-time and early morning. This is consistent with the results of Mårtensson et al. (2006) and Harrison et al. (2012). These studies reported that positive upward aerosol fluxes at Stockholm (Sweden) and London (UK) were the most frequent and that the observed occasional downward fluxes were very small in magnitude and only occur during low aerosol loading conditions. These authors attributed the urban negative fluxes to the stochastic nature of turbulence and uncertainty of the eddy covariance measurements. However, in this case, most of negative fluxes were relatively high

Table 4.1 - Statistical summary of 30-min aerosol number concentrations and fluxes measured at Granada from November 2016 to April 2018. SD is the standard deviation.

	Winter	Spring	Summer	Autumn	All period
Concentrations (10^3 cm^{-3})					
Mean±SD	12.0 ± 8.0	8.3 ± 5.3	7.5 ± 4.0	9.9 ± 6.5	9.6 ± 6.6
Median	9.6	6.9	6.5	8.1	7.8
1^{st} - 3^{rd} quartiles	6.0-15.5	4.5-10.8	4.5-9.5	5.2-12.7	5.0-12.2
Number of data	5216	4775	2964	3437	16393
(data coverage)	(60%)	(63%)	(67%)	(60%)	(62%)
Fluxes (10^6 m^{-2} s^{-1})					
Mean±SD	230 ± 300	210 ± 240	140 ± 160	160 ± 210	190 ± 240
Median	170	180	115	120	150
1^{st} – 3^{rd} quartiles	45-360	60-325	30-225	20-250	40-300
Number of data	5216	4775	2964	3437	16393
(data coverage)	(60%)	(63%)	(67%)	(60%)	(62%)

in magnitude (median value of -53×10^6 m^{-2} s^{-1}, with the 1^{st} and 3^{rd} quartiles of -130×10^6 m^{-2} s^{-1} and -20×10^6 m^{-2} s^{-1}, respectively) and were observed during high aerosol loading conditions (median aerosol number concentration was 9236 cm^{-3}, and the 1^{st} and 3^{rd} quartiles were 6000 cm^{-3} and 14300 cm^{-3}, respectively). Thus, these results indicate that the downward aerosol fluxes observed over Granada were not caused by stochastic effects in the data. Downward particle fluxes can be attributed to updrafts of relatively particle depleted air from surface or to downdrafts of relatively particle enriched air from aloft (entrainment). Thus, the downward fluxes observed here during high aerosol loading were probably the result of downdrafts of particle enriched air from aloft. The lack of additional information on aerosol characteristics during these events such as vertical aerosol distribution from ground surface to top of boundary layer and chemical aerosol composition as well as aerosol size distribution make difficult the accurate identification of the sources

of these downward fluxes. Thus, no attempt is made here to investigate the origin of these downward fluxes, however, a detailed analysis of the different sources of all these large number of negative flux cases will be done in future.

Until date the reported long-term aerosol flux data for urban sites are scarce (Donateo et al., 2019; Järvi et al., 2009; Kurppa et al., 2015; Ripamonti et al., 2013; Vogt et al., 2011). In general, the direct comparison of the results obtained in Granada with those reported for other urban areas is difficult and large differences in the aerosol number concentrations and fluxes between these urban sites may result from differences in the measured size ranges, measurement heights, instrumentation and sampling periods. Nevertheless, aerosol number fluxes measured at Granada were of the same order of magnitude as in other urban or suburban areas in Europe (e.g., Conte et al., 2018; Contini et al., 2012; Dorsey et al., 2002; Järvi et al., 2009; Mårtensson et al., 2006; Martin et al., 2009; Schmidt and Klemm, 2008). Particularly, the mean aerosol number flux obtained in Granada is similar to that reported (mean value of 180×10^6 m^{-2} s^{-1} during July 2011-June 2013) for two urban sites in Helsinki (Finland) using similar instrumentation and experimental design as used here (Kurppa et al., 2015). On the other hand, the average aerosol concentration measured at Granada was in the range of those obtained at ground level (8000-16000 cm^{-3}) in other European and Spanish urban sites (e.g., Aalto et al., 2005; Hofman et al., 2016; Morawska et al., 2008; Reche et al., 2011).

4.3 /Monthly variation of particle number concentrations and fluxes

Figure 4.2 shows the monthly variation of aerosol fluxes and concentrations measured above Granada urban site from November 2016 to April 2018. The average monthly aerosol flux is always positive regardless of the month, indicating

that the studied urban area is a particle source at a monthly scale. As can be seen, both, aerosol flux and concentration, showed large seasonal variation presenting their maxima in winter (December-February) and minima in summer (June-August). The median aerosol flux value in winter (170 × 10^6 m^{-2} s^{-1}) was 50% larger than that measured in summer (115 × 10^6 m^{-2} s^{-1}). Meanwhile, the median aerosol number concentration also increased by 50% from 6500 cm^{-3} in summer to 9600 cm^{-3} in winter. Similar seasonal variations in aerosol number fluxes and concentrations have been observed in other urban areas, with highest values in winter and lowest ones in summer (e.g., Donateo et al., 2019; Järvi et al., 2009; Ripamonti et al., 2013). These seasonal variations are driven by a combination of changes in emission rates and seasonal meteorology as well as planetary boundary layer structure and dynamic.

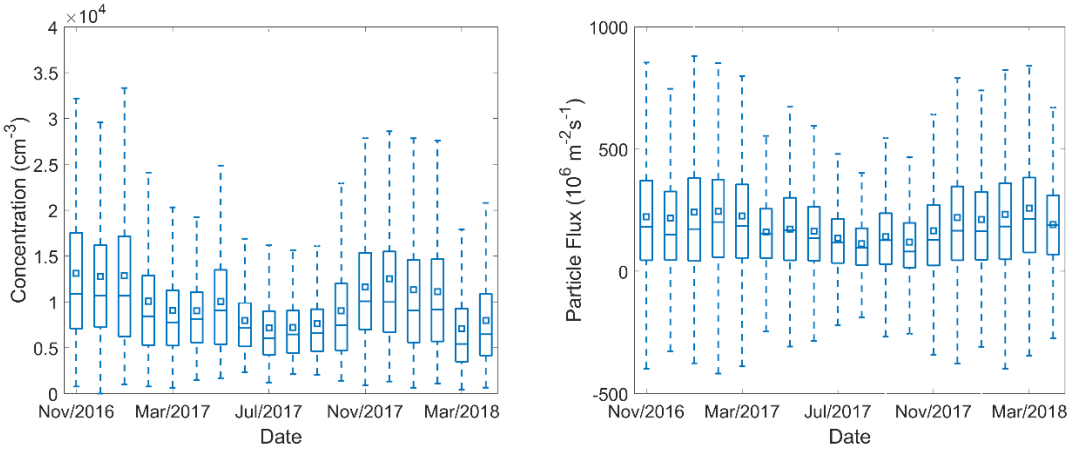

Figure 4.2 - Monthly aerosol concentration (left) and aerosol flux (right) observed over Granada from November 2016 to April 2018. The center rectangle and line show the mean and median, respectively, where the box around represents one standard deviation and whiskers the 25% and 75% percentiles.

The high aerosol number fluxes and concentrations observed in winter are mainly attributed to the increased emissions from domestic heating and burning of residual agricultural waste in the agricultural area surrounding the site (Lyamani et al., 2010; Titos et al., 2017). The summertime mixing layer in Granada reached significantly higher altitudes (1900 ± 500 m) than in winter (1100 ± 400 m) and the

summer wind speed values (3.0 ± 1.8 m s^{-1}) were also significantly higher than those registered in winter (2.0 ± 1.6 m s^{-1}), Table 4.2. Thus, the reduced mixing volume and low wind speed in winter, which favors lower vertical and horizontal dilution of the actual aerosol emissions in the atmospheric column, may also contribute to the increase in aerosol concentration in winter months. Furthermore, particles emissions associated with motor vehicles increase with decreasing ambient air temperature because low temperature promote and enhance the nucleation and condensation processes of condensable gaseous compounds emitted in vehicle exhaust (e.g., Ripamonti et al., 2013). Thus, the increased number of particles due to the enhanced new particle formation in vehicle exhaust by winter cold temperatures (Table 4.2) may also contribute to the high levels of aerosol number fluxes and concentrations observed in Granada in winter months.

Table 4.2 - Statistical summary of meteorological variables and mixing layer height registered at Granada during the analyzed period. SD is the standard deviation.

	Winter	**Spring**	**Summer**	**Autumn**
Maximum mixing layer height (m)				
Mean ± SD	1100 ± 400	1800 ± 600	1900 ± 500	1500 ± 600
Median	1100	1700	1800	1500
Minima / Maxima	500 / 2200	700 /3500	1150 /3600	680 / 2700
Wind speed (m s^{-1})				
Mean ± SD	2.0±1.6	3.0±2.0	3.0±1.8	2.2±1.5
Median	1.8	2.4	2.6	1.9
Minina / Maxima	0.03 / 10.00	0.10 / 14	0.10 / 10	0.06 / 9
Temperature (º C)				
Mean ± SD	10±4	15±6	29±5	19±7
Median	10	14	28	19
Minima / Maxima	-2 / 20	3 / 33	16 /41	4 / 34

It is worth to note that, although aerosol number fluxes and concentrations show almost similar seasonal variation, both metrics show some differences in their behaviours. The median aerosol concentration value in autumn (8100 cm^{-3}) was 15% larger than that observed in spring (6900 cm^{-3}), Table 4.1. However, the median aerosol flux value in autumn (120 × 10^6 m^{-2} s^{-1}) was 33% lower than that observed in spring (180 × 10^6 m^{-2} s^{-1}), which may indicate that surface emissions are not the main cause of the high aerosol concentration in autumn as compared with spring. Aerosol fluxes are mainly controlled by surface emissions and turbulence strength whereas atmospheric aerosol concentrations do not only depend on the actual surface emissions, but also on atmospheric boundary layer dynamics and meteorological conditions. The boundary layer mixing height in autumn (1500 ± 600 m a.g.l.) was lower than in spring (1800 ± 600 m a.g.l.), indicating a smaller volume for aerosol vertical dilution in autumn in comparison to spring. Also, wind speeds in autumn (2.2 ± 1.5 m s^{-1}) were lower than in spring (3.0 ± 2.0 m s^{-1}). Thus, since there was a decrease in aerosol fluxes from spring to autumn, the less vertical and horizontal aerosol dilution effects in autumn as compared to spring can at least partially explain the higher aerosol concentrations observed in autumn.

4.4 /Aerosol number concentrations and fluxes dependence on wind sector

Atmospheric aerosol number concentrations are largely dependent on emission source/sink spatial distributions and their strengths, synoptic and mesoscale meteorology, boundary layer dynamics and chemical processes, while aerosol number fluxes are mainly driven by local emissions and turbulence strength. On an inhomogeneous surface with different land uses and cover types, both aerosol number concentration and flux measurements depend strongly on wind direction due to the non-uniform spatial distribution of surface aerosol sources and sinks. In this

sense, studies conducted in different urban areas (e.g., Donateo et al., 2019; Järvi et al., 2009; Martin et al., 2009; Ripamonti et al., 2013) revealed that aerosol number concentration and flux measurements are largely controlled by the surface sources/sinks within the footprint area (i.e., the source surface area affecting the site measurements). However, some of these studies also revealed that aerosol flux can have a different footprint source area than the corresponding number concentration, being the concentration footprints generally larger than the flux footprints (e.g., Rannik et al., 2012). Therefore, both metrics can be influenced by different aerosol sources and hence can have different behaviour because distant aerosol sources located outside the flux footprint can affect aerosol concentration measurements but not flux levels. Thus, the combined analysis of both aerosol number concentrations and fluxes by wind sector will help us to identify the potential sources and sinks of aerosols affecting our site, providing insight on the contributions of local and/or distant sources/sinks to both metrics. In order to assess the spatial patterns of emissions and identify the potential sources of aerosols in the study area, we analyzed the dependence of both aerosol number concentrations and fluxes on wind direction. Figure 4.3 shows aerosol number concentrations and fluxes as a function of wind direction in bins of 45º for the period between November 2016 and April 2018. The corresponding frequency of occurrence of wind direction in each 45º wind sector is included in Figure 4.3.

The predominant wind direction (30% of the cases) was the west-northwest direction (270º-315º), while the less frequent (5%) corresponds to the wind sectors 0º-45º (north-northeast) and 135º-180º (south-southeast). In the rest of the wind sectors the frequency was almost similar with values in the range 10-14% (Figure 4.3). Therefore, statistically robust information on aerosol sources from 0-45º and 135-180º sectors (direction from urban area; Figure 4.1) cannot be derived and the results from these two wind directions will be treated with caution. As can be seen in Figure 4.3, the mean and median values of aerosol fluxes are positive in all wind

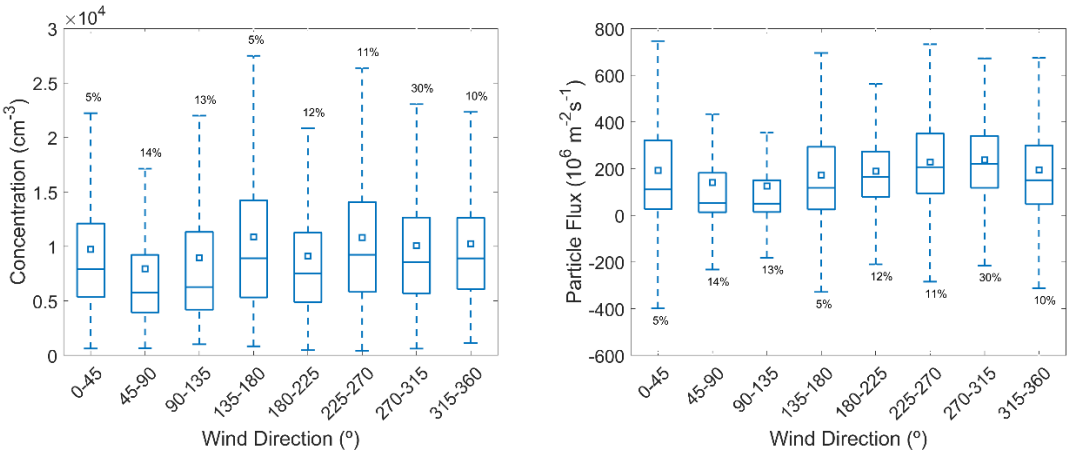

Figure 4.3 - Aerosol number concentrations (left) and fluxes (right) according to 45º wind sectors for the period between November 2016 and April 2018. The corresponding wind frequencies of occurrence in each 45º wind sector are inserted in the figures.

directions, indicating that aerosol emission dominated over the deposition and on average all land type sectors affecting the measurement site acted as sources. Negative fluxes were occasionally observed in all wind sectors, indicating that there was no specific sink area of aerosols around the measurement site. Unexpectedly, aerosol flux values were highest with median value of 220 × 10^6 m^{-2} s^{-1} from the SW-W-NW directions (225-315º), where the suburban area is located (including agricultural area and the principal highway), and lowest with mean value of 51 × 10^6 m^{-2} s^{-1} from NE-E-SE (45-135º) sectors which include densely built up residential and commercial areas (Figure 4.3). It is important to note that the suburban sector is crossed from south to north by the main highway that surrounds the city. Furthermore, not only the median value of the aerosol fluxes in the SW-W-NW sector was higher than that obtained in the NE-E-SE sector, but also the mean, third and first quartile values were higher in this sector than in the NE-E-SE sector (Figure 4.3). Furthermore, the Mann-Whitney test with a significance level of 0.01 confirms that the aerosol fluxes and concentrations from SW-W-NW sector were also statistically significantly higher than those from NE-E-SE sector. Thus, the results suggest the presence of strong local emission sources in SW-W-NW wind sectors as compared to the urban sector in NE-E-SE wind directions.

In depth analysis of data showed that wind from suburban sector (225º-360º) occurred more frequently (more than 70%) during daytime, when local anthropogenic emissions are activated. In contrast, the majority of wind (more than 70%) from the urban sector (0º to 225º) occurred during night-time, when local anthropogenic activities are reduced, which may explain the low aerosol number concentrations and fluxes recorded for this urban sector in comparison to those observed from the suburban sector. Therefore, to avoid misleading interpretation of the results and obtain reliable information about the emission/sink sources in our area, we repeated the same analysis but separating the data for day and night. In addition, as mentioned in Section 4.1, for a robust statistical analysis of the data, we regrouped the data in two groups: urban (corresponding to 0-225º wind sector) and suburban (corresponding to 225-360º wind sector) sectors (Figure 4.1). The data were separated into these two sectors due to their completely different land-use while aerosol sources distribution and land use types within each sector are very similar. Urban sector (0-225º) contains the city center, densely built up residential and commercial areas and traffic roads, including one of the city streets with more dense traffic that is located just at 500 m from the measurement site. In contrast, suburban sector (225-360º) contains extensive agricultural areas, poorly built up area and the main highway of the city that crosses this sector from south to north at a distance of at least 500 m from the measurement site.

The results of this analysis are given in Table 4.3. The results show again that both aerosol number concentrations and fluxes from suburban sector were statistically significantly higher than those from urban sector (as confirmed by Mann-Whitney test at 0.01 significance level) during both day and night-time, evidencing again the presence of strong local emission sources in suburban sector. This result points to the intense traffic on the highway that crosses the suburban sector from south to north as a potential source of local emissions that affect our

Table 4.3 - Statistical summary of aerosol concentration and fluxes measured at Granada from November 2016 to April 2018 for urban and suburban sectors separated into day and night time periods. SD is the standard deviation.

	Mean ± SD	Median (1^{st} - 3^{rd} quartiles)	Number of data
Concentration (10^3 cm^{-3})			
Urban sector - Day time	9.1 ± 6.7	7.1 (4.8 - 10.9)	2392
Suburban sector - Day time	10.5 ± 6.6	8.9 (5.8 - 13.3)	5883
Urban sector - Night time	8.9 ± 6.9	6.7 (4.2 - 11.2)	5518
Suburban sector - Night time	9.8 ± 5.8	8.5 (5.7 - 12.2)	2600
Flux (10^6 m^{-2} s^{-1})			
Urban sector - Day time	250±240	210 (110-350)	2392
Suburban sector - Day time	270±210	240 (140-370)	5883
Urban sector - Night time	120±250	50 (10-150)	5518
Suburban sector - Night time	140±240	110 (30-230)	2600

study area. However, the highest aerosol concentrations and fluxes in the suburban sector may also be attributed to emissions from agricultural waste burning activities and biomass burning for domestic heating in this sector, especially in cold season. Previous studies performed in our study area revealed that, during winter, the burning of agricultural residues represent an important additional local source of aerosol particles in Granada urban area (e.g., Patrón et al., 2017; Titos et al., 2017). In this sense, Titos et al. (2017) reported that agricultural waste burning activities in the suburban and rural areas surrounding the city of Granada are as important as vehicle exhaust emissions, contributing around 40% to the carbonaceous particle concentrations observed in Granada urban area during winter season. So, in order to assess and distinguish the possible effects of traffic emissions from the highway and agricultural waste burning emissions from suburban sector on aerosol concentrations and fluxes at our urban site, data were further divided into winter

(when open waste burning is allowed) and summer (when this practice is forbidden) periods. The results are shown in Figure 4.4 and Table 4.4.

In summer season, aerosol number concentrations from suburban sector were significantly larger than those from urban sector, especially during night-time periods (Figure 4.4 and Table 4.4). The mean aerosol number concentrations from suburban sector at day and night periods were 30% and 50%, respectively, higher than those observed from urban sector. The higher aerosol number concentrations observed in suburban sector in comparison with urban sector were associated with significantly high aerosol fluxes in this sector at both day and night-time (Figure 4.4), indicating high local aerosol emissions from suburban sector in summer. The day-time mean aerosol flux from suburban sector was 45% higher than that from urban sector whereas at night-time it was more than twice that from urban sector.

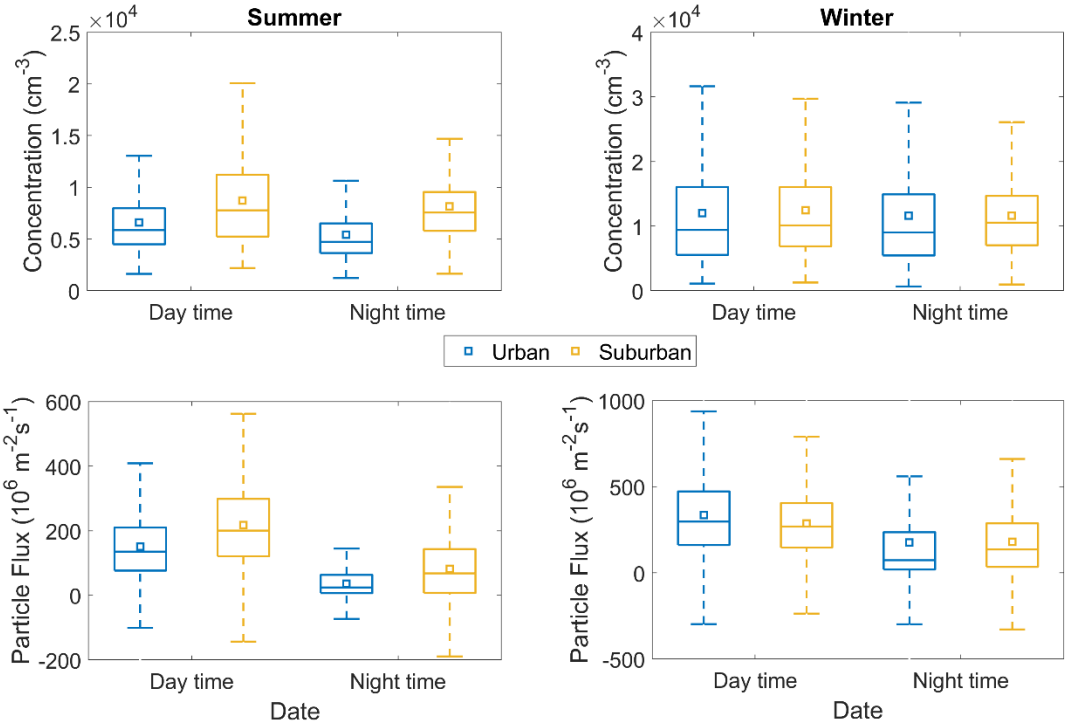

Figure 4.4 - Particle number concentrations (top) and fluxes (down) in urban (blue) and suburban (yellow) sectors for day-time and night-time for summer (left) and winter (right) seasons.

In winter season, however, no statistically significant differences were observed between aerosol number concentrations from suburban and urban sectors during both day and night-time (Figure 4.4). In the same way, the differences between aerosol fluxes from suburban and urban sectors were small especially in night-time, and were significantly lower than the differences between these sectors in summer season, indicating almost similar contributions of aerosol emissions from both sectors to the aerosol population over the study area in winter season. This finding confirms that traffic emission from the highway crossing the suburban sector is an important source of aerosol in summer at our urban area study.

Table 4.4 - Statistical summary of aerosol number concentration and fluxes measured at Granada from November 2016 to April 2018 in urban and suburban sectors for winter and summer and separated into day and night-time periods.

	Winter				**Summer**			
	Urban sector		**Suburban sector**		**Urban sector**		**Suburban sector**	
	Day	Night	Day	Night	Day	Night	Day	Night
Concentration (cm^{-3})								
Mean	12.0	11.5	12.5	11.6	6.6	5.4	8.7	8.2
SD	9.0	8.6	7.7	6.5	3.4	2.7	4.5	3.6
Median	9.4	9.0	10.1	10.5	5.9	4.7	7.8	7.6
1st quartile	5.5	5.4	6.8	7.0	4.4	3.6	5.2	5.7
3rd quartile	16.0	14.9	16.0	14.7	7.8	6.5	11.2	9.5
Flux (10^6 m^{-2} s^{-1})								
Mean	340	175	290	180	150	35	220	80
SD	300	300	200	260	130	100	170	160
Median	300	75	270	135	135	25	200	70
1st quartile	160	20	140	30	75	5	120	7
3rd quartile	480	240	400	300	210	65	300	145
Number of data	651	2182	1595	788	517	686	1288	474

Another important observation is that the winter aerosol number concentrations and fluxes from suburban sector as well as from urban area were significantly higher, both at day and night-time, than those observed in these sectors in summer season, reflecting a pronounced increase in local aerosol emissions from both sectors in winter. As we mentioned before, in addition to traffic emissions, other sources of aerosols, such as domestic heating in the urban area and the agricultural waste burning activities in the suburban area, are activated in winter season in the Granada area. Thus, the results point to domestic heating as the main source emission that has caused the increase observed in winter aerosol concentrations and fluxes from urban sector and to agricultural waste burning activities as the potential sources responsible for this increase in suburban sector.

Furthermore, it is important to note that the increase in aerosol number concentrations and emissions from summer to winter were more pronounced in the urban sector than in the suburban sector, especially during night when agricultural burning waste activities are not active and domestic heating still operating. In urban sector, the day time aerosol fluxes increased by a factor of 2.2 from median value of 135×10^6 m^{-2} s^{-1} in summer to 300×10^6 m^{-2} s^{-1} in winter, whereas the night time aerosol fluxes increased by a factor of 3 from mean value of 25×10^6 m^{-2} s^{-1} in summer to 75×10^6 m^{-2} s^{-1} in winter. For suburban sector, the day time aerosol fluxes increased by a factor of 1.4 from median value of 200×10^6 m^{-2} s^{-1} in summer to 270×10^6 m^{-2} s^{-1} in winter, while the night time aerosol fluxes increased by a factor of 1.9 from median value of 70×10^6 m^{-2} s^{-1} in summer to 135×10^6 m^{-2} s^{-1} in winter. This finding demonstrates that, in addition to traffic activities, domestic heating and agricultural waste burning are two important emission sources that affect aerosol population and the air quality of the Granada urban area in winter. Furthermore, the results show that the impact of domestic heating emissions from the urban area, especially at night, is much stronger than the impact of agricultural waste burning emissions from the suburban sector. This information is crucial for the

implementation of effective mitigation measures to improve air quality in the area of Granada. The findings reveal the usefulness of eddy covariance technique for the determination and quantification of aerosol sources in the urban area as well as for providing insight on the processes affecting urban air quality.

In 2014, the local authorities in Granada implemented a series of control measures with the aim of reducing air pollution, especially with respect to aerosol particles and NO_2. Most of these control measures focused on traffic emissions in the city center but no measures were taken to reduce traffic emissions on the city's main highway. In fact, emission abatement measures led to a decrease in particles and black carbon concentrations in this restricted traffic area, but were not effective outside this area (Titos et al., 2015). Therefore, to improve air quality in Granada, emission reduction measures focusing on traffic emissions on the city's main highway, which is the main source of aerosols, should be implemented. In addition, stringent control measures on emissions from agricultural waste burning activities, and especially on domestic heating emissions, should be implemented to improve air quality and protect human health, particularly in the winter season.

4.5 /Diurnal and weekly variations in aerosol number concentrations and fluxes

Weekly variations of aerosol concentrations and fluxes can only be explained by local anthropogenic activities, especially traffic, which shows a considerable decrease on the weekend in comparison with working days. Thus, to investigate the role of local emission sources and their influences on aerosol population over our study area, the weekend data were compared to working days. For this, the data were grouped on working days from Monday to Friday and other groups representing

Saturdays and Sundays, respectively. For this analysis we only used data collected in daytime hours when traffic activity is high. Figure 4.5 shows the seasonal weekly variations of aerosol concentrations and fluxes averaged over all day-time data available from November 2016 to April 2018.

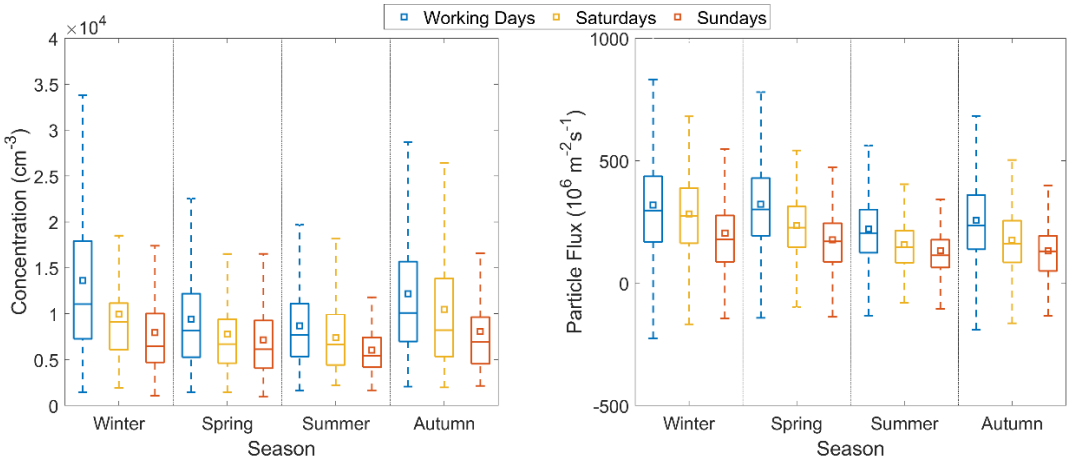

Figure 4.5 - Seasonal weekly variations of particle number concentrations (left) and fluxes (right) averaged over all day-time data available from November 2016 to April 2018.

In all season, the average aerosol fluxes were upward on weekend and working days, indicating that particles emissions dominate on weekly scale. As expected, the highest weekly aerosol fluxes were observed in winter (median value of 300 × 10^6 m^{-2} s^{-1} during working days and 180 × 10^6 m^{-2} s^{-1} on Sundays) due to the activation of additional sources such as domestic heating. The lowest weekly aerosol fluxes were observed in summer (with average value of 205 × 10^6 m^{-2} s^{-1} during working days and 110 × 10^6 m^{-2} s^{-1} during Sundays), indicating weaker emissions in this season in comparison with other seasons. It is worth noting that weekly aerosol fluxes in spring were also significantly high with median aerosol flux during working days similar to that observed in winter (300 × 10^6 m^{-2} s^{-1}) and a median value of 165 × 10^6 m^{-2} s^{-1} on Sundays, indicating higher emissions in this season. The increase in aerosol emissions in spring cannot be explained as in the case of winter by the activation of additional anthropogenic sources, but it seems

that this increase was most likely due to an increase in production rates of aerosols partly due to the increased frequency of occurrence of regional new particle formation events in this season (Casquero-Vera et al., 2021). These authors showed that the frequency of occurrence of NPF events in Granada during 2018 showed large seasonal variability with high NPF event frequency (>50%) in spring.

As a common feature, aerosol concentrations and fluxes in all seasons showed pronounced reduction during weekends, especially on Sundays, evidencing that in each season weekly cycles were primarily driven by traffic emissions. This finding demonstrates that traffic was an important source of aerosol in each season in this urban area. Furthermore, the results show that the weekend aerosol flux reduction in winter (35%) was lower than that observed in other season (>40%). In addition to traffic activities, domestic heating is an active source of aerosol emission in Granada during the winter, but this emission source is not expected to show a significant change during the week, which may explain the lower reduction in aerosol fluxes on the weekend in winter compared to other seasons. This finding reveals the importance of domestic heating emissions in winter in this urban area.

It is important to note that the median aerosol fluxes on working days were similar and highest on winter and spring seasons (300×10^6 m^{-2} s^{-1}) and that the highest weekend aerosol flux decrease of 45% was observed in spring while the lowest reduction of 40% was observed in winter. In contrast, the highest weekend reduction in aerosol concentration was observed in winter season which decreased by 42% from 13 600 cm^{-3} on working days to 7900 cm^{-3} on Sundays, while the lowest weekend reduction was observed in spring season with a reduction of 24% from 9400 cm^{-3} on working days to 7200 cm^{-3} on Sundays. The increase of the mixing layer height from winter (1100 ± 400 m) to spring (1800 ± 600 m) will result

in more aerosol vertical dilution effect in spring (Table 4.2). Thus, the opposite behaviour observed in the seasonal weekly features of aerosol fluxes and concentrations is possibly caused by low vertical dilution effect in winter compared to spring. In this sense, less change in aerosol emissions in winter when mixing layer height is low will produce a large change in aerosol concentration than in spring when mixing layer height is higher. These results indicate that aerosol emissions are not the only drivers controlling aerosol concentration, and that mixing layer dynamic may explain a larger fraction of the concentration change.

To gain more insight on the role of local sources, particularly traffic, in aerosol concentration and flux, an analysis of the weekly variation of both metrics for urban and suburban sectors was carried out. As can be seen in Figure 4.6, aerosol concentration and particularly aerosol fluxes showed a pronounced increase from weekends to working days in both sectors. In both sectors, aerosol fluxes increased on working days by more than 40% whereas aerosol concentration increased by approximately 33%, further demonstrating that traffic was the main important source of aerosol in both sectors. Another interesting finding is that both aerosol concentrations and aerosol fluxes from urban sector (where high density of anthropogenic sources in the city are located) were lower than those from suburban sector during working days and weekends, as confirmed by Mann-Whitney test at 0.01 significance level. This finding demonstrates again the strong impact of aerosol emissions from traffic circulating on the highway that crosses suburban sector on aerosol population over our measurement site. Therefore, measures focusing on traffic emissions, especially at the main highway of the city, will be an efficient way to improve air quality over Granada.

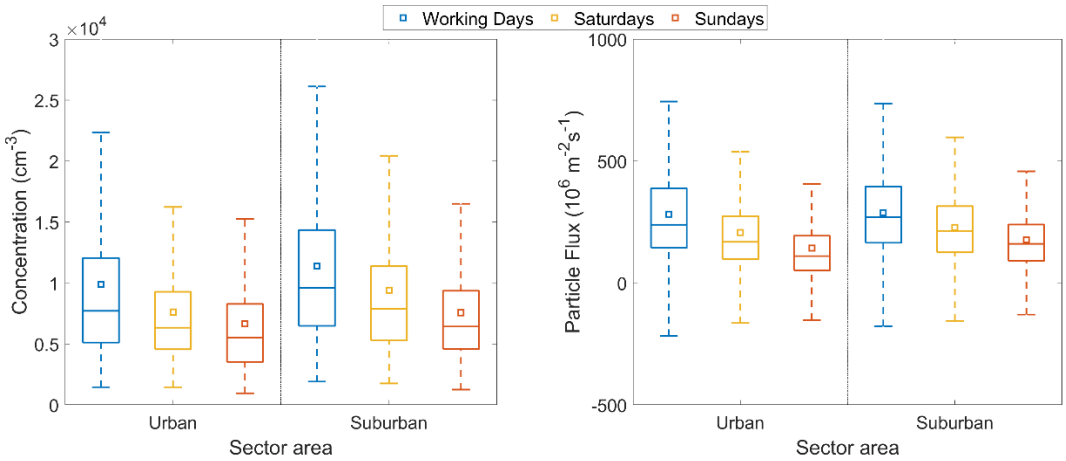

Figure 4.6 - Weekly variations of particle number concentrations (left) and fluxes (right) in urban and suburban sectors averaged over all day-time data available from November 2016 to April 2018.

The study of the diurnal variations can offer further insight into the underlying processes that control the evolution of aerosol concentration and flux in Granada and can help to identify local and regional sources. This source identification is very useful for developing local and regional strategies to reduce air pollution for health and climatic reasons. Figure 4.7 shows the seasonal diurnal cycles of aerosol number concentrations and fluxes averaged over all data available from November 2016 to May 2018. As a common feature, the aerosol concentration presented a clear diurnal pattern, in all seasons, with two local maxima in coincidence with the morning and late afternoon traffic rush hours. Similar diurnal cycle was observed for black carbon at ground level, good tracer of traffic emissions, in the same urban area by Lyamani et al. (2011), which was attributed to the daily variation in both mixing layer dynamic and anthropogenic activities. In summer and spring, a third small peak was observed at around 14:00 h local time. This third peak derives from the enhanced new particle formation processes favored by the increased solar radiation intensity and the availability of precursor vapours during summer and spring seasons (Casquero-Vera et al., 2021; del Águila et al., 2018). Ground surface measurements of aerosol size distribution obtained during the

analyzed period near the site measurements (at approximately 100 m from the tower) corroborate this explanation (not shown here). It is worth to note that the morning concentration peak in winter was almost similar to that observed for the late afternoon peak, whereas, in the other season the second afternoon peak was much lower than the first morning peak. This finding reveals again the significant impact of domestic heating emissions on aerosol concentration in winter season.

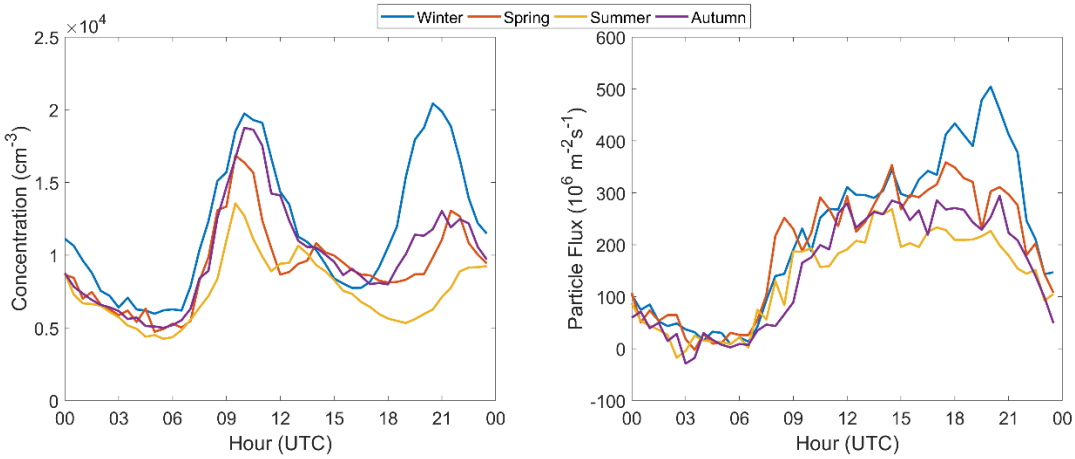

Figure 4.7 - Seasonal diurnal variations of aerosol number concentration (left) and aerosol flux (right) observed over Granada averaged over all data available from November 2016 to April 2018.

On the other hand, aerosol number flux showed a completely different diurnal behaviour. In all seasons, the aerosol flux begins to increase early in the morning around 07:00 h and reaches high values at noon, remaining relatively constant throughout the day until it began to decrease after 19-20 h. However, in all seasons, the aerosol flux did not show a double peak pattern observed in the aerosol concentration. Also, the aerosol flux did not show the large decrease observed in the aerosol concentration around 12:00-14:00 h. The high aerosol fluxes associated with the low aerosol concentration in the middle of the day can be explained by the entrainment of particle depleted air from above the measurement site due to mixing layer growth (see Figure 4.8). Similar diurnal aerosol concentration and flux

behaviours were observed in other urban areas (e.g., Contini et al., 2012; Dorsey et al., 2002; Järvi et al., 2009; Mårtensson et al., 2006; Martin et al., 2009). It is important to note that aerosol flux in winter showed a large increase in the evening between 18:00-22:00 h, which was associated with high aerosol concentration. This finding reveals again the significant influence of domestic heating emissions on aerosol concentrations and fluxes in winter season.

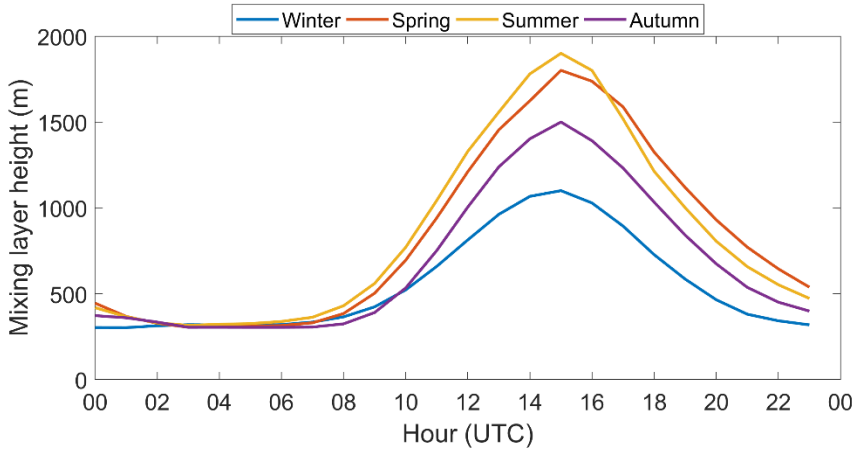

Figure 4.8 - Seasonal diurnal variations of PBL height over Granada averaged over all data available from November 2016 to April 2018.

4.6 /Conclusions

In this section, continuous measurements from November 2016 to April 2018 obtained by Eddy Covariance method were used to examine the diurnal, weekly, seasonal, and spatial variability of aerosol number flux and concentration at an urban site in Granada, Spain. The majority of aerosol number flux values were positive, and negative fluxes were only observed in 12 % of the cases, suggesting that Granada urban site acted as a net source of aerosol particles to the atmosphere. Most of negative fluxes were relatively high in magnitude and were observed during high aerosol load conditions, as a result of downdrafts of particle enriched air from aloft the

measurement height. Aerosol number concentrations and fluxes measured in winter were higher than those observed in summer due to increased emissions from domestic heating and agricultural waste burning and less intense vertical mixing in winter.

The aerosol concentration presents a clear diurnal pattern in all seasons, with two local maxima coinciding with the morning and the evening traffic rush hours, evidencing the large impact of traffic emissions throughout the year. Beside the two diurnal maxima, a third aerosol concentration peak was also observed around midday during summer and spring, which was associated to enhanced new particle formation processes in these seasons. In all seasons, aerosol flux did not show the two peaks associated with traffic observed in the diurnal cycle of aerosol concentration, which was explained by the entrainment of particle depleted air from above the measurement site due to mixing layer grows throughout the day. Strong weekly cycles were also observed with weekend aerosol number concentrations and fluxes significantly lower than working days, mainly due to decrease in traffic activities on weekends.

Aerosol fluxes were positive in all wind direction, indicating that on average all land type sectors affecting the measurement site acted as sources and that there was no specific sink area of aerosols around the measurement site. Large aerosol number concentrations and fluxes were observed from suburban sector which contains an extensive agricultural area and the main highway of the city and low ones were observed for urban sector which includes the city center, densely built up residential and commercial areas and traffic roads. This finding points to the traffic emission from the highway that crosses the suburban sector from south to north as a potential source of local emissions that affect our area of study. A detailed seasonal analysis by wind sector demonstrates that, in addition to traffic activities, domestic heating in urban sector and agricultural waste burning in suburban sector are two important emission sources that affect aerosol population and the air quality of the

study area in winter. In addition, this wind sector analysis shows that the impact of domestic heating emissions from the urban area, especially at night, is much stronger than the impact of agricultural waste burning emissions from the suburban sector. This information is crucial for the implementation of effective mitigation measures to improve air quality in the study area.

5 /Quantifying traffic, biomass burning and secondary source contributions to atmospheric particle number concentrations at urban and suburban sites

This chapter is adapted from "***Quantifying traffic, biomass burning and secondary source contributions to atmospheric particle number concentrations at urban and suburban sites***" by J.A. Casquero-Vera, H. Lyamani, G. Titos, M.C. Minguillón, L. Dada, A. Alastuey, X. Querol, T. Petäjä, F.J. Olmo and L. Alados-Arboledas. Published in Science of The Total Environment, Volume 768, 145282, 2021.

As discussed in previous section, biomass burning is an additional aerosol source in the study area during winter period. The main objective of this chapter is the quantification of the contribution of different sources and processes to sub-micrometric particle concentrations in ambient air at urban and suburban sites influenced by biomass burning emissions. For this purpose, using SMPS and AE33 measurements obtained during winter AMICUS campaign at urban and suburban sites, a new approach based on the Rodríguez and Cuevas (2007) and Sandradewi et al. (2008) methods is proposed to determine the contribution of both vehicle and biomass burning primary emissions and secondary aerosol to the size-segregated particle number concentrations. In addition, this new approach is also applied to an extended dataset at the urban area in order to investigate the extent of each of the source's contribution to particle number concentrations along the year.

5.1 /Sub-micrometric particle number and black carbon mass concentrations

In order to identify the sources and processes contributing to particle number concentration over urban and suburban sites, in this section, the particle number concentrations measured in the range 12-600 nm (N_{Tot}) was separated into three different diameter ranges ($N_{12–25}$ from 12 to 25 nm, $N_{25–100}$ from 25 to 100 nm and $N_{100–600}$ from 100 to 600 nm). In the following sub-sections, the size segregated particle number and BC mass concentrations, obtained during the AMICUS winter campaign (18-12-2015 to 01-04-2016) are analyzed, and BC source apportionment is also presented and discussed.

5.1.1 Campaign overview

Table 5.1 shows the average and standard deviation of particle number concentrations for the different aerosol size ranges obtained at both sites during the whole campaign period. Only concurrent measurements at both sites are considered here. N_{Tot} mean concentration (± standard deviation) at the urban site ($13.4 \pm 9.3 \times 10^3$ cm^{-3}) is slightly higher (13%) than at the suburban site ($11.6 \pm 8.8 \times 10^3$ cm^{-3}). The first streaking pattern here is the very small difference between suburban and urban N_{Tot} levels, the second is that the urban site yields averages close to the typical urban averages for total aerosol number concentration (Cassee et al., 2019). The observed total aerosol number concentrations at both sites are similar to those reported (mean value 12×10^3 cm^{-3} during winter 2017) in Section 4.2 for urban tower site. Nevertheless, the observed concentrations during the AMICUS winter campaign in the urban and suburban sites are slightly higher than those observed in winter season in other Spanish cities like Barcelona, Madrid or A Coruña (Alonso-Blanco et al., 2018). However, the observed concentrations are lower than those

observed in other European cities like Leipzig, London, Bern or Glasgow (Putaud et al., 2010). It is worth to note that large part of differences in the aerosol number concentrations among these sites may result from differences in the measured size ranges, measurement height, instrumentation and sampling period.

Table 5.1 - Statistical overview of size-segregated particle number concentrations measured at urban and suburban stations during AMICUS winter campaign. Std is standard deviation.

		N_{Tot} (10^3 cm^{-3})	N_{12-100} (10^3 cm^{-3})	N_{12-25} (10^3 cm^{-3})	N_{25-100} (10^3 cm^{-3})	$N_{100-600}$ (10^3 cm^{-3})
Urban	Mean	13.4	10.1	2.1	8.0	3.3
	SD	9.3	7.4	1.8	5.9	2.3
Suburban	Mean	11.6	7.9	1.0	6.9	3.7
	SD	8.8	6.0	1.0	5.5	3.2

When comparing size segregated contributions to the total particle number concentration, particles in the nucleation mode (12-25 nm) have the smallest contribution to the total particle number concentrations, being this contribution slightly larger at the urban site (N_{12-25} represents only 16% and 9% of N_{Tot} at the urban and suburban sites, respectively). The low contribution of nucleation particles to the total number concentration during AMICUS winter campaign at both sites may be explained by the low frequency of occurrence of NPF events during the winter campaign (only 3 NPF events). In contrast, N_{25-100} represents the largest contribution to N_{Tot} (59% at both sites), being the concentrations in this size range slightly larger (by 14%) at the urban site compared to the suburban site. Despite possible discrepancy could be caused by different instrumentation cut-off sizes, the average contribution of UFP (<100 nm) to the total particle number concentrations is about 75% and 68% at the urban and suburban sites, respectively, which are in the range of those observed by Putaud et al. (2010), who reported 76% as European mean contribution of UFP to the total particle number concentration.

As expected, larger aerosol number concentrations are observed in the 12-25 and 25-100 nm size ranges at the urban site compared to the suburban site (Table 5.1) due to the proximity of the urban site to traffic roads. In fact, diurnal patterns of $N_{12–25}$ and $N_{25\text{-}100}$ at both sites exhibit distinct morning and evening peaks in coincidence with traffic rush hours, being these peaks much more pronounced in the urban site (Figure 5.1), which evidence the large impact of traffic emissions, especially at the urban site. In this sense, the large $N_{12–25}$ observed in the urban site could be attributed to larger contribution of the so-called delayed primary particles which are formed in the atmosphere from precursor gases released in hot vehicle exhaust after it dilutes and cools in ambient air (Rönkkö et al., 2017). In addition, the large $N_{25–100}$ observed in urban site could be also related to traffic emissions since carbonaceous particles emitted by EURO standards vehicles contribute to the Aitken mode size fraction (Rodríguez and Cuevas, 2007). In contrast to $N_{12–25}$ and $N_{25–100}$, the mean $N_{100–600}$ concentration at suburban site is 12% larger than that obtained at urban site (Table 5.1) with less pronounced $N_{100–600}$ morning and evening peaks (Figure 5.1). Meanwhile, $N_{100–600}$ concentration represents 32% and 25% of the total particle number concentration at suburban and urban sites, respectively. The additional contribution of other sources different to traffic or aging processes during the aerosol transport to suburban site are probably the reason of the larger $N_{100–600}$ concentration observed at suburban station. Assuming spherical particles and constant particle density for the whole size distribution, particles in accumulation size range (100-600 nm) contribute 92% and 93% to the total mass concentration (12-600 nm) at urban and suburban sites, respectively. Thus, larger particle number concentrations in accumulation mode could imply a significant contribution to particle mass concentrations with important repercussions for air quality. Furthermore, at night time, the total aerosol number concentrations as well as the concentrations of particles in the different ranges in suburban site are quite higher than those observed at the urban site (Figure 5.1), supporting the presence of

important emission sources other than traffic at suburban site. Subsequently, a more detailed analysis of the contribution of different sources to the aerosol number concentrations at both sites will be carried out.

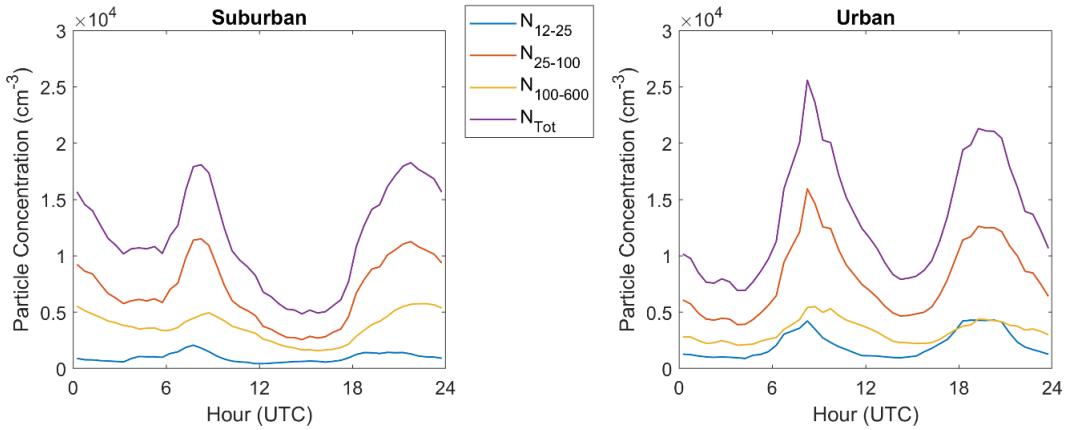

Figure 5.1 - Daily mean pattern of aerosol number concentration in different diameter size rages at suburban and urban sites

Although the suburban site is relatively far from the direct influence of traffic, surprisingly, the concentrations of BC obtained at the urban and suburban sites are similar. In fact, BC concentration ranges from 0.1 to 31 μg m^{-3} with a mean value of 3.0 ± 3.0 μg m^{-3} at the urban site and from 0.1 to 22 μg m^{-3} with a mean value of 2.9 ± 3.0 μg m^{-3} at the suburban site. This result suggests that in addition to traffic there are other important sources of BC particles at the suburban site. The BC concentrations measured at the urban station are in the range of those found during cold season in other European urban areas. For example, recent studies by Liakakou et al. (2019) in Athens (Greece) and by Costabile et al. (2017) in Rome (Italy) have reported winter mean BC concentrations of 2.8 and 2.9 μg m^{-3}, respectively. However, the BC concentrations obtained at the suburban site are significantly much larger than those reported for suburban sites by Laj et al. (2020) (e.g., SIRTA or Ispra sites).

Figure 5.2 shows the mean diurnal variation of BC concentrations measured at the urban and suburban sites. As for the total particle number concentration, BC presents a clear diurnal cycle with two distinct peaks associated with traffic emissions at both sites. Furthermore, significantly higher BC concentrations are observed in the suburban site during night hours, which again indicates an additional contribution to BC particles over suburban site from sources other than traffic. Previous observational study in Granada urban area has identified vehicle exhaust and biomass burning as main sources of BC during winter period (Titos et al., 2017). To quantify the contributions of traffic and biomass burning sources to BC concentrations at both sites and confirm whether the night BC increase at the suburban station is due to biomass burning emissions, the source apportionment analysis of BC particles at both sites will be performed in the following section.

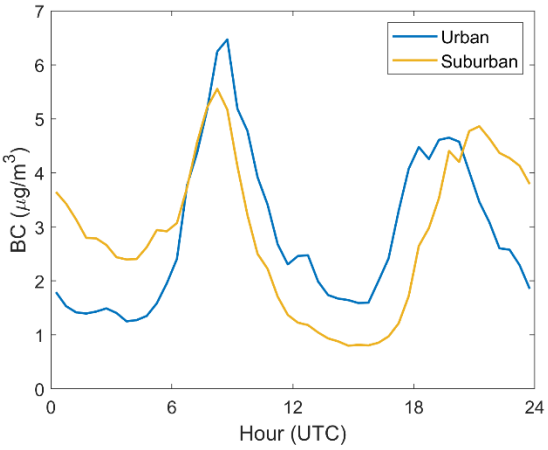

Figure 5.2 - Daily mean pattern of BC concentration at the urban and suburban sites

5.1.2 Source apportionment of BC particles

In order to quantify the contribution of vehicle exhaust and biomass burning emissions to ambient BC particles in the urban and suburban sites, the source apportionment method proposed by Sandradewi et al. (2008) was used. This method assumes that the total aerosol absorption is solely due to the combination of absorption from fossil fuel and biomass burning aerosols. The model is based on the

spectral dependency of the absorption coefficient (particles absorption Ångström exponent, α_{ap}) assuming that aerosol absorption from fossil fuel and biomass burning emission sources follows different spectral dependencies and therefore considers the preselection of suitable α_{ap} values for fossil fuel (α_{ap}^{ff}) and biomass burning (α_{ap}^{bb}). Values of α_{ap} ranging from 0.8 to 1.1 indicate the predominance of BC particles from fuel combustion emissions while α_{ap} values larger than 1.5 indicate considerable contribution of BC from biomass burning (e.g., Helin et al., 2018; Patrón et al., 2017; Titos et al., 2017). Several approaches exist to optimize the selection of α_{ap}^{ff} and α_{ap}^{bb}, depending on the ancillary measurements available, such as biomass burning tracers from filter samples (e.g., Fuller et al., 2014; Titos et al., 2017) or online chemical speciation measurements (e.g., Ealo et al., 2016). During the AMICUS campaign, an ACSM was operating during a short period at the urban site (from 28 January to 18 February 2016). Thus, following the procedure described by Ealo et al. (2016), optimization of Sandradewi et al. (2008) model was done based on the best correlation between carbonaceous material from fossil fuel (CM_{ff}) and biomass burning (CM_{bb}) with hydro-carbon like organic aerosols (HOA) and biomass burning organic aerosols (BBOA), respectively, obtained from the source apportionment of organic aerosols from the ACSM measurements (Minguillón et al., 2015). Applying this procedure during the period in which the ACSM was operative at UGR urban station, α_{ap}^{ff}= 1.0 and α_{ap}^{bb}= 1.9 were obtained. These values of α_{ap}^{ff} and α_{ap}^{bb} have been used for BC source apportionment at both sites.

Considering only simultaneous measurements at both sites, the BC, BC_{bb} and BC_{ff} concentrations obtained at the suburban and urban sites during the studied period are shown in Figure 5.3. Mean BC_{ff} concentrations of 1.9 ± 2.2 μg m^{-3} and 2.3 ± 2.6 μg m^{-3} are obtained for the whole campaign at the suburban and urban sites, respectively. Thus, the BC_{ff} concentration is only slightly larger at the urban

site (1.2 times larger than at suburban site). Furthermore, significantly larger concentrations of BC_{bb} are observed at the suburban site (1.4 times larger than at the urban station), with mean concentrations of 1.0 ± 1.2 μg m^{-3} and 0.7 ± 0.7 μg m^{-3} at the suburban and urban sites, respectively, revealing the strong impact of biomass burning emissions on ambient BC concentrations at the suburban site. Figure 5.3 shows the diurnal evolution of the relative contribution of biomass burning to total BC concentrations. The contribution of biomass burning along the day is always larger at the suburban site with maximum contribution at both sites (about 40-50%) during night-time (Figure 5.3). The lowest contribution of biomass burning is observed during traffic rush hours at both sites. However, despite the large contribution of traffic to BC concentrations during rush hours, the biomass burning contribution during morning rush hours accounted for the 20% of the total BC concentrations observed at the suburban site and only 10% at the urban station. Overall, biomass burning represents an average contribution of 34% and 23% to the total BC at the suburban and urban sites, respectively, evidencing again the large impact of biomass burning emissions on BC concentrations at the suburban site, especially at night-time (Figure 5.3). Biomass burning contribution to BC concentration at the urban site is in the range of those observed in other European cities. Indeed, a biomass burning contribution of about 25% has been reported for urban and suburban areas in Paris (Favez et al., 2009), 24% in Zurich (Herich et al., 2011) and 23% in London (Fuller et al., 2014). On the other hand, the biomass burning contribution to BC concentration at the suburban station is in the range of those reported for other European metropolitan areas highly influenced by biomass burning like Helsinki (Helin et al., 2018) or those observed in rural areas in Switzerland (Herich et al., 2011), with contributions of 40% and 33%, respectively.

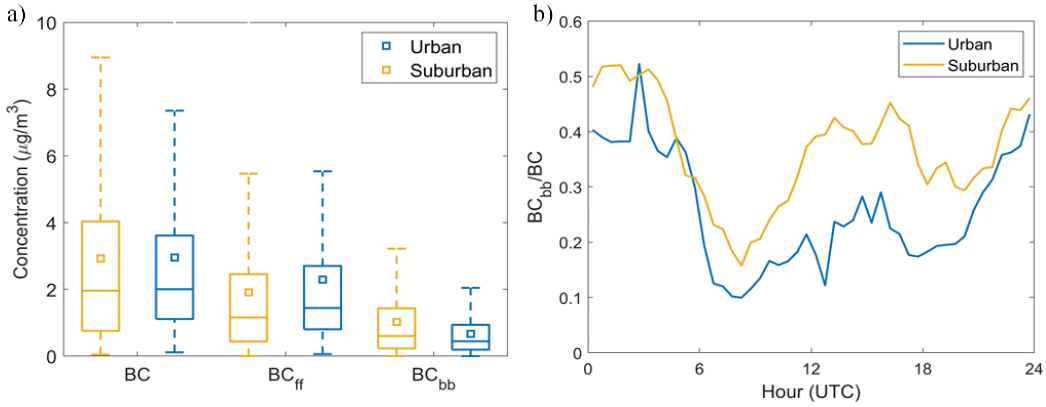

Figure 5.3 - (a) Box and whisker plots of BC, BC_{bb} and BC_{ff} for the suburban and urban sites. The line represents the median of the data, the square represents the mean of the data and the lower and upper edges of the box represent 25th and 75th percentiles of the data, respectively. The length of the whiskers represents 1.5× interquartile range which includes 99.3% of the data. (b) Diurnal evolution of BC_{bb} contribution to BC retrieved for the suburban and urban sites during the study period.

5.2 /Contributions of different aerosol sources to total aerosol number concentration

The estimation of the different source contributions to particle number concentration is important for designing efficient measures to reduce air pollution. In order to quantify the sources and processes contributing to the particle number concentrations, Rodríguez and Cuevas (2007) separated total particle number concentrations into two components: primary and secondary particles. Following Rodríguez and Cuevas (2007) criteria, primary component (N_1) comprises particles directly emitted in the particle phase (such as BC, organic matter compounds, polycyclic aromatic hydrocarbons, some trace elements) and particles nucleating immediately after the emissions, so-called delayed primary particles (Rönkkö et al., 2017). On the other hand, secondary component (N_2) includes particles formed by NPF driven via atmospheric photochemistry or grown by condensation of low-volatility compounds. In this sense, volatile gaseous compounds emitted by traffic are photochemically transformed in the atmosphere to less volatile species, enabling

and enhancing secondary aerosol particle formation via condensation or NPF. Whereas the primary particles emissions affect mostly the air quality near the emission source, the effects of the secondary processes are more important on a regional scale (Rönkkö et al., 2017).

To distinguish between particle number concentrations originating from primary emissions and those from secondary processes, Rodríguez and Cuevas (2007) estimated the concentration of primary aerosol particles (N_1) from BC concentrations using the relation:

$$N_1 = S_1 \cdot BC \qquad \text{Eq. (5.1)}$$

where S_1 is a semi-empirical scaling factor derived from the N_{Tot} vs BC scatter plot (Figure S1 in Appendix), that is interpreted as the minimum number of primary particles arising from vehicle exhaust emissions per each nanogram of BC and is calculated by the quantile linear regression for the 5th percentile.

The results of applying this methodology to all the 30-min averaged data at both stations are shown in Table 5.2. The obtained value of S_1 is slightly larger (by 14%) at the urban site, meaning that there are 14% more particles per ng of BC at the urban site. This result reveals the large impact of so-called delayed primary particles at the urban station, that could be larger as near as traffic sources are. The obtained S_1 values are in the lower range of the values (2-9 10^6 particles ng(BC)$^{-1}$) reported for other European areas (Fernández-Camacho et al., 2010; Hama et al., 2017; Kulmala et al., 2016; Reche et al., 2011; Rodríguez and Cuevas, 2007; Wang et al., 2016). The lower S_1 values obtained in this study could be related with the implementation of more stringent EURO emissions standards along the last years. In this sense, Euro VI standards (implemented in 2015) are 5 times stricter than Euro IV (implemented in 2006), reducing the limit of particles matter emissions from 25 mg/km (98/69/EC) to 5 mg/km (715/2007/EC). In addition to the stringent measure

Table 5.2 - Mean particle number concentration (10^3 cm^{-3}) and contribution to total particle concentrations in parentheses as well as scaling factors (10^6 particles $ng(BC)^{-1}$) obtained by the different approaches used. N_1 and S_1 are the concentration of primary particles and scaling factor obtained by Rodriguez and Cuevas (2007) while N_1^{ff}, N_1^{bb} and N_2 are the concentrations of primary vehicle exhaust, primary biomass burning and secondary particles, respectively, and S_1^{ff} is scaling factor determined by the proposed method.

	Particle number concentration				Scaling factors	
	N_1	N_1^{ff}	N_1^{bb}	N_2	S_1	S_1^{ff}
Urban	6.67 (50%)	5.44 (41%)	1.23 (9%)	6.73 (50%)	2.20	2.38
Suburban	6.04 (52%)	4.49 (39%)	1.55 (13%)	5.56 (48%)	1.93	2.29

to reduce particles matter emissions in the last decade, control of particle number concentration emissions started since EURO V implementation limiting the emissions to 6×10^{11} part/km (692/2008/EC) to all car registrations since 2013. Nevertheless, part of the differences in S_1 values reported in the literature could be also related to the influence of different ambient air conditions on new particle formation during dilution and cooling of vehicle exhausts. Also, it is worth to mention that the comparison among studies depends on the instrumentation used and it is especially sensitive to the CPC cut-off size or SMPS diameter range.

Although the minimum particles emitted per ng of BC (S_1) in this study is below those reported in other areas, the contribution of primary particles to the total particle number concentration (50% and 52% at urban and suburban sites, respectively) was slightly larger than the contribution observed in other cities like Barcelona (46%), Santa Cruz de Tenerife (46%) or Leicester (43%) (Reche et al., 2011).

At this point, it is important to recall that the Rodriguez and Cuevas (2007) method, as was devised, assumes that BC particles are only originated from traffic emissions. However, this assumption is not valid in areas influenced by biomass burning emissions, where the application of this methodology can lead to significant overestimation of the primary particles associated to vehicle emissions. Therefore, new approach is proposed in this study to separate the contributions of primary

vehicle exhaust and primary biomass burning emissions to ambient aerosol in urban areas influenced by biomass burning. To this end, in this section it is proposed the use of BC originated only from traffic emissions, BC_{ff}, previously estimated with the Aethalometer model:

$$N_1^{ff} = S_1^{ff} \cdot BC_{ff} \qquad \text{Eq. (5.2)}$$

where S_1^{ff} is a scaling factor derived from the N_{Tot} vs BC_{ff} scatter plot, and N_1^{ff} is the concentration of primary particles from traffic exhaust (Figure S1 in Appendix). The results of applying this methodology to all the 30-min averaged data at both stations are shown in Table 5.2. The estimated N_1^{ff} mean concentration is of 5.44 × 10^3 cm^{-3} and 4.49 × 10^3 cm^{-3} at the urban and suburban sites, respectively, showing that the application of Rodríguez and Cuevas (2007) method in the study area lead to the overestimation of the concentration of primary particles emitted from vehicle exhaust by about 18% and 26% at urban and suburban sites, respectively (Table 5.2). Thus, this proposed method lead to a reduced contribution of primary emission of vehicle exhaust to the total aerosol number concentration during the whole campaign, decreasing from 50% and 52% at urban and suburban stations, respectively, estimated by the Rodríguez and Cuevas (2007) method, to 41% and 39% at the urban and suburban sites, respectively, estimated by the proposed method.

Considering the main aerosol emission sources on the study region, it can be assumed that the only significant combustion process contributing to BC concentrations at urban and suburban environments are traffic exhaust and biomass burning. Thus, the concentration of primary particles from biomass burning (N_1^{bb}) can be estimated as:

$$N_1^{bb} = N_1 - N_1^{ff} \qquad \text{Eq. (5.3)}$$

and, following Rodríguez and Cuevas (2007) definition, the concentration of secondary particles (N_2) could be estimated as:

$$N_2 = N_{Tot} - N_1^{ff} - N_1^{bb} \quad \text{Eq. (5.4)}$$

A statistical summary of the particle number concentrations of primary particles from biomass burning and secondary particles are reported in Table 5.2. The results show that primary biomass burning particles with concentrations of 1.23×10^3 cm^{-3} and 1.55×10^3 cm^{-3} contributed 18% and 26% to the total primary particles at the urban and suburban sites, respectively. These N_1^{bb} concentrations represent 9% and 13% of the total particle concentrations at the urban and suburban sites, respectively, revealing that the contributions of primary biomass burning source to particle number concentration cannot be neglected. Finally, with concentrations of 6.73×10^3 cm^{-3} and 5.56×10^3 cm^{-3} at the urban and suburban sites, secondary source contribution to total particle number concentrations (50% at the urban site and 48% at the suburban site) is comparable to the contribution of both primary sources.

Although primary and secondary sources show similar relative contributions to the total aerosol number concentrations at both sites, Figure 5.4 shows that these contributions vary with the total particle number concentration. Figure 5.4 also shows that secondary aerosol is the main contributor to the total particle number concentrations at low concentrations at both sites, especially at urban site. However, at urban site, the contribution of traffic source shows a slight increase with the increase of N_{Tot}, reaching a contribution of up to 65% at high ambient total particle number concentrations. Thus, a reduction in exhaust traffic emissions will help to reduce substantially high total particle concentrations at urban site. On the other hand, biomass burning source is the smaller contributor to total particle number concentrations at both sites with no clear variation of this source contribution with the variation of the total particle concentration.

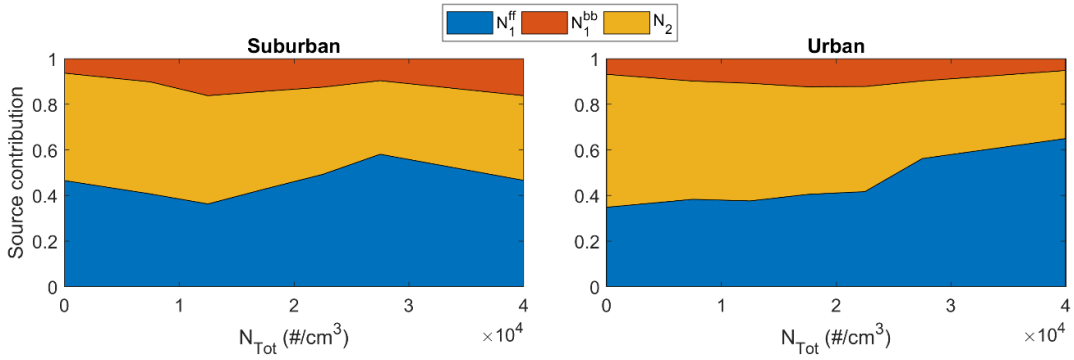

Figure 5.4 - Contributions of primary traffic and biomass burning as well as secondary particles to total particle number concentrations as function of total particle number concentration.

5.3 /Mode-segregated particle sources contribution

As mentioned above, knowledge of the contribution of primary and secondary sources to the total particle number concentration gives valuable information for improving current abatement strategies. However, understanding the contribution of these sources as a function of particle size could provide definite evidence to help tackling high air pollution levels and providing valuable information in terms of health effects. As was done by Kulmala et al. (2016), the analysis presented in the previous section is extended to the three aerosol size ranges (12-25, 25-100 and 100-600 nm), which will allow us not only to split the total particle number concentrations into N_1^{ff}, N_1^{bb}, N_1 and N_2, but also to split it for each single size range. Thus, using the new methodology presented in Section 5.2 and following the mentioned criteria, the total particle number concentration in nucleation size range (12-25 nm) is split into four components: N_{11} (total primary particles), N_{11}^{ff} (primary vehicle exhaust particles), N_{11}^{bb} (primary biomass burning particles) and N_{21} (secondary particles). Similarly, particle number concentration for the other size

ranges is split into N_{12}, N_{12}^{ff}, N_{12}^{bb} and N_{22} for 25-100 nm size range and N_{13}, N_{13}^{ff}, N_{13}^{bb} and N_{23} for 100-600 nm size range.

A statistical summary of the particle number concentrations of the four components (total primary particles, primary particles from biomass burning and vehicle exhaust and secondary particles) for the three size ranges (12-25, 25-100 and 100-600 nm) and scaling factors are reported in Table 5.3. Strong to moderate correlations (r>0.70) between particle number concentrations in 25-100 and 100-600 nm size ranges and BC concentration are observed at both sites (not shown). However, the nucleation mode particle concentration (12-25 nm size range) has relatively weak correlations with BC at the suburban and urban sites (correlation coefficient of 0.44 and 0.67, respectively). This is because a large fraction of nucleation mode particles is probably not associated with fresh traffic emissions, especially at suburban site. Thus, the results of source contributions to nucleation mode aerosol should be interpreted with caution.

The results of applying the methodology presented in this study to size-segregated particle number concentrations evidences a distinct contribution of primary and secondary sources to each size mode. As shown in previous section, secondary aerosol is the main contributor to total particle number concentrations at the urban and suburban sites, followed by primary particles from vehicle emissions and primary biomass burning particles. Looking at size-segregated contributions, secondary aerosol is also the main contributor in the 12-25 and 100-600 nm size ranges at the urban and suburban sites. In this sense, secondary aerosol represents 70% and 82% of the particles in the 12-25 nm size range and 55% and 60% in the 100-600 nm size range, at the urban and suburban sites, respectively. However, the contribution of primary particles (from both vehicle exhaust and biomass burning) is similar to that of secondary particles in the 25-100 nm size range, where the

Table 5.3 - Mode segregated particle number concentrations (10^3 cm^{-3}) from primary vehicle exhaust, primary biomass burning and secondary origin and scaling factors (10^6 particles $ng(BC)^{-1}$) at urban and suburban sites. N_{11}, N_{11}^{ff}, N_{11}^{bb} and N_{21} are the concentrations of total primary, primary vehicle exhaust, primary biomass burning and secondary particles in the 12-25 nm size range, respectively. N_{12}, N_{12}^{ff}, N_{12}^{bb} and N_{22} and N_{13}, N_{13}^{ff}, N_{13}^{bb} and N_{23} are the corresponding concentrations in 25-100 nm and 100-600 nm size ranges, respectively. The contribution of each source to total particle concentration in each size mode is given in parentheses.

Particle number concentration

	N_{11}^{ff}	N_{11}^{bb}	N_{11}	N_{21}	N_{12}^{ff}	N_{12}^{bb}	N_{12}	N_{22}	N_{13}^{ff}	N_{13}^{bb}	N_{13}	N_{23}
Urban	0.59 (28%)	0.05 (2%)	0.64 (30%)	1.46 (70%)	3.52 (44%)	0.51 (6%)	4.03 (50%)	3.97 (50%)	1.20 (36%)	0.30 (9%)	1.50 (45%)	1.80 (55%)
Suburban	0.18 (18%)	0.00 (0%)	0.18 (18%)	0.82 (82%)	2.67 (39%)	0.86 (12%)	3.53 (51%)	3.37 (49%)	1.07 (29%)	0.41 (11%)	1.48 (40%)	2.22 (60%)

Scaling factors

	S_{11}^{ff}	S_{11}	S_{12}^{ff}	S_{12}	S_{13}^{ff}	S_{13}
Urban	0.26	0.22	1.54	1.37	0.53	0.51
Suburban	0.09	0.05	1.37	1.18	0.55	0.50

primary particles represent 50% and 51% of the particle number concentration at the urban and suburban sites, respectively. When looking at primary particles, vehicle exhaust is the main contributor to primary particles accounting for more than 70% of the total primary particles in all the studied size ranges. These results are in agreement with the source apportionment of BC, where BC_{ff} originated from traffic emissions accounted for 66% and 77% of the total BC at suburban and urban sites, respectively.

When comparing particle number concentration at the urban and suburban sites, primary vehicle exhaust and total primary particles concentrations are larger at the urban site in all the size ranges. However, secondary aerosol presents larger concentrations at suburban site in the 100-600 nm size range, with concentrations of 2.20×10^3 and 1.80×10^3 cm^{-3} at the suburban and urban sites, respectively. In

addition, the concentration of primary biomass burning particles at suburban site is 1.7 and 1.4 times larger than at urban site in the 25-100 and 100-600 nm size ranges, respectively. In this sense, the concentration of primary biomass burning particles represents 24% and 13% of the total primary particle number concentrations in the 25-100 nm size range and 28% and 20% in the 100-600 nm size range at the suburban and urban sites, respectively. Thus, considering that the particles in the 100-600 nm size range represents more than 90% of the total mass concentration, this significant contribution of biomass burning particles especially in the 100-600 nm size range would imply a significant contribution of this source to particle mass concentrations with important repercussions for air quality.

Diurnal patters of the mode segregated particle number concentrations of primary and secondary particles at the urban and suburban sites are shown in Figure 5.5. The primary vehicle exhaust particle concentration in the different size ranges considered exhibits a marked morning and evening peaks in coincidence with traffic rush hours. This pattern is observed at both suburban and urban sites, however, a peak delay is observed between both sites as it was observed for BC on Section 5.1. In this sense, the morning peak on vehicle primary exhaust particle concentration at suburban site is observed prior to that at urban site and during the evening hours the suburban peak is delayed few hours respect to the observed on urban site. This delay can be explained by the variation of the wind diurnal pattern observed in the study area and the location of the main sources of particles. The urban site is ~3 km away from suburban site and between both stations is located the main highway that surrounds the city (400 m away from urban site). In this sense, the study region has a characteristic mountain-valley wind regime, with up-valley winds from NW-W during day time and down-valley winds from SE-E during night (Ortiz-Amezcua, 2019) that could explain the dissimilarities observed in diurnal patterns of the primary vehicle exhaust particle concentration at the suburban and urban sites.

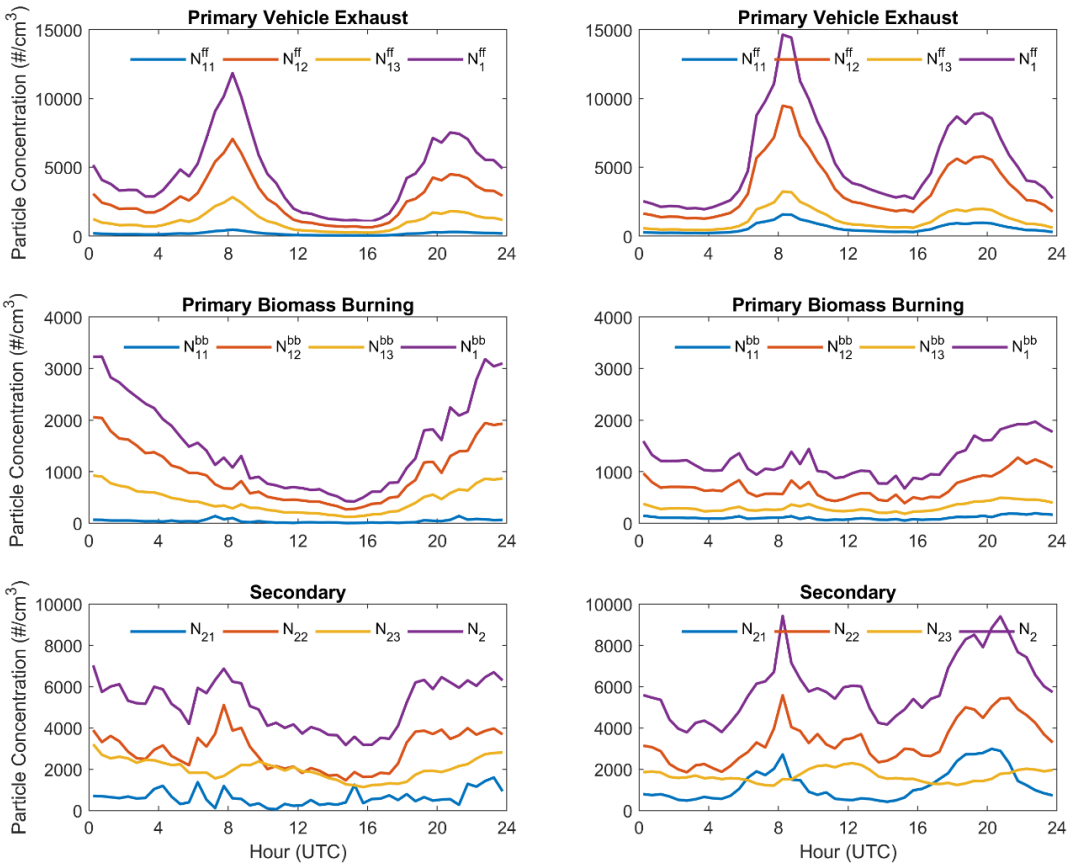

Figure 5.5 - Diurnal evolution of mode segregated and total particle number concentrations from primary vehicle exhaust, primary biomass burning and secondary origin at suburban (left column) and urban sites (right column). N_{11}, N_{11}^{ff}, N_{11}^{bb} and N_{21} are the concentrations of total primary, primary vehicle exhaust, primary biomass burning and secondary particles in the 12-25 nm size range, respectively. N_{12}, N_{12}^{ff}, N_{12}^{bb} and N_{22} and N_{13}, N_{13}^{ff}, N_{13}^{bb} and N_{23} are the corresponding concentrations in 25-100 nm and 100-600 nm size ranges, respectively.

The size segregated concentrations of secondary particles at suburban site do not show clear daily pattern during the study period. However, at urban site the concentration of secondary particles shows two marked peaks in all the size ranges, except in 100-600 nm size range, in coincidence with traffic rush hours. At urban site, the secondary particles in 12-25 nm size range is the main contributor along the whole day. In this sense, lower temperatures during winter season may be more favorable for secondary particle formation through particle condensation and nucleation during cooling and dilution of vehicle exhaust (Rönkkö et al., 2017).

Also, the increase on N_2, especially during evening- and night-time, could be a consequence of the contribution of secondary organic aerosol formation from biomass burning emissions.

5.4 /Seasonal variability of aerosol number concentrations originating from different primary and secondary sources

The variability of aerosol number concentration in urban environments is largely determined by local emission sources and atmospheric processes. Particle emission sources has been widely recognized to present seasonal variability. In Granada metropolitan area, domestic heating (based on fuel oil combustion and biomass burning) and agricultural wastes burning for land clearing represent an additional local source of aerosols in winter (Titos et al., 2017). In opposite, traffic activity in Granada city remains almost constant along the year, with only a slight decrease during summer due to holidays period. On the other hand, the occurrence of new particle formation events at Granada shows a marked seasonal variability, with high occurrence frequency in spring and summer (as can be seen below). So, to investigate the impact of these different aerosol sources and their contributions to the total aerosol number concentrations throughout the year, in this section the newly proposed methodology is applied to aerosol number and BC concentrations measured during 2018 in the UGR urban station. As until now there is no reference source apportionment method that can be used to quantitatively evaluate the performance of the new method proposed, the following seasonal analysis may help to qualitatively address its feasibility as well as to investigate the temporal variability of primary and secondary sources in the Granada urban area.

A statistical summary of aerosol number concentrations of primary vehicles exhaust, primary biomass burning and secondary particles as well as scaling factors obtained at UGR urban station for each season is displayed in Table 5.4. In this section, winter corresponds to the months from December to February, spring from March to May, summer from June to August and autumn from September to November.

Table 5.4 - Seasonal statistical summary of particle number concentration (10^3 cm^{-3}) and the corresponding contribution of the different sources to total particle concentrations (in parentheses) as well as scaling factors obtained at UGR station for 2018. N_1 and S_1 are the concentration of total primary particles and scaling factor obtained by Rodriguez and Cuevas (2007) while N_1^{ff}, N_1^{bb} and N_2 and S_1^{ff} are the concentrations and scaling factor (10^6 particles $ng(BC)^{-1}$) determined by the proposed method.

	Particle number concentration				Scaling factors	
	N_1	N_1^{ff}	N_1^{bb}	N_2	S_1	S_1^{ff}
Winter	7.27 (48%)	5.66 (37%)	1.61 (11%)	7.90 (52%)	2.50	2.72
Spring	4.40 (45%)	3.91 (40%)	0.49 (5%)	5.44 (55%)	3.30	3.30
Summer	4.62 (51%)	4.27 (47%)	0.35 (4%)	4.41 (49%)	3.16	3.15
Autumn	5.78 (48%)	5.32 (43%)	0.46 (5%)	6.35 (52%)	2.60	2.78

In all seasons, total particle number and BC concentrations shows strong to moderate correlations ($r>0.66$). The estimated S_1^{ff} slope shows an evident seasonal variation with the highest slope values during warm seasons and lowest during cold season (Table 5.4). This seasonal behaviour is probably associated with a smaller reduction of particulate emission rates in comparison with the reduction of BC emission rates from cold to warm period due to the seasonal change in meteorological conditions (e.g., relative humidity and temperature). In this sense, it is well known that both aerosol particles and especially BC emissions from fuel combustion increase with decreasing temperature (e.g., Chan et al., 2014; Olivares et al., 2007).

Total particle number concentration at UGR urban station shows a clear seasonal pattern. Largest and smallest total particle number concentrations are observed during winter (1.51×10^4 cm^{-3}) and summer (0.90×10^4 cm^{-3}), respectively (N_1+N_2 on Table 5.4). Similar seasonal variations in aerosol number concentrations were reported for other urban areas (e.g., Järvi et al., 2009; Ripamonti et al., 2013). This seasonal variation is attributed to the increased emissions from domestic heating, burning of residual agricultural waste in the agricultural area surrounding the site. Furthermore, the reduced mixing volume and low wind speed observed in the study area during cold period would favour lower vertical and horizontal dilution of the aerosol emissions, contributing to the increase in aerosol concentration in winter months.

As can be seen in Table 5.4 and as expected, vehicle exhaust is the main source of primary particles along the year in UGR urban station with mean concentrations ranging from 5.66×10^3 cm^{-3} in winter to 3.91×10^3 cm^{-3} during spring season. Since traffic activity remains almost constant along the year in Granada city, this difference on vehicle exhaust primary particles could not be due to larger traffic activity during winter period. Thus, the increase of vehicle exhaust primary particles could be due to lower atmospheric boundary layer heights and lower ambient temperatures. In this sense, ambient temperatures could influence the vehicle particle emissions, with emissions increasing at colder temperatures and during cold start conditions that lead to inefficient combustion, inefficient catalyst operation and the potential for the vehicle operation under fuel-rich conditions (Nam et al., 2010).

Despite the concentration of vehicle exhaust primary particles peaks in winter, it coincides with the lowest contribution of traffic primary particles to total primary particles due to the highest biomass burning primary particle concentrations observed during winter period with concentrations of 1.61×10^3 cm^{-3}, that represents 22% of the total primary particles concentration. For the other seasons, as expected,

the absolute concentration as well as the contribution of biomass burning source to the measured aerosol number concentrations are negligible (below 4%). In this sense, agricultural waste and biomass burning from domestic heating practices are common in the study area during the cold season, and especially domestic heating based on olive pits burning has significantly increased over the past years (Titos et al., 2017). However, these sources are negligible during warm season due to the prohibition of open-air biomass burning activities during that period and the absence of domestic heating.

As it was previously observed in other urban areas, secondary particles presented an important contribution to total aerosol number concentration at UGR urban station through the year with contributions ranging from 49% to 55. The high winter concentration (7.90×10^3 cm^{-3}) and contribution (52%) of secondary particles is, in large part, associated with the lower temperatures during this cold season which favour more secondary particle formation during cooling and dilution of vehicle exhaust through nucleation and condensation processes of emitted condensable gaseous compounds. Summarizing, in winter the secondary particles are the main contributor to total number concentration (52%) at UGR urban station followed by primary exhaust particles (37%) and biomass burning particles (11%) while in summer season the secondary particles and primary exhaust particles contribute 49% and 47% to the total aerosol number concentration, respectively.

Analysis of seasonal diurnal variability can give us more insights about the seasonal change in source emission rates and processes affecting aerosol load. Figure 5.6 shows the seasonal diurnal evolutions of the particle number concentrations from each primary source and secondary origin at urban site. As expected, in all season, the concentration of traffic primary particles shows a clear diurnal pattern with two marked peaks in coincidence with traffic rush hours, being primary particles from vehicle exhaust the main contributor to the total number

concentration during the morning traffic rush hours. The diurnal evolution of secondary particle concentrations during autumn and winter shows similar evolution to traffic diurnal pattern with two peaks in coincidence with traffic rush hours. However, the evening peak at both seasons shows longer duration, ending much later than the primary vehicle exhaust peak. In addition, the evening peak of secondary particle concentration is much pronounced than the morning one, especially in winter season, being secondary particles the most important contributor to the total number concentration during evening and night-time. This diurnal behaviour is different to the showed by the concentration of primary vehicle exhaust particles, which showed higher concentration during the morning peak than during evening peak in all seasons. Thus, this result points to an important contribution of domestic heating emissions to secondary aerosol number concentration at evening-night hours during cold period.

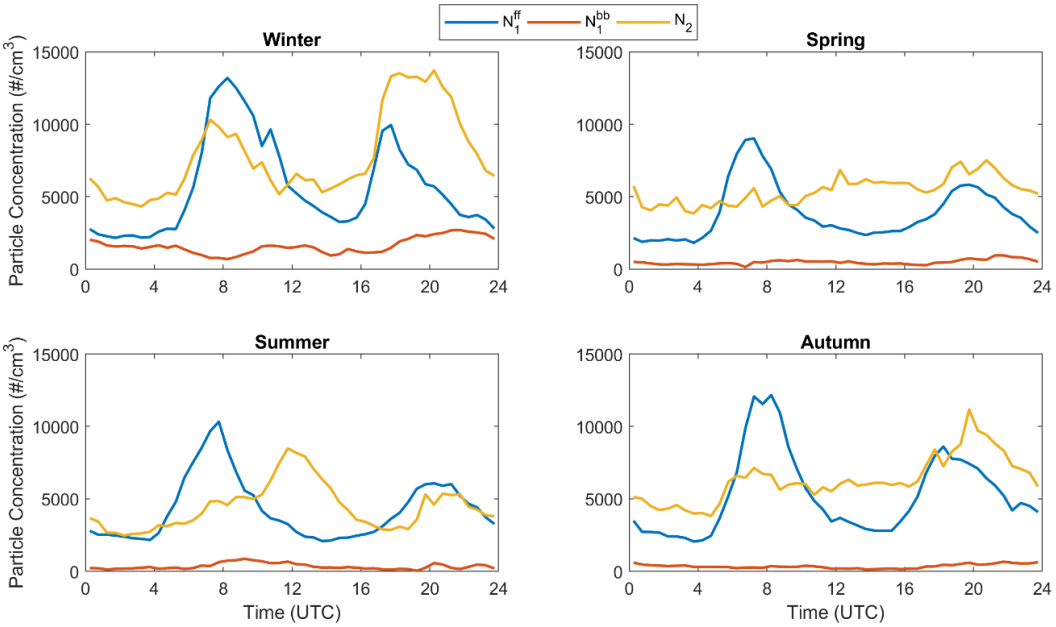

Figure 5.6 - Seasonal diurnal evolution of total particle number concentration from primary (fossil fuel and biomass burning) and secondary origin at urban site.

On the other hand, the secondary particle concentration in summer shows a pronounced increase at noon four hours after the morning peak of primary traffic

particles, indicating that is not directly related to vehicle emissions. Also, this pronounced noon peak is not observed in the rest of seasons. This noon peak in concentration of secondary particles is attributed to the high occurrence frequency of regional NPF events during warm period, as discussed below.

In order to determine the significance and relative contribution of atmospheric NPF events to particle number concentrations, the NPF events that occurred during 2018 were analyzed. Following Dal Maso et al. (2005) procedure, days has been classified as event, non-events, undefined and bad-data days. The results show 99 days of NPF events, 132 non-event and 33 undefined days for a total of 264 analyzed days, with an event frequency of 38% for 2018 year. However, despite the event frequency is in the range of those observed in other southern area of Spain (Sorribas et al., 2015) or Finnish boreal forest (Dal Maso et al., 2005), the monthly variability of NPF events frequency is significantly larger than that observed in those studies. Figure 5.7 shows that the occurrence of NPF events in the study region have a large variability along the year, with an event frequency ranging from 4% on December to 100% on July. In this sense, NPF events occurs mainly during the warm season, later spring and early autumn.

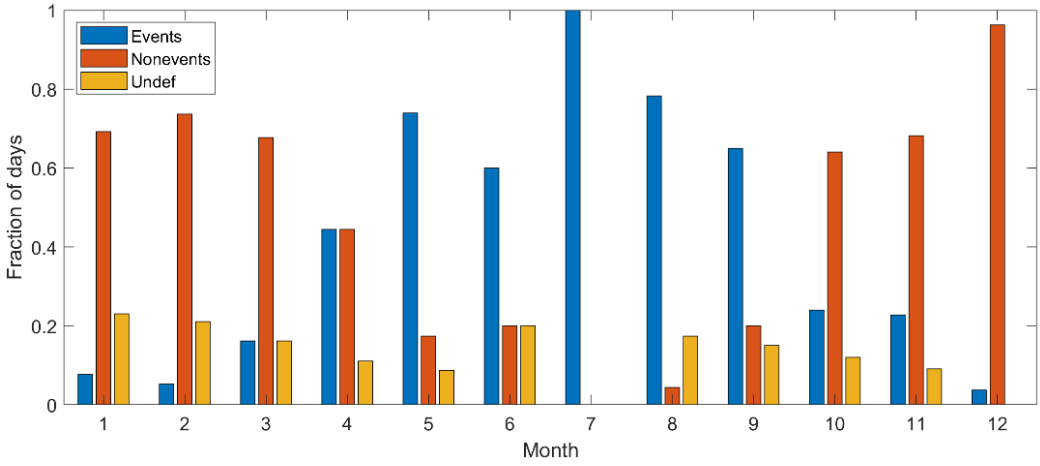

Figure 5.7 - Monthly fraction of days classified as NPF events, nonevents and undefined.

In order to study the relative concentration increment of particles from NPF with respect to the particles originating from all other sources on event days, Salma et al. (2014) methodology was applied for 2018 NPF events. Salma et al. (2014) defined the nucleation strength factor (NSF) as the particle number concentration ratio of ultrafine particles to the regional aerosol in accumulation mode on NPF days to non-NPF days, respectively:

$$NSF = \frac{(N_{12-100}/N_{100-600})_{events}}{(N_{12-100}/N_{100-600})_{non-events}} \quad \text{Eq. (5.5)}$$

The importance of atmospheric NPF is negligible if NSF<1.0. In case of 1.0<NSF<2.0, NPF shows comparable importance to all other sources. When NSF>2.0, the NPF has the highest contribution to ambient particles than any other sources.

Mean nucleation strength factor of 1.05 has been obtained in Granada urban site during 2018. This implies that, on average, regional new particle formation does not implicate a considerable contribution of NPF events to total urban particles. This value is significantly lower than those observed in central European cities Budapest, Vienna, and Prague, with NSF values of 1.58, 1.54, and 2.01, respectively (Németh et al., 2018). Large part of these differences in NSF factor is attributed to the differences in cut-off sizes of the used instruments. On the other hand, the summer diurnal pattern of NSF shows that the nucleation strength factor varies from ~0.7 during early morning to ~2 at noon (not shown). Thus, in summer, NPF events is an important source of particles during hours of high solar radiation, however, traffic primary particles and secondary particles from other sources different to NPF events are the main sources of particles in the urban area of Granada.

5.5 /Conclusions

In order to implement effective abatement measures, it is critical to identify the sources of aerosol particles and their contributions to the total aerosol population. For this purpose, a new approach based on Rodríguez and Cuevas (2007) and Sandradewi et al. (2008) methods was proposed to determine the contributions of both vehicle exhaust and biomass burning primary as well as secondary particles to total and mode segregated particle number concentrations. For that, simultaneous measurements of aerosol size distribution in 12-600 nm size range and black carbon (BC) concentration performed at urban and suburban sites in Granada, Spain, during AMICUS winter campaign in 2015-2016 were used.

As expected, larger aerosol number concentrations, especially in the 12-25 and 25-100 nm size ranges, are observed at the urban site compared to the suburban site. Surprisingly, similar concentrations of BC are observed at both sites due to the larger contribution of biomass burning particles to the observed BC at suburban (34%) in comparison to urban site (23%). Due to the significant biomass burning contribution, it has been found that in the study areas the application of Rodriguez and Cuevas (2007) method, which only assume primary particles from vehicle exhaust, leads to the overestimation of the concentration of primary particles emitted from vehicle exhaust by about 18% and 26% at urban and suburban sites, respectively.

The results of the new proposed approach show that at both sites secondary particles are the main contributor to mode segregated particle number concentrations, especially in the 12-25 and 100-600 nm size ranges, followed by primary particles from vehicle emissions and primary biomass burning particles, respectively. In both sites, primary particles from vehicle exhaust dominated the total primary particles (>70%) at all the studied size ranges. The concentration of primary biomass burning particles in the 25-100 nm and 100-600 nm size ranges at suburban site is 1.7 and 1.4 times larger than at urban site, respectively, being the

contribution of primary biomass burning particles to the total primary particle number concentrations 24% and 13% in the 25-100 nm size range and 28% and 20% in the 100-600 nm size range at the suburban and urban sites, respectively. The different source contributions vary with the total particle number concentration, being secondary particles the main contributor at low particle number concentrations at both sites. At urban site, the contribution of primary particles from traffic emissions shows a slight increase with the increase of total particle number concentration, reaching a contribution of up to 65% at high ambient particle number concentrations. Thus, these results could give valuable information on the qualitative effect of various types of air pollution abatement measures.

Finally, this new approach was applied to an extended dataset at the urban site in order to examine sources' strength along the year and their contributions to particle number concentrations. As expected, vehicle exhaust is the main source of primary particles along the year in UGR urban station. The concentrations of primary particles from biomass burning source was highest in winter (1.6×10^4 cm^{-3}), when this source contributed about 22% to the total concentration of primary particles. New Particle Formation process (NPF) has been found to be an important source of particles only during summer noon hours but, on average, NPF events does not implicate a considerable contribution to atmospheric particles in the urban environment.

The proposed new approach has been shown to be a useful tool for assessing and quantifying sources contributing to particle number concentrations into different aerosol size ranges under the influence of vehicle exhaust and biomass burning emissions. Thus, considering the instrumentation used, this new approach could be useful in assessing the impact of these sources around the globe since this methodology can be applied to larger datasets (as those generated by ACTRIS or SARGAN networks), giving more insights into secondary and primary contributions (vehicle exhaust and biomass burning) and into the health effects of these aerosol sources.

6 /New particle formation at urban and high-altitude remote sites

This chapter is adapted from "***New particle formation at urban and high-altitude remote sites in the south-eastern Iberian Peninsula***" by J.A. Casquero-Vera, H. Lyamani, L. Dada, S. Hakala, P. Paasonen, R. Román, R. Fraile, T. Petäja, F.J. Olmo-Reyes and L. Alados-Arboledas. Published in Atmospheric Chemistry and Physics, Volume 20, 14253–14271, 2021.

In previous sections, NPF events have been found to be an important source of particles during summer in the study area. These NPF events are of great importance for the production of cloud condensation nuclei (CCN) and cloud formation, and hence, the characterization of their vertical distribution is of special interest. Thus, this section is devoted to the study of the occurrence frequency, characteristics and factors that promote/inhibit NPF processes at two contrastive sites: urban (UGR) and high-altitude remote (SNS) sites. To this end, aerosol size distributions in the size range 4-500 nm measured simultaneously during SLOPE II summer campaign are investigated and the role of precursor gases such as sulfuric acid and volatile organic compounds and their contribution to the formation and growth of aerosol particles at these two different environments are explored. In addition, in order to get insight about the processes and the constituent components that lead to the formation of new particles during Saharan dust intrusions, a closer analysis of NPF events during a Saharan dust episode is presented.

6.1 /Classification of NPF events and determination of their physical characteristics

The classification of NPF event days was done by visual inspection of the daily particle number size distribution data according to the guidelines presented by Dal Maso et al. (2005). According to this classification criteria, days are classified and separated into four groups: event (E), non-event (NE), undefined (UN) and bad-data days (BD). (1) "E" days are days during which sub-25 nm particle formation and their consequent growth are observed; (2) "NE" days are days on which neither new growing modes or production of sub-25 nm particles are observed; (3) "UN" days are the days which do not fit either of the previous classes; (4) "BD" days are the days during which data are not valid or inexistent. In addition, event days are separated into two different groups: class I and II events. NPF events are classified as class I events when the NPF growth rate retrieval is possible from 7 to 25 nm, and class II when it is not possible.

The automatic DO-FIT algorithm (Hussein et al., 2005) is used to describe the measured particle number size distributions by fitting multiple lognormal distributions to the measured data. The geometric mean diameters of the fitted distributions are then used for calculating particle growth rates during NPF events. This is done by calculating the slope of the linear fit to the geometric mean diameters as a function of time, which were identified to represent the growing particle mode formed in an NPF event. Thus, the growth rate (GR) is obtained as:

$$GR_{\Delta D_p} = \frac{dD_p}{dt} = \frac{\Delta D_p}{\Delta t} \qquad \text{Eq. (6.1)}$$

where D_p is the representative diameter of the NPF mode at time *t*. In this work, the growth rates in the range 4-7 ($GR_{4\text{-}7}$) and 7-25 nm ($GR_{7\text{-}25}$) were calculated. The uncertainties in the calculated GRs was estimated on 19% and 8% for the 3-7 and 7-20 nm size ranges (Yli-Juuti et al., 2011).

The formation rate (J_{D_p}) is defined as the flux of particles past the lower limit of the size range (ΔD_p), and it is obtained by adding up the observed change in the observed particle number concentration and the losses of particles due to coagulation and growth out of the size range (ΔD_p) and it is calculated following the methodology described by Kulmala et al. (2012):

$$J_{D_p} = \frac{dN_{\Delta D_p}}{dt} + CoagS_{\Delta D_p} \cdot N_{\Delta D_p} + \frac{GR_{\Delta D_p}}{\Delta D_P} \cdot N_{\Delta D_p} \qquad \text{Eq. (6.2)}$$

where the first term on the right hand side represents the rate of change of particle concentration with time (where $N_{\Delta D_p}$ is the particle number concentration in the size range ΔD_p); the second term describes the loss of particles due to coagulation with larger aerosol particles (where $CoagS_{\Delta D_p}$ is the coagulation sink); and the third term considers the growth out of the considered size range. The coagulation sink was calculated from the geometric mean of the considered size range (ΔD_p) to the upper SMPS diameter limit (500 nm), according to Kulmala et al. (2001). In this study, the formation rates at diameters (D_P) 4 nm (J_4) and 7 nm (J_7) were calculated using the diameter range (ΔD_p) of 4-7 and 7-25 nm, respectively.

The condensation sink (CS) describes how rapidly vapour molecules will condense onto pre-existing aerosols. CS is dependent on the effective surface area of the pre-existing particle size distribution (Kulmala et al., 2012). Accordingly, the CS is calculated from each size distribution as:

$$CS = 2\pi D \int_{D_{min}}^{D_{max}} D_p \, \beta_M \, N_{D_p} \, dD_p = 2\pi D \sum_{D_p} D_p \, \beta_M \, N_{D_p} \qquad \text{Eq. (6.3)}$$

where D is the diffusion coefficient of condensable vapour, that is assumed to be sulfuric acid, and β_M is the transitional correction factor (Fuchs and Sutugin, 1971) that depends on the mean free path of vapour molecules and aerosol diameter (e.g., Kulmala et al., 2001; Pirjola et al., 1999).

In order to quantify the contribution of H_2SO_4 to new particle formation and growth, the concentration of condensable vapour required for a growth rate of 1 nm h^{-1} (C_v) was calculated following Nieminen et al. (2010) procedure. For better estimation of condensable vapour concentration, C_v was retrieved by using the mass and density of the sulfuric acid-water-mixture (Kurtén et al., 2007) taking into account the differences of temperature and RH between SNS and UGR station.

Since concentration of H_2SO_4 was not measured at either stations, a proxy of H_2SO_4 concentration is used in order to define whether H_2SO_4 is the precursor vapour responsible for NPF at both stations and if so to link the new particle formation rates with the H_2SO_4 concentrations The proxy calculation was first proposed by Petäjä et al. (2009) which derives H_2SO_4 concentration from its formation through SO_2 concentration in the presence of global radiation, UV-B or OH and its loss to CS. To estimate the H_2SO_4 concentration for our two stations, the following formula was used (Petäjä et al., 2009):

$$H_2SO_4 = k \cdot \frac{SO_2 \cdot UVB}{CS} \qquad \text{Eq. (6.4)}$$

where SO_2 is sulfur dioxide concentration, UV-B is the radiation with wavelength from 280 to 320 nm and *k* is a scaling factor. For this work, the *k* value reported by Petaja et al. (2009) based on measurements in the Hyytiala SMEAR II station ($k = 8.4 \times 10^{-7} \cdot UVB^{-0.68}$ [$m^2W^{-1}s^{-1}$]) was used. The choice of *k* value will have an influence on the absolute value of the H_2SO_4 concentrations, but not on the relative variability. Then, the particle growth rate by sulfuric acid is calculated directly as the ratio of H_2SO_4 and the concentration of condensable vapours required for a growth rate of 1 nm h^{-1} (C_v).

Finally, the dimensionless survival probability parameter (*P*) proposed by Kulmala et al. (2017) was calculated as:

$$P = \frac{CS'}{GR'} \qquad \text{Eq. (6.5)}$$

where CS' = CS / (10^{-4} s^{-1}) and GR' = $GR_{7\text{-}25}$/ (1 nm h^{-1}). The used CS and GR values were calculated with the methods described previously. The larger the survival parameter is, the smaller percentage of newly formed particles will survive to greater sizes. Values of *P* smaller than 50 are typically required for NPF occurrence in clean and moderately polluted environments, although higher values of *P* (up to 200) are observed for NPF events in highly polluted atmospheres (M. Kulmala et al., 2017).

6.2 /Atmospheric aerosol number concentrations

During the intensive SLOPE II campaign, 32 days of coincident aerosol number concentration measurements at SNS and UGR station were recorded. To take insight about the sources of aerosol particles, the 5-min particle size distributions measured by SMPS were segregated into three diameter ranges: nucleation mode from 4 to 25 nm ($N_{4–25}$), Aitken mode from 25 to 100 nm ($N_{25–100}$) and accumulation mode from 100 to 500 nm ($N_{100–500}$). This is because these distinct particle modes result from different emission sources and chemical and physical processes (e.g., Hama et al., 2017 and reference therein). In addition, total particle number concentration is calculated from the whole 4 to 500 nm range (N_{Tot}).

A statistical summary of daily mean particle number concentrations in different size ranges ($N_{4–25}$, $N_{25–100}$, $N_{100–500}$ and N_{Tot}) at SNS and UGR station are presented in Table 6.1. As expected, the average total particle number concentration during the whole campaign period at UGR urban station was clearly 2 folds larger (mean value of 8.4 × 10^3 cm^{-3}) than that at the remote SNS station (3.4 × 10^3 cm^{-3}) due to a large contribution from local anthropogenic emissions in the urban

environment. In general, the direct comparison of the results obtained in this section with those reported in literature is difficult and large differences in the aerosol number concentrations between the different sites may result from differences in the measured size ranges, instrumentation, sampling period, site location and proximity to the sources. However, the average aerosol concentration measured at UGR urban station was in the range of those obtained in summer season (4-24 × 10^3 cm^{-3}) in other European urban sites (e.g., Birmili et al., 2016; Gómez-Moreno et al., 2011; Pérez et al., 2010; Pey et al., 2010). On the other hand, the mean aerosol concentration at SNS was slightly higher than that observed at Puy de Dôme (research station located at 1465 m a.s.l. in central France), where $N_{10–1000}$ were 2.5 × 10^3 cm^{-3} in summer (Venzac et al., 2009). However, the mean aerosol concentrations at SNS was significantly higher than that reported (mean $N_{10–1000}$ of 767 cm^{-3} in July) for Jungfraujoch (high-alpine station located at 3580 m a.s.l. in the central Swiss Alps) by Weingartner et al. (1999). Aerosol number concentrations at remote sites are rather influenced by long-range transport or/and by transport from lower altitudes in the case of remote mountain sites. Therefore, aerosol transport from lower altitudes (i.e., from Granada city) could partly explain the high aerosol concentration observed over SNS station.

Table 6.1 - Statistical overview of daily aerosol concentrations in different size ranges in 10^3 cm^{-3} at SNS and UGR station.

	SNS				UGR			
	N_{4-25}	N_{25-100}	$N_{100-500}$	N_{Tot}	N_{4-25}	N_{25-100}	$N_{100-500}$	N_{Tot}
Min	0.2	0.4	0.1	1.0	1.1	1.2	0.4	2.4
Median	1.3	1.2	0.4	3.2	3.8	3.3	1.0	9.1
Max	6.2	3.8	0.7	9.6	8.0	5.3	1.7	14.9
Mean	1.7	1.4	0.4	3.5	4.0	3.2	0.9	8.1
St. Dev.	1.4	0.9	0.2	2.3	1.8	1.2	0.4	3.2

Table 6.1 also shows that the ratios between aerosol number concentrations measured at SNS and UGR are similar for all size ranges (N_{Tot} – 41%, $N_{4\text{-}25}$ – 43%, $N_{25\text{-}100}$ – 44% and $N_{100\text{-}500}$ – 44%). Consequently, the contributions of each aerosol mode to the total aerosol number concentration are similar at both locations. For example, accumulation mode ($N_{100\text{-}500}$) has a contribution of 11% at both sites, whereas Aitken mode ($N_{25\text{-}100}$) contributed 40% to the total aerosol number concentrations at both measurement sites. Finally, nucleation mode ($N_{4\text{-}25}$) is the main contributor to the total aerosol number concentration at both sites during the whole campaign, representing 49% of the total aerosol number concentration at both sites.

Although the contributions of the different modes to total particle number concentration are similar at both sites, Figure 6.1 shows that diurnal patterns differ from one site to another, revealing that the aerosol concentrations at both sites are influenced by different sources and mechanisms. $N_{25\text{-}100}$ and $N_{100\text{-}500}$ diurnal patterns at UGR station show two peaks (one in the morning and other in the evening) in coincidence with those observed in black carbon (BC; a good tracer of traffic emissions; Lyamani et al., 2011) diurnal pattern (Figure S2. in Appendix). These diurnal patterns are evidence for the large impact of anthropogenic emissions, mainly traffic emissions, on the aerosol concentrations at UGR site. Similar pattern is observed for N_{Tot} at this site, but with a third peak overlapping the morning traffic rush hours peak. This third peak is observed around 10-12h UTC in coincidence with an increase of nucleation mode aerosol number concentration ($N_{4\text{-}25}$). This peak is related to the occurrence of NPF events at UGR due to an increase in atmospheric photochemistry as can be seen later. On the other hand, the total aerosol concentration at SNS shows an evident diurnal cycle with a peak around 12-16h UTC. This peak is probably associated with the evolution of the boundary layer that transports gases and aerosol from lower altitudes (Figure S2) or to the occurrence of NPF events at SNS site, since an increase in nucleation mode aerosol concentration is also observed.

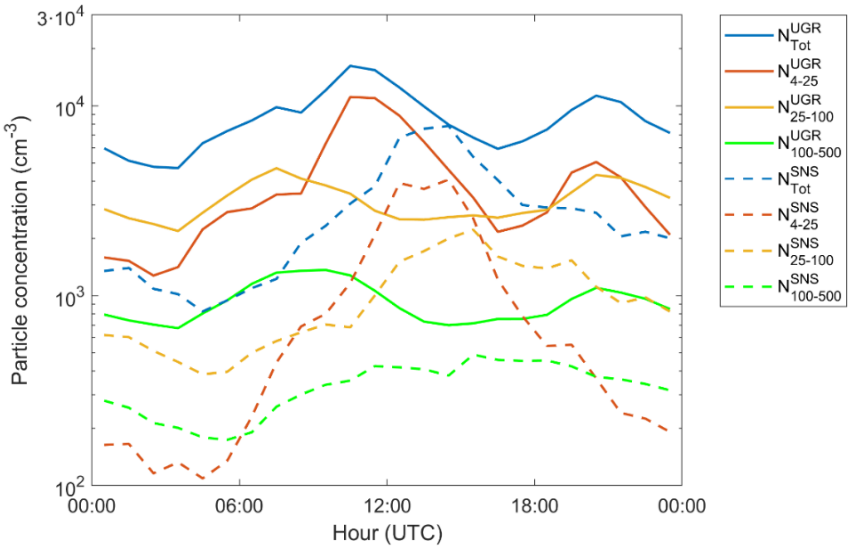

Figure 6.1 - The mean diurnal variation of particle concentrations in different size ranges at SNS and UGR for the whole analysed period.

Although on average the total particle number concentration at UGR is larger than at SNS station, temporal evolution of N_{Tot} shows that during some days the total aerosol concentrations at SNS was higher than those observed at UGR urban station. These high aerosol total concentrations at SNS are also associated with high $N_{4\text{-}25}$ concentrations, both peaking around 12h UTC. The observed peaks in $N_{4\text{-}25}$ concentrations (~4×10^3 cm^{-3}) are more than 40 times larger than the background concentrations (~100 cm^{-3}) observed during night-time, suggesting that these cases are probably associated with strong NPF events occurring at SNS site. Due to the observed high contribution of nucleation mode and the suggested relevance of NPF events at both sites, an in-depth study of NPF events is carried out in the next section.

6.3 /New particle formation analysis

The results of NPF classification (events, non-events or undefined and bad-data days) are summarised in Table 6.2. At both sites, a high NPF event frequency (>70%) is observed with 19 and 23 events at SNS and UGR, respectively. For many

years, it was thought that NPF events cannot take place in urban areas, where the high pre-existing aerosol concentrations was considered detrimental in suppressing the formation and growth of particles due to high condensation sink. However, our results show slightly higher frequency of NPF events at UGR urban site in comparison to the remote site, which could be attributed to the higher availability of precursor gases at the urban site. Our results oppose Boulon et al. (2011) observations, who found that nucleation process is more frequent in a high-altitude site than in nearby urban area. Currently, the cause of the high frequency of NPF in polluted urban atmospheres, such as those in Chinese megacities, is still an open question (Kulmala et al., 2017; Yao et al., 2018).

Table 6.2 - Number of NPF event (E), non-event (NE) or undefined (UN) NPF days and bad-data (BD) observed at SNS and UGR.

	E (days)	NE (days)	UN (days)	BD (days)
SNS	19	5	3	5
UGR	23	4	1	4

In general, NPF event days at SNS station seem to be connected to the events observed at UGR station, as all the event days observed at SNS are also classified as event days in UGR station. This results in 17 coincident event days at both sites, and suggests a regional scale of NPF events. In this work, class I events have been considered when a growing mode is observed below 25 nm and the retrieval of GR in the 7-25 nm size range is possible. In this sense, at SNS station 10 of the 19 observed events were classified as class I events, while at UGR station 17 of the 23 observed events were classified as class I events.

It is important to note that the $GR_{7\text{-}25}$ retrieval is not unambiguous for some NPF events occurring at SNS station due to the appearance of two modes at same time in the nucleation range (<25 nm) during these cases (Figure S3). These two modes are not always well separated, making difficult or impossible the retrieval of

growth and formation rates for these cases. In some cases, these two modes show similar temporal evolution, but in other cases, completely different behaviour is observed, suggesting different precursor vapours origin or different formation processes of both aerosol modes. The appearance of these two nucleation modes is probably associated to the advection of nucleated particles probably from lower altitude levels (i.e., from Granada city) over mountain site, but also the influence of precursor gases advected over SNS station that leads to the occurrence of NPF events at the proximities of SNS station. In this sense, the predominant western winds at SNS during NPF events support the advection of nucleated aerosol particles and precursor gases to SNS from the valley (Figure S4). The appearance of two modes in the nucleation size range were also observed in other mountain sites (e.g., García et al., 2014; Rose et al., 2017) and the cause for their appearance during some NPF events is an open question as remarked in the review of Sellegri et al. (2019).

While regional NPF events are usually observed after 11:00 UTC at SNS station probably due to the upslope transport of precursors vapours from lower altitudes, at UGR urban site, the frequent occurrence of a local event (burst event) is observed around 07:00-08:00 UTC followed by another event lasting for few hours (see Figure S3). First event at urban site coincides with morning traffic rush hours and could be attributed to the so-called delayed primary particles which are formed in the atmosphere from precursor gases released from hot vehicle exhaust after it dilutes and cools in ambient air (Rönkkö et al., 2017). This local event is followed by another event that is associated with the occurrence of regional NPF events at both stations (Figure 6.2). The regional NPF events at UGR station appear in the time range from 9:00 UTC to 12:00 UTC, while NPF events at SNS station are usually observed after 11:00 UTC. It is worth to mention that the production of 4 nm particles can be observed at SNS even though their production has already ended at UGR, which suggests that completely new particles are being formed at high altitudes.

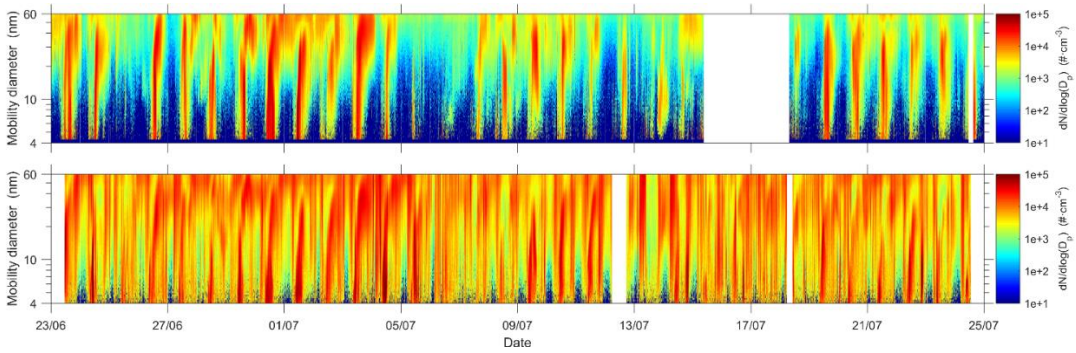

Figure 6.2 - Size distribution time evolution from 23 June to 24 July at SNS (top) and UGR (bottom) station.

6.4 /Growth and formation rate

Figure 6.3 presents the box-whiskers and time series of GRs recorded at SNS and UGR during the campaign. The $GR_{7\text{-}25}$ ranges from 4.5 to 9.5 nm h^{-1} at SNS, with a mean value (± standard deviation) of 6.9 ± 1.7 nm h^{-1}, and from 2.8 to 6.2 nm h^{-1} at UGR, with a mean value of 4.5 ± 1.0 nm h^{-1}. Also, $GR_{4\text{-}7}$ ranges from 3.0 to 5.9 nm h^{-1} at SNS, with a mean value of 4.1 ± 0.9 nm h^{-1}, and from 2.6 to 5.0 nm h^{-1} at UGR, with a mean value of 3.6 ± 0.8 nm h^{-1}. These values are in the range of GRs for urban and high-mountain environments reviewed by Nieminen et al. (2018) and Sellegri et al. (2019). The results show that $GR_{7\text{-}25}$ and $GR_{4\text{-}7}$ mean values at SNS remote station are larger than those observed at UGR station (Figure 6.3.a) and that $GR_{7\text{-}25}$ is always larger at SNS station (comparing same NPF class I event days) (Figure 6.3.b). It is surprising that the growth rates, especially $GR_{7\text{-}25}$, are on average larger at SNS than at UGR since higher precursor vapour concentrations are expected at the urban environment. This fact could have a special importance on cloud formations, since larger GR at SNS mountain station could be translated to larger survival probability of NPF particles to reach CCN sizes, due to shorter time needed for the growth. However, this fact is of importance after considering that ceiling size and shrinkage are not limiting factors to reach CCN size. Since ceiling

of particle growth mode ranges from 25 to 60 nm with a mean value of 41 nm during class I events at SNS site and shrinkage has not been observed at this site, NPF events at SNS site can affect CCN concentrations at least at high SS (e.g., Fan et al., 2018; Leaitch et al., 2016; Leng et al., 2014).

Another important result is that the difference between GRs at SNS and UGR stations is lower for the small size range, being 53% and 14% for the size range of 7-25 and 4-7 nm, respectively. It is important to note that, although it is not a direct method, the GR at lowest diameter ranges is a good indicator of the quantity of the condensable gases that contribute to the early growth of new particles. Thus, this result suggests that the initial steps of the aerosol formation have almost similar precursors and availability at both sites, resulting in only 14% relative difference of GR at 4-7 nm range. Also, the results suggest higher differences of the available gas

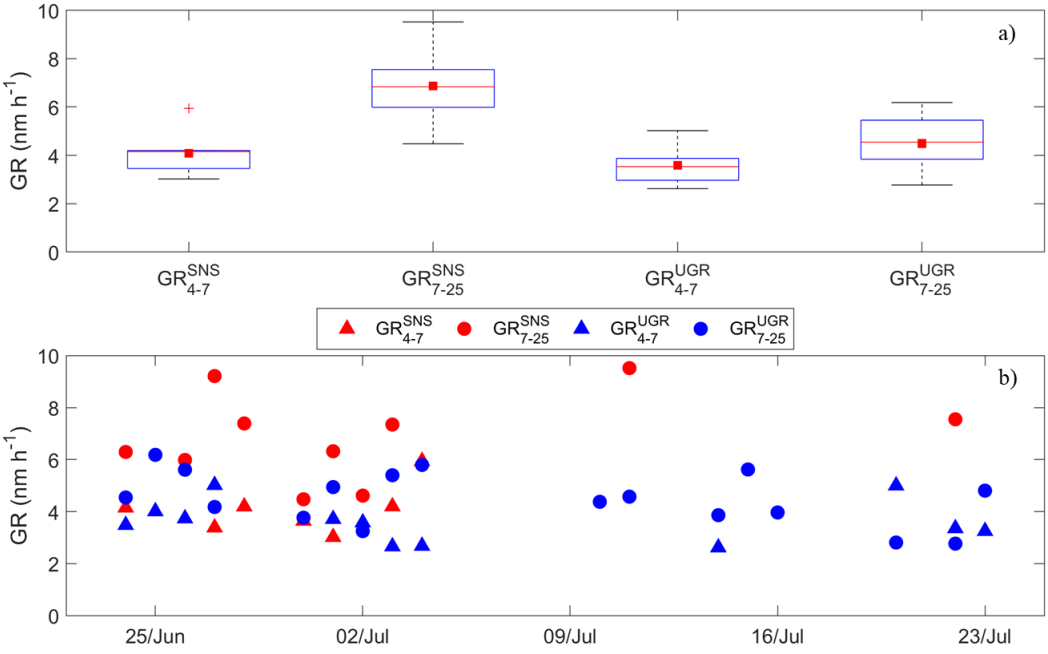

Figure 6.3 - (a) Box and whisker plot of growth rates recorded at SNS and UGR stations. The red line represents the median of the data, the square represents the mean of the data and the lower and upper edges of the box represent 25th and 75th percentiles of the data, respectively. The length of the whiskers represents 1.5× interquartile range which includes 99.3% of the data. (b) Growth rates time series at SNS and UGR station.

precursors for further steps of the aerosol growth, increasing the differences in GRs from 14% in 4-7 nm to 53% in 7-25 nm range. Also, the increase of GR as a function of the particle size suggests that the growth of the particles is not only due to the same vapours that form particles through nucleation.

However, due to the difference of altitude, the differences in temperature, RH and UV-B between both stations could contribute, at least partly, to this difference in GRs between SNS and UGR. In this sense, lower temperatures at SNS than at UGR (mean temperatures of 14 and 29 ºC during event days, respectively) can decrease the evaporation rates, enhancing the effective condensation and thus particle growth at lower temperatures. H_2SO_4 is produced from the $SO_2 + OH \rightarrow SO_3$ reaction and OH radicals are produced from water vapour UV absorption. Thus, higher RH and UV-B radiation at SNS (mean values of 44% and 2.6 W m^{-2} at SNS and 21% and 2.3 W m^{-2} at UGR) can increase the H_2SO_4-water nucleation and H_2SO_4 production, respectively, and thus enhance particle growth, especially in the initial NPF steps. Also, as Boulon et al. (2011) and Manninen et al. (2010) pointed, ion-mediated nucleation could be promoted at higher altitudes compared to low altitudes, and therefore can contribute to the observed differences. However, as Lehtipalo et al. (2016) showed, this mechanism only accelerates the growth of newly formed particles at low concentrations of base compounds. When a strongly basic compound is present, the growth of newly formed particles can be greatly enhanced by acid-base clusters. Thus, the presence of stabilizing vapours could also be responsible of the differences observed.

Figure 6.4 presents the box-whisker and time series of the Js (Formation Rates, J_4 and J_7), showing J_7 mean values of 1.3 ± 0.8 and 1.1 ± 1.2 cm^{-3} s^{-1} at SNS and UGR, respectively, and J_4 mean values of 2.1 ± 1.3 and 3.7 ± 5.2 cm^{-3} s^{-1}, respectively. The values of J_4 and J_7 show a large variability at both sites, ranging over one order of magnitude. These results differ from GRs results. In this case, J_4

mean value is 43% larger at UGR station, while J_7 mean value is 15% larger at SNS station. This result differs from that reported by Nieminen et al. (2018) since J_7 is expected to be higher at stations with higher anthropogenic influence. As can be seen in Figure 6.4, $GR_{4\text{-}7}$ takes slightly larger values at SNS station, and in contrast, J_4 shows significantly larger values at UGR station. This difference again points to the decoupling of the mechanisms leading to the initial particle formation and the subsequent growth of the particles. Also, in contrast to the particle formation rate, the particle growth rate increases as a function of particle size, suggesting the participation of other vapours than sulfuric acid. However, it is worth to mention that the formation rate of 4 and 7 nm particles are not only affected by the new particle formation rate but also by the scavenging of newly formed particles by coagulation into pre-existing particles.

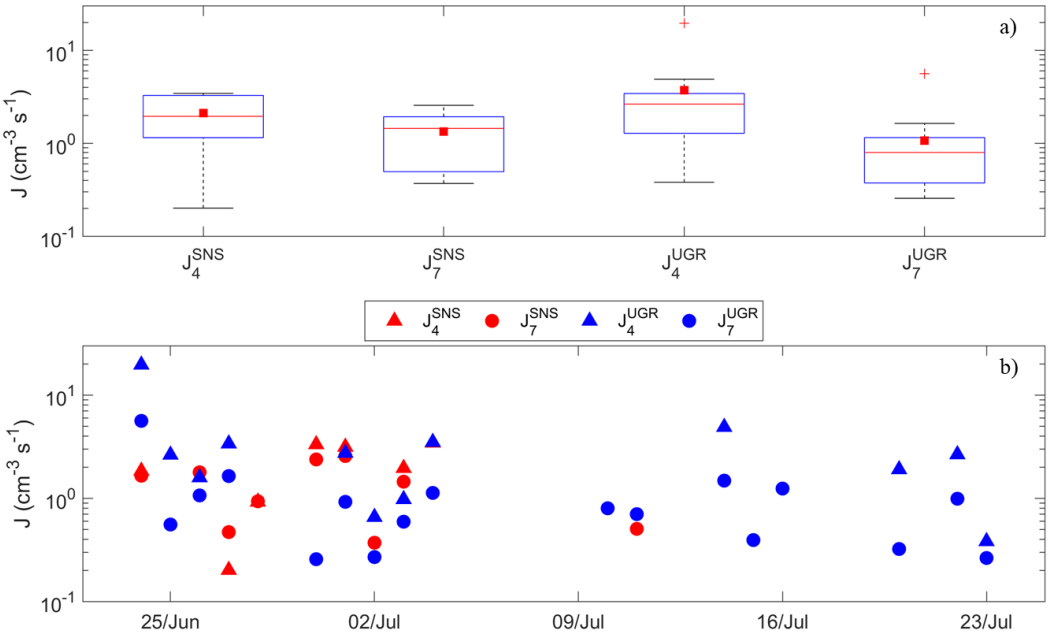

Figure 6.4 - (a) Box and whisker plot of formation rates recorded at SNS and UGR stations. The red line represents the median of the data, the square represents the mean of the data and the lower and upper edges of the box represent 25th and 75th percentiles of the data, respectively. The length of the whiskers represents 1.5× interquartile range which includes 99.3% of the data. (b) Formation rates time series at SNS and UGR station.

In order to quantify the contribution of sulfuric acid to the initial steps of the particle formation, the growth due to sulfuric acid was estimated in both 4-7 and 7-25 nm size ranges, GR^{SA}_{4-7} and GR^{SA}_{7-25}, respectively. Figure 6.5 shows the resulting sulfuric acid contribution to the total experimental growth rates at SNS and UGR. It is clear that sulfuric acid can only explain a small fraction of the growth rates retrieved in the ranges 4-7 and 7-25 nm at both measurement sites. The ratio GR^{SA}_{4-7}/GR_{4-7} is 9% at both stations, and the ratios GR^{SA}_{7-25}/GR_{7-25} are 0.8% and 1% at SNS and UGR, respectively. Thus, sulfuric acid explains similar small fraction of the experimental GRs at both sites during the study period and, despite a proxy sulfuric acid concentration was used here, these results strongly suggest a significant contribution of other vapours in this period at both sites. Furthermore, despite sulfuric acid is traditionally considered as one of the main factors for NPF events to occur, SO_2 and sulfuric acid concentrations are lower at SNS when events take place than on non-events days (figure not shown), indicating that sulfuric acid concentrations are sufficient for events to take place but not the factor that drives NPF events.

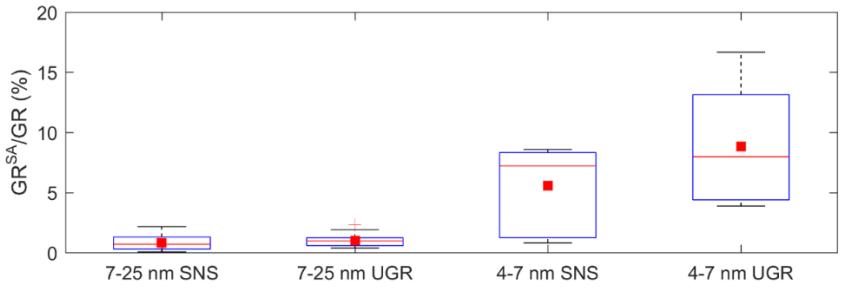

Figure 6.5 - Box and whisker plot of sulfuric acid contribution to the total measured growth rate at SNS and UGR. The red line represents the median of the data, the square represents the mean of the data and the lower and upper edges of the box represent 25th and 75th percentiles of the data, respectively. The length of the whiskers represents 1.5× interquartile range which includes 99.3% of the data.

Recent studies have suggested that volatile organic compounds (VOCs), especially extremely low-volatility ones, play vital roles in NPF processes promoting the initial growth of newly formed particles in the atmosphere (e.g., Tröstl et al., 2016). Unfortunately, VOC measurements are not available for the most part of the period

analyzed here. However, simultaneous measurements of VOCs were recorded at SNS and UGR during a short intensive period from 15 to 30 June 2017. Surprisingly, the analysis of these measurements shows that mean VOCs concentrations at SNS remote site was higher than at UGR urban station. Mean total VOCs concentrations of 9.9 and 5.1 $\mu g \cdot m^{-3}$ were observed at SNS and UGR, respectively, during the period 15 to 30 June. Thus, higher concentrations of VOCs at SNS, doubling approximately the UGR concentrations, could explain, at least partly, the higher growth rates observed at SNS as low-volatile vapours produced by photo–oxidation of VOCs could promote particle growth (e.g., Bianchi et al., 2019; Mohr et al., 2019).

6.5 /Condensation Sink and Survival Parameter

High pre-existing aerosol particle concentrations might also influence NPF events, inhibiting the process by increasing the competition for available condensable gases. In order to investigate the role of pre-existing aerosols, CS has been retrieved for the whole campaign period and averaged each day for 9.00-12.00 UTC time interval. As expected, the average CS obtained at UGR (6.7×10^{-3} s^{-1}) was higher than the average value of 2.2×10^{-3} s^{-1} obtained at SNS due to higher anthropogenic aerosol emissions close to UGR urban site. When considering event and non-event days, the CS was higher on event days (2.9 and 6.7×10^{-3} s^{-1} at SNS and UGR, respectively) compared to non-event days (1.8 and 6.6×10^{-3} s^{-1} at SNS and UGR, respectively), indicating that CS does not play a significant role in NPF processes at both sites. It is worth mentioning that the role of CS in NPF processes differs from one high altitude site to other as Sellegri et al. (2019) pointed out. For example, Boulon et al. (2011) at Puy de Dôme station, Venzac et al., (2008) at the Nepal Climate Observatory Pyramid station and Lv et al. (2018) at Mount Tai found that higher CS inhibits the occurrence of NPF events. However, Boulon et al. (2010) at

Jungfraujoch station, García et al. (2014) at Izaña station and Rose et al. (2015) at Chacaltaya station found that higher CS observed in these sites does not inhibits the occurrence of NPF events. Overall, a detailed understanding of the role of CS in NPF events remains an open question and the chemical composition of CS could play an important role on the NPF processes (Tuovinen et al., 2020).

Looking on event days, Figure 6.6 shows the relationship between CS and J_7 and $GR_{7\text{-}25}$ at both measurement sites. As can be seen J_7 increases with increasing CS at both measurement sites. This result is contrary to the expected one, since concentration of vapours participating in NPF are expected to decrease with increasing CS due to their faster loss rate. However, this result suggests that CS and the concentrations of condensing vapours are connected. This is also supported by our previous observation showing that both CS and H_2SO_4 are higher during the NPF event days than during non-event days. On other hand, $GR_{7\text{-}25}$ tends to decrease as CS increases, especially at SNS site (Figure 6.6). Thus, this result shows that lower CS favours the growth of particles as should be expected. In this sense, as our previous results suggested, this difference in the relationship between CS and J_7 and $GR_{7\text{-}25}$ points again to the decoupling of the mechanisms leading to the initial particle formation and the subsequent growth of the particles.

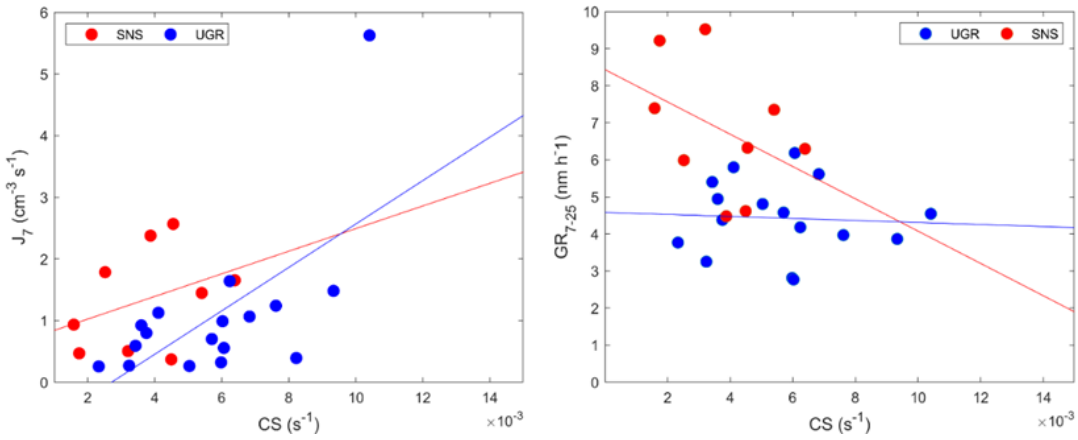

Figure 6.6 - Relationship between CS (time window: 9:00-16:00 UTC) and J_7 (left) and $GR_{7\text{-}25}$ (right) during study period.

The survival probability of growing clusters links the competition between their growth and scavenging by pre-existing aerosol particles. The key parameter to estimate the clusters survival was defined by Kulmala et al. (2017) as the ratio between the CS and GR (Eq. 6.5). Our results show that the survival parameter (*P)* ranges from 2 to 10 at SNS with a mean value of 6 ± 3 and from 6 to 24 at UGR with a mean value of 13 ± 6. At both sites, the values of *P* are below the threshold value of 50 for NPF to take place (Kulmala et al., 2017). Larger survival parameter indicates that a smaller percentage of newly formed particles will survive to greater sizes (smaller survival probability). In this sense, lower P values observed at SNS suggests that survival probability of newly formed particles at this site is higher than at UGR urban station.

6.6 /Case study: NPF during Saharan dust intrusion

Mineral dust contributes to a major fraction of the global coarse mode aerosol load, with an emission rate into the atmosphere currently estimated at 1,000–3,000 Tg yr^{-1} from the Earth's surface (Tegen and Schepanski, 2009). Due to its proximity to the African continent, Granada region is frequently affected by Saharan dust intrusions, especially in summer (Mandija et al., 2017; Valenzuela et al., 2015). These African dust intrusions usually transport large mineral dust loads to our study area (e.g., Benavent-Oltra et al., 2019; Lyamani et al., 2006). During the analysed period, there was an intrusion of Saharan dust over the region of study from 24 to 27 June, as confirmed by CALIMA warning system (www.calima.ws; Figure S5). For the confirmation of desert dust intrusions over different regions in the Iberian Peninsula, CALIMA network uses information derived from different sources, including models, air mass back-trajectory analysis, synoptic meteorological charts, satellite and surface PM_{10} data. As shown in Figure 6.7.a, there was a significant

increase in the coarse particle number concentration (N_C, aerodynamic size range 1-20 μm) during 24-27 June, supporting the presence of desert dust over SNS station during these days. According to the N_C analysis it seems that the dust event ended around 10:00 UTC on 27 June, when N_C began to decrease reaching concentrations similar to those observed before the dust intrusion on 23 June. Figure 6.7.b shows the 24-h PM_{10} mass concentration (starting at 07:00 UTC) and the percentage of mineral aerosol on each measurement filter from 07:00 of 23 June to 07:00 of 29 June. It is worth to mention that the last PM_{10} filter measurement was collected during a period of 48-h from 07:00 UTC of 27 June to 07:00 UTC of 29 June. As can be seen, PM_{10} mass concentrations recorded at SNS remote station were higher than 23 μg m^{-3} from 24 June until 27 June and after this period PM_{10} concentration decreases drastically to 7 μg m^{-3} on 27-29 June; typical background PM_{10} concentration reported for European mountain sites (e.g., Dinoi et al., 2017). Also, mineral aerosol component contributed more than 65% to the total aerosol mass

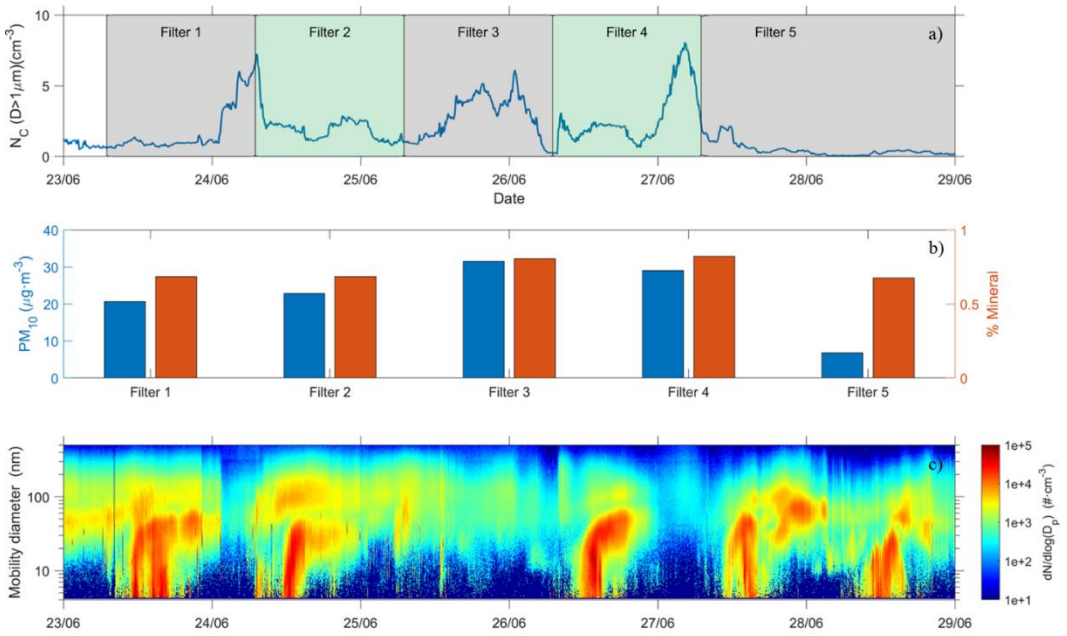

Figure 6.7 - Temporal evolution of (a) coarse mode aerosol number concentration, (b) PM_{10} concentration and mineral matter fraction (%) and (c) aerosol size distribution from 23 to 29 June at SNS station.

concentration for each measurement day, reaching highest mineral contribution on filters 3 and 4 (25 and 26 June) with a relative contribution above 80% (Figure 6.7.b). Also, high concentrations of Fe_2O_3 and Ca (good tracers of desert dust aerosol) were observed (Table 6.3), confirming again the presence and the large impact of Saharan desert dust on aerosol population over our site during 24-27 June.

Table 6.3 - Concentration of Ca, K, Fe_2O_3 and Fe_2O_3 during the period 23-29 June.

($\mu g\ m^{-3}$)	**Filter 1 23 June**	**Filter 2 24 June**	**Filter 3 25 June**	**Filter 4 26 June**	**Filter 5 27-29 June**
Ca	1.05	0.91	1.22	0.94	0.46
K	0.30	0.34	0.53	0.47	0.13
Fe_2O_3	1.00	1.18	1.91	1.89	0.33
TiO_2	0.13	0.15	0.24	0.24	0.04

As discussed before, high pre-existing aerosol particle loadings have been thought to suppress NPF events due to high condensation and coagulation sinks. In this sense, the NPF events are not expected to occur under desert dust episodes, especially at remote sites where the concentrations of condensable vapours are expected to be low. Also, desert dust intrusions with high concentrations of mineral dust particles are expected to reduce the concentrations of condensing vapours and the clustering by limiting solar radiation and hence photochemical oxidation of gaseous precursors, which also reduce the probability of occurrence of NPF events during desert dust events. However, although Saharan dust and NPF events are not expected to occur simultaneously at SNS site, two NPF events classified as class I were observed at SNS on 24 and 26 June during the desert dust intrusion that occurred in the period 24 to 27 June (Figure 6.7.c). However, no NPF event was observed on dusty day on 25 June although PM_{10} concentration on this day was similar to that registered on 24 and 26 June. Below, the factors that promote or inhibit the occurrence of NPF events in the presence of mineral dust will be investigated.

The evolution of the averaged daily CS (from 9:00 to 12:00 UTC) during these three days shows higher values on 24 June (5.6×10^{-3} s^{-1}), decreasing more than 40% and 70% on 25 (3.2×10^{-3} s^{-1}) and 26 June (1.6×10^{-3} s^{-1}), respectively. Thus, CS seems not to be a limiting factor for the occurrence of NPF event on 25 June (dusty day). It is important to note that in these cases, the number concentration of coarse mode particles has been considered for CS retrievals. However, the contributions of coarse particles to the CS during these cases are below 10%, because the contribution of coarse particles in the continuum regime is proportional to the particles diameter (D_p) instead of D_p^2 (Pirjola et al., 1999).

Figure 6.8.a shows sulfuric acid and VOCs (24h filter sampling starting 07:00 UTC) concentrations and Figure 6.8.b shows GRs and Js retrievals at SNS site during 23-28 June period. Mean J_7 value of 1.72 cm^{-3} s^{-1} was retrieved for the two NPF events observed on 24 and 26 June dusty days. This J_7 value is slightly higher than the mean value observed for the whole campaign (1.35 cm^{-3} s^{-1}), suggesting that during these dusty days there were larger production rates of condensing vapours or more

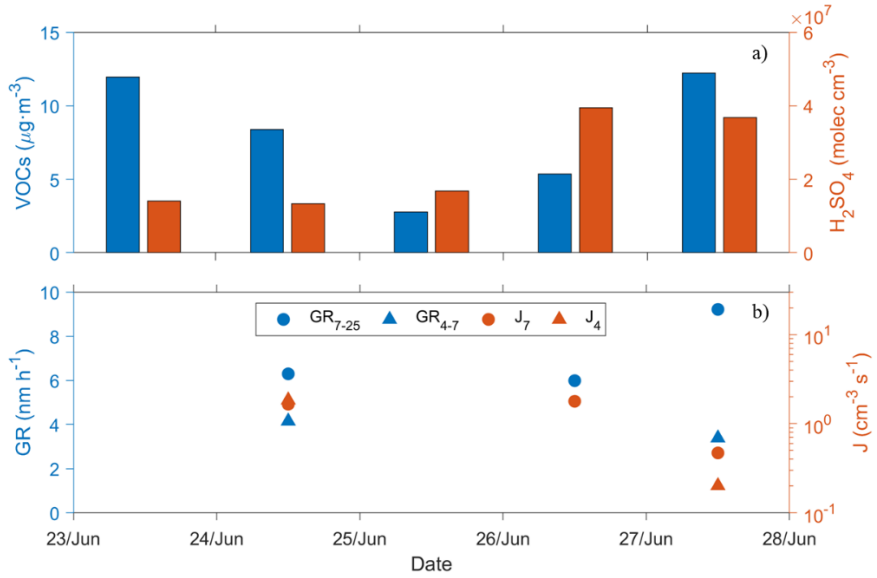

Figure 6.8 - (a) VOCs and H_2SO_4 concentration and (b) GR and J in different size ranges from 23 to 28 June observed at SNS station.

favourable conditions for condensation. The opposite behaviour is found for $GR_{7\text{-}25}$, since $GR_{7\text{-}25}$ value of 6.1 nm h^{-1} was retrieved for the two NPF events observed on 24 and 26 June, which is slightly lower (14% relative difference) than the value observed during the overall campaign (6.9 nm h^{-1}). This lower GR values obtained on NPF events on dusty days may be due to the increase of CS or to its effectiveness during dusty days, which again points to the decoupling of the mechanisms leading to the initial particle formation and the subsequent growth of the particles.

The $GR_{7\text{-}25}$ shows similar values on 26 June (6.0 nm h^{-1}) and 24 June (6.3 nm h^{-1}). This is contrary to the expected from CS and H_2SO_4 concentrations. Firstly, on 26 June the CS mean value was 70% lower than on 24 June. Secondly, despite no direct measurements of sulfuric acid were available, the sulfuric acid concentration estimated by proxy on 26 June (4.0×10^7 molec cm^{-3}) was 3 times higher than on 24 June (1.3×10^7 molec cm^{-3}). As discussed before, the estimated concentrations of sulfuric acid could only explain less than 10% of the observed GRs. These results evidence that sulfuric acid and CS don't play a relevant role in the particle growth during the NPF events observed during these dusty days. However, the significantly high VOCs concentration observed on 24 June (8.4 µg m^{-3}) as compared to 26 June (5.4 µg m^{-3}) can explain at least partly the differences observed on GR from 24 to 26 June.

Furthermore, the results suggest that sulfuric acid is not a limiting factor for the occurrence of NPF event on 25 June dusty day, since an increase on sulfuric acid concentrations is observed from 24 to 25 June (Figure 6.8.a). However, as can be seen in Figure 6.8.a, VOCs concentration showed a decrease by ~67% from 24 to 25 June. The significant reduction of VOCs concentrations on 25 June could be a possible factor limiting the occurrence of NPF on this dusty day. Thus, the results point to VOCs as one of the main driving factors controlling the occurrence of NPF event and subsequent particle growth at SNS site during Saharan dust events.

Finally, the chemical composition of desert dust particles (acting as CS) may be another important factor that can play a significant role in the occurrence of NPF events during dust events. In fact, recent laboratory and observational studies (Dupart et al., 2012; Nie et al., 2014) revealed that the presence of TiO_2 and Fe_2O_3 (which are common components of mineral dust) under UV light could promote the occurrence of NPF can enhance the formation of OH and other radicals that favour oxidation reactions, promoting the occurrence of NPF during dusty conditions. These components, acting as catalysts, are not consumed in the photo-catalytic reaction and can accelerate atmospheric photochemistry repeatedly. The PM_{10} elemental analysis shows that both components reached their highest concentrations on 25 and 26 June, with TiO_2 concentrations of 0.24 μg m^{-3} on both days and F_2O_3 concentrations of 1.91 and 1.89 μg m^{-3} on 25 and 26 June, respectively (Table 6.3). It is worth noting that the effectiveness of photochemical reactions in promoting the occurrence of NPF depends largely on the available precursor gases. Thus, the increased TiO_2 and F_2O_3 concentrations together with the high concentrations of H_2SO_4 and VOCs observed on 26 June, could explain, at least partly, the occurrence of NPF and the observed high formation rates during this dusty day (26 June). However, although the concentrations of TiO_2 and F_2O_3 on June 25 (non-event day) were high and comparable to those observed on 26 June, the low availability of precursor gases on this dusty day seems to be the cause of the non-occurrence of NPF event. Summarizing, these findings suggest that TiO_2 and Fe_2O_3 could promote NPF events during dusty conditions, but the availability of VOCs seems to be the main factors controlling the occurrence of NPF events in this area. To improve our understanding in this topic, further investigation accompanied by multiplatform measurement campaigns is needed.

6.7 /Conclusions

In this section, the aerosol size distribution was investigated at two stations located close to each other (~20 km), but at different altitudes: urban (UGR; 680 m a.s.l.) and high-altitude remote (SNS; 2500 m a.s.l.) site, both in the area of Granada (Spain). Results show the important contribution of nucleation mode aerosols to the total particle number concentration at both sites, with a contribution of 47% and 48% at SNS and UGR, respectively. Despite SNS remote site is less influenced by anthropogenic emissions, temporal evolution of aerosol total concentration shows larger concentrations at SNS site during some days, associated with high concentrations of nucleation mode particles.

New particle formation (NPF) events were studied in detail due to their high frequency of occurrence (>70% at both sites) and their significant contributions to total aerosol number concentrations. Our analysis suggests that NPF events at SNS remote site are associated with the transport of precursor vapours from lower altitudes by orographic buoyant upward flows. NPF events at SNS site are always observed from the smallest measured sizes of the aerosol size distribution (4 nm), implying that NPF takes place at or in the vicinity of the high altitude SNS station rather than transported from lower altitudes. However, despite the connection between the occurrence of NPF events at the mountain and urban site, different growth rates (GRs) were observed at both stations; the GRs at SNS site were larger than those at UGR site ($GR_{7\text{-}25}$ of 6.9 and 4.5 nm h^{-1} and $GR_{4\text{-}7}$ of 4.1 and 3.6 nm h^{-1} at SNS and UGR, respectively). This fact could have a special importance on the production of cloud condensation nuclei (CCN) and therefore on cloud formations which may affect regional/global climate, since larger GR at mountain sites could be translated to larger survival probability of NPF particles to reach CCN sizes, due to shorter time needed for the growth. The increase in GR differences between SNS and UGR with increasing size (increasing from 14% in the size range of 4-7 nm to 53%

in the range 7-25 nm) suggests higher concentrations of the available gas precursors, other than sulfuric acid, for further steps of the aerosol growth. This was also supported by the low contribution of sulfuric acid to the observed GRs at both sites (<1% and <10% for 7-25 and 4-7 nm size range, respectively). A deep analysis of the role of precursor gases in NPF processes points to the volatile organic compounds (VOCs) as one of the main factors controlling the NPF events at both sites.

Higher condensation sink (CS) values on event days compared to non-event days were observed at both measurement sites, suggesting that CS is not the limiting factor of NPF processes at either of the sites. In fact, the obtained results suggest that the availability of condensable vapours at SNS is closely connected to CS. In this sense, although Saharan dust and NPF events are not expected to occur simultaneously at SNS remote site, two NPF events were identified during an intrusion of Saharan dust. A close analysis of these two NPF events suggest that TiO_2 and Fe_2O_3 could promote NPF events, but the availability of VOCs seems to be the main factor controlling the occurrence of NPF events during dusty conditions. Despite further investigation is needed to improve our understanding in this topic, this result suggests that climate effects of mineral dust and NPF are not disconnected from each other as it was commonly thought. Therefore, since mineral dust contributes to a major fraction of the global aerosol mass load, dust-NPF interaction should be taken into account in global aerosol-climate modelling for better climate change prediction.

7 /General conclutions and perspectives

Throughout this thesis, at the end of each of the results chapters, the main conclusions obtained have been presented. Thus, this section presents the main conclusions on fine atmospheric aerosol particles sources (their strength, spatial and temporal variability as well as their contributions to ambient aerosol concentrations) at three different environments in the south-eastern Iberian Peninsula, including urban, suburban and high-altitude remote environments.

The results showed that the aerosol number concentrations and the strength of aerosol sources exhibit large temporal and spatial variability at the study area. First, long dataset of total atmospheric particle number concentrations ($N_{>2.5}$) in a 50 m height tower at Granada urban area was analysed (Section 4). The $N_{>2.5}$ showed a clear seasonal variability of aerosol number concentration with the highest aerosol number concentrations during winter (12.0×10^3 cm^{-3}) and the lowest during summer season (7.5×10^3 cm^{-3}). The overall mean aerosol number concentration at this urban site was of 9.6×10^3 cm^{-3} which was in the typical range observed in other European urban areas. On the other hand, the results regarding the spatial variability of aerosol number concentrations were presented and discussed in Sections 5 and 6. As expected, large differences were observed in total aerosol number concentrations measured at the urban and high-altitude remote sites during the SLOPE II summer campaign (Section 6), with average total particle number concentration two-fold at urban environment ($N_{4\text{-}500} = 8.4 \times 10^3$ cm^{-3}) than at the high-altitude remote environment ($N_{4\text{-}500} = 3.4 \times 10^3$ cm^{-3}). By contrast, unexpected similar (13%

difference) total aerosol concentrations were measured at the urban ($N_{12\text{-}600}$ = 13.4 × 10^3 cm^{-3}) and suburban ($N_{12\text{-}600}$ = 11.6 × 10^3 cm^{-3}) environments during the AMICUS winter campaign (Section 5), both with average values in the typical range for European urban sites. The large temporal and spatial variability of aerosol number concentrations in Granada urban area was mainly due to the variability in (1) emissions sources and their strength, (2) meteorological conditions and (3) atmospheric boundary layer dynamic as was shown in Section 4.

The analysis of the aerosol number flux measurements obtained by eddy covariance technique on the top of the tower at a height of 50 m above ground level at Granada urban area showed that Granada acted as a net source of aerosol particles to the atmosphere at different time scales. Furthermore, a close analysis of the diurnal, weekly and sectorial variability of aerosol number fluxes showed a significant impact of traffic emissions on ambient aerosol concentrations over Granada urban area in all seasons, and a relatively important impact of domestic heating and agricultural waste burning emissions in winter, as well as the influence of new particle formation processes in summer and spring seasons.

In addition to the unexpected similar total aerosol concentrations observed at the urban and suburban environments during AMICUS winter campaign, very similar black carbon (BC) concentrations were also observed at both sites. Source apportionment of BC showed that these similar concentrations have in fact different origins, with larger impact of biomass burning sources at the suburban site in comparison to the urban site In this sense, 34% and 23% of the observed BC concentrations during the AMICUS winter campaign at suburban and urban sites, respectively, were associated with BC from biomass burning origin, evidencing the relevant role of aerosol particles from biomass burning sources in the study area during winter. Thus, in order to quantify the contribution of the different aerosol sources to the ambient aerosol number concentration at these sites influenced by

biomass burning emissions, a new approach based on the Rodriguez and Cuevas (2007) and Sandradewi et al. (2008) methods was developed and presented in Section 5. This new approach made possible the quantification of the contributions of both vehicle and biomass burning primary emissions as well as secondary aerosol to the size-segregated particle number concentrations at both measurement sites. This new method was applied to the simultaneous measurements of aerosol size distribution in the 12–600 nm size range and black carbon (BC) concentrations obtained at suburban and urban sites sites during winter AMICUS campaign, when the study area is usually influenced by biomass burning emissions from domestic heating and agricultural waste burning. The results showed that (1) secondary aerosol particles concentrations were the main contributor to the ambient aerosol number concentrations in all aerosol particles size ranges at both sites, (2) primary vehicle exhaust particles concentrations were the main contributor to primary particles (>70%) in all size ranges at both sites and (3) primary biomass burning particles concentrations contribute significantly to the primary particles in the 25–100 and 100–600 nm size ranges at the suburban (24% and 28%, respectively) and urban (13% and 20%, respectively) sites. In order to examine sources' strength along the year and their contributions to particle number concentrations, the new approach was also applied to an extended dataset obtained at the urban site. As expected, vehicle exhaust was found to be the main source of primary particles along the year in the urban station. In addition, new particle formation (NPF) events were found to be an important aerosol source only during summer noon hours but, on average, these events do not implicate a considerable contribution to urban particles.

Despite the low contribution of NPF events to the total particle number concentration in the urban area, especially in the winter season, these events are of great importance for the production of cloud condensation nuclei (CCN), affecting clouds formation. Therefore, the characterization of NPF vertical distribution is of special interest, especially at high altitudes where clouds are usually formed. To this

end, a detailed characterization of NPF events and investigation of the factors that promote/inhibit NPF processes was performed at two contrastive sites: urban (UGR) and high-altitude remote (SNS) sites. For this, simultaneous measurements of aerosol size distributions (4-500 nm) measured during SLOPE II summer campaign at these contrastive sites were used. In addition to the expected large differences on aerosol number concentrations at both measurement sites (urban concentrations were two-fold than at high-altitude remote site), the analysis showed that nucleation mode particles contribute greatly to the total aerosol number concentration at both sites (47 % and 48 % at SNS and UGR, respectively). This high contribution was mainly due to the large NPF event frequency (>70%) observed at both sites during this summer campaign. At SNS, NPF events were found to be associated with the transport of gaseous precursors from lower altitudes by orographic buoyant upward flows. Nevertheless, NPF events at SNS site were always observed from the smallest measured sizes of the aerosol size distribution (4 nm), implying that NPF takes place in or in the vicinity of the high-altitude SNS station rather than being transported from lower altitudes. Although NPF events at the mountain site seemed to be connected with those occurring at the urban site, the growth rates (GRs) at SNS were higher than those at the UGR site. The analysis of sulfuric acid (H_2SO_4) concentrations showed that the concentrations of H_2SO_4 only explain a marginal fraction of the observed GRs at both sites (<1% and <10% for the 7–25 and 4–7 nm size ranges, respectively), indicating that other condensing vapours were responsible for the majority of particle growth, as well as the differing growth rates between the two sites. The results also showed that the condensation sink (CS) did not play a relevant role in NPF processes at both sites and pointed to the availability of volatile organic compounds (VOCs) as one of the main factors controlling the NPF events at both sites.

Future research will be necessary in order to continue advancing in the aspects approached in this thesis, making emphasis in some important topics:

- Further efforts are needed to identify the cause and the sources of the high aerosol load events observed at Granada urban area during downward particle fluxes. These downward particle fluxes can be attributed to (1) updrafts of relatively particle depleted air from surface or (2) to downdrafts of relatively particle enriched air from aloft (entrainment). Thus, a detailed information on the vertical distribution of aerosol size distribution and the aerosol chemical composition will help to address this issue.
- Since SMPS and AE33 data are readily available from open databases as those generated by ACTRIS or SARGAN networks, the new approach developed in the frame of this thesis will be applied to assess the impact of traffic, biomass burning and secondary sources around the globe, giving more insights into secondary and primary contributions to total particle number concentrations.
- These aerosol sources contributions will be also linked with the impact of each source on health but also on the production of potential cloud condensations nuclei and their different activation properties depending on the aerosol source.
- Further efforts will also be done to study the new particle formation pathways in the study area using a larger dataset, with especial emphasis on the organic compounds involved on the formation and growth processes. Real-time measurements of the organic compounds will be useful to improve our understanding of the formation pathways.
- The role of condensation sink on new particle formation events will be investigated from a multi-site perspective, with special emphasis on

the impact of dust particles on the inhibition or promotion of NPF. For this, online measurements of dust particles chemical composition during ambient NPF events and laboratory experiments will give more insight about the role of dust on the inhibition or promotion of NPF.

/Conclusiones generales y perspectivas

A lo largo de esta tesis, al final de cada uno de los capítulos de resultados, se han presentado las principales conclusiones obtenidas. Por tanto, en esta sección se presentan las principales conclusiones sobre la variabilidad de las fuentes de partículas finas de aerosol atmosférico (su variabilidad espacio-temporal y de intensidad, así como sus contribuciones a las concentraciones de partículas) en tres ambientes diferentes del sureste de la Península Ibérica: urbano, suburbano y remoto de alta montaña.

Los resultados mostraron que la concentración numérica de partículas y la intensidad de las fuentes presentan una gran variabilidad espacio-temporal en el área de estudio. En primer lugar, se ha analizado la concentración total de partículas ($N_{>2.5}$) en una torre de 50 m de altura en el entorno urbano de Granada (Sección 4). Dicha base de datos ha mostrado la clara variabilidad estacional de la concentración total de aerosol, con las mayores concentraciones numéricas de partículas observadas durante el invierno (12.0×10^3 cm^{-3}) y las más bajas durante el verano (7.5×10^3 cm^{-3}). Por otro lado, los resultados sobre la variabilidad espacial de la concentración numérica de partículas se han discutido en las Secciones 5 y 6. Como era de esperar, se han observado grandes diferencias en las concentraciones numéricas totales de partículas entre el ambiente urbano y el de alta montaña durante la campaña SLOPE II, llevada a cabo en verano (Sección 6). En este sentido, la concentración total de partículas en el ambiente urbano ($N_{4\text{-}500} = 8.4 \times 10^3$ cm^{-3}) fue dos veces superior a la observada en el entorno de alta montaña ($N_{4\text{-}500}$ = 3.4 ×

10^3 cm^{-3}). Por el contrario, se han encontrado concentraciones de aerosoles totales inesperadamente similares (13% de diferencia) en los entornos urbano ($N_{12\text{-}600}$ = 13.4 × 10^3 cm^{-3}) y suburbano ($N_{12\text{-}600}$ = 11.6 × 10^3 cm^{-3}) durante la campaña de invierno, AMICUS, ambos entornos con valores medios en el rango típico de los observados para otros sitios urbanos europeos (Sección 5). La gran variabilidad espacio-temporal en las concentraciones numéricas de aerosoles en el área de estudio se debe principalmente a la variabilidad en (1) las fuentes de emisión y su intensidad, (2) las condiciones meteorológicas y (3) la dinámica de la capa límite atmosférica, como se ha mostrado en la Sección 4.

El análisis de las medidas de flujo vertical de partículas obtenidas mediante la técnica *eddy covariance* en la parte superior de una torre de 50 m de altura en el entorno de urbano de Granada ha mostrado que Granada actúa como fuente neta de partículas de aerosol a diferentes escalas temporales. Además, el análisis de la variabilidad diurna, semanal y sectorial (sectores de vientos) de los flujos de aerosol ha mostrado un impacto significativo de las emisiones de tráfico en las concentraciones numéricas de partículas en el área urbana durante todas las estaciones del año. Además, se ha mostrado un impacto relativamente importante en invierno por parte de las emisiones de los sistemas de calefacción doméstica y de la quema de residuos agrícolas, así como un impacto importante de los procesos de formación de nuevas partículas durante los meses de verano y primavera.

Además de las inesperadas similares concentraciones de aerosol en el entorno urbano y suburbano durante la campaña de invierno (AMICUS), también se han observado concentraciones similares de carbono negro (BC) en ambos ambientes. En este sentido, durante dicha campaña AMICUS el 34% y el 23% de las concentraciones de BC observadas en los emplazamientos suburbanos y urbanos, respectivamente, estaban asociadas al BC procedente de la quema de biomasa. Esto puso de manifiesto el papel relevante de las partículas procedentes de la quema de biomasa en la zona de

estudio durante el invierno. Por tanto, para cuantificar la contribución de las diferentes fuentes de aerosol a la concentración numérica total de partículas en estos sitios influenciados por las emisiones de la quema de biomasa, se ha desarrollado un nuevo método basado en los métodos de Rodríguez y Cuevas (2007) y Sandradewi et al. (2008) y presentado en la Sección 5. Este método ha permitido cuantificar las contribuciones de las emisiones primarias de los vehículos y de la quema de biomasa, así como de los aerosoles secundarios, a las concentraciones de número de partículas segregadas por tamaño en ambos sitios de medida. Este nuevo método se ha aplicado a las medidas simultáneas de la distribución numérica de partículas en el rango de tamaño de 12-600 nm y a las concentraciones de carbono negro (BC) obtenidas en ambos entornos durante la campaña de invierno de AMICUS, cuando el área de estudio suele estar influenciada por las emisiones de la quema de biomasa procedentes de la calefacción doméstica y la quema de residuos agrícolas. Los resultados mostraron que (1) el aerosol secundario es el principal contribuyente en todos los rangos de tamaño de las partículas en ambos sitios, (2) la concentración numérica de partículas primarias emitidas por los vehículos es el principal contribuyente a las partículas primarias (>70%) en todos los rangos de tamaño en ambos sitios y (3) las concentraciones de partículas primarias procedentes de la quema de biomasa contribuyen significativamente a las partículas primarias en los rangos de tamaño de 25-100 y 100-600 nm en los entornos suburbano (24% y 28%, respectivamente) y urbano (13% y 20%, respectivamente). Además, este nuevo método se ha aplicado a una base de datos más extensa en la estación urbana para examinar la intensidad de las fuentes a lo largo del año y sus contribuciones a las concentraciones numéricas de partículas. Como se esperaba, el tráfico ha resultado ser la principal fuente de partículas primarias a lo largo del año en la estación urbana. Además, se ha encontrado que los eventos de formación de nuevas partículas (NPF) son una fuente importante de aerosoles durante las horas centrales del día en verano, pero, en promedio, estos eventos no implican una contribución considerable a las partículas urbanas.

A pesar de la baja contribución de los eventos de NPF a la concentración total de número de partículas en la zona urbana, estos eventos son de gran importancia para la producción de núcleos de condensación de nubes, afectando a la formación de estas. Por lo tanto, la caracterización de la distribución vertical de los eventos de NPF es de especial interés. Para ello, se ha llevado a cabo una investigación detallada de las características de los eventos de NPF y de los diferentes factores que promueven/inhiben los procesos de NPF en dos ambientes distintos: urbano y remoto en alta montaña. Para ello, se han utilizado mediciones simultáneas de las distribuciones de tamaño de los aerosoles (4-500 nm) medidas en ambos sitios. El análisis muestra que, con una frecuencia de eventos NPF >70% en ambos sitios, las partículas del modo de nucleación contribuyen en gran medida a la concentración numérica total de aerosoles en verano (47% y 48% en la estación de alta montaña y urbana, respectivamente). En la estación de alta montaña, se ha encontrado que los eventos de NPF están asociados al transporte de precursores gaseosos desde altitudes más bajas gracias al transporte ascendente debido a la orografía del terreno. Sin embargo, los eventos de NPF en la estación de alta montaña siempre se han observado a partir de los tamaños más pequeños medidos de la distribución de tamaño de aerosoles (4 nm), lo que implica que los eventos de NPF tienen lugar en la estación de alta montaña (o en sus proximidades), en lugar de ser transportados desde altitudes inferiores. Aunque los eventos de NPF en la estación de montaña parecen estar conectados con los que ocurren en el sitio urbano, las tasas de crecimiento (GR, por sus siglas en inglés) en la estación de montaña son más altas que las de la estación urbana. El análisis del ácido sulfúrico (H_2SO_4) muestra que las concentraciones de H_2SO_4 pueden explicar una contribución mínima a las tasas de crecimiento observadas en ambos sitios (< 1 % y < 10 % para los rangos de tamaño de 7-25 y 4-7 nm, respectivamente), indicando que otros vapores de condensación son los responsables de la mayor parte del crecimiento de las partículas, así como de las diferentes tasas de crecimiento entre los dos ambientes.

Los resultados también muestran que el sumidero de condensación (CS) no juega un papel relevante en los procesos de NPF en ambos sitios y apunta a la disponibilidad de compuestos orgánicos volátiles como uno de los principales factores que controlan los eventos de NPF en los ambientes urbanos y remotos investigados.

Será necesario realizar futuras investigaciones para seguir avanzando en los aspectos desarrollados en eta tesis, haciendo hincapié en algunos aspectos:

- Es necesario investigar la causa y las fuentes de los eventos de flujos negativos de aerosol en el área urbana de Granada. Estos eventos de flujos negativos pueden deberse a (1) corrientes ascendentes de aire desde la superficie relativamente pobres de partículas o (2) a corrientes descendentes de aire relativamente ricas en partículas desde capas más altas. Por lo tanto, más información sobre la distribución vertical de la distribución tamaño de partículas y de la composición química de los mismos ayudará a abordar esta cuestión.
- Dado que los datos de SMPS y AE33 están fácilmente disponibles en bases de datos abiertas como las generadas por las redes ACTRIS o SARGAN, el nuevo método desarrollado en el marco de esta tesis se aplicará para evaluar el impacto del tráfico, la quema de biomasa y las fuentes secundarias en más áreas, lo que permitirá conocer mejor las contribuciones de las partículas secundarias y primarias a las concentraciones totales de número de partículas.
- Estas contribuciones de las fuentes de aerosol también se relacionarán con el impacto de cada fuente en la salud, pero también en la potencial producción de núcleos de condensación de nubes por cada una de las fuentes.

- El estudio de las vías de formación de nuevas partículas en la zona de estudio se realizará con un conjunto de datos más amplio, haciendo hincapié en los compuestos orgánicos implicados en los procesos de formación y crecimiento.
- El papel de los sumideros de condensación (*condensation sink*, CS) en los eventos de formación de nuevas partículas se investigará desde una perspectiva multisitio, con especial énfasis en el impacto de las partículas de polvo en la inhibición o promoción de la formación de nuevas partículas.

Supplementary figures

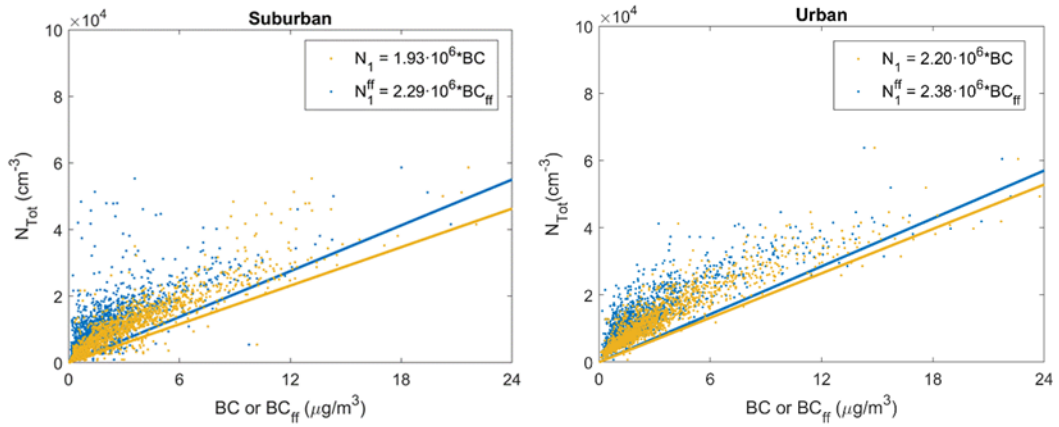

Figure S1 - Total particle number concentration vs BC or BC_{ff} scatters plots for the urban and suburban sites.

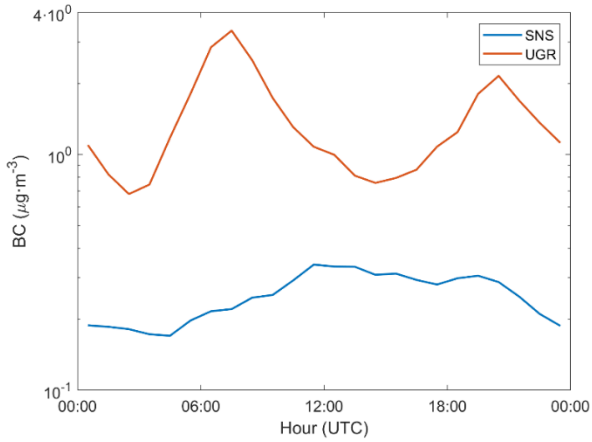

Figure S2 - Mean diurnal variation of BC concentration (µg m^{-3}) at SNS and UGR for the whole analysed campaign period.

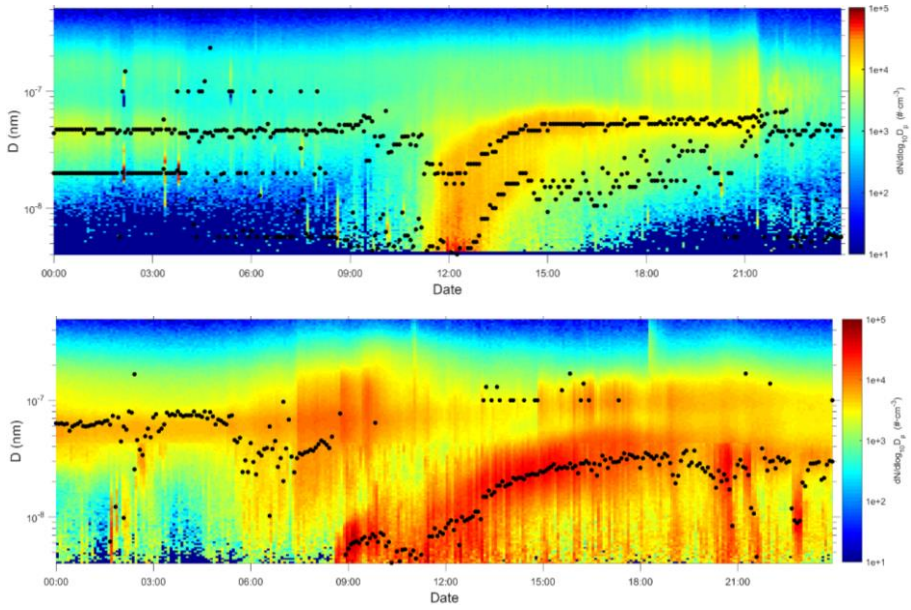

Figure S3 - An example illustrating a case where (top) two aerosol modes appears at same time at SNS site and (bottom) local and regional event take place at UGR site.

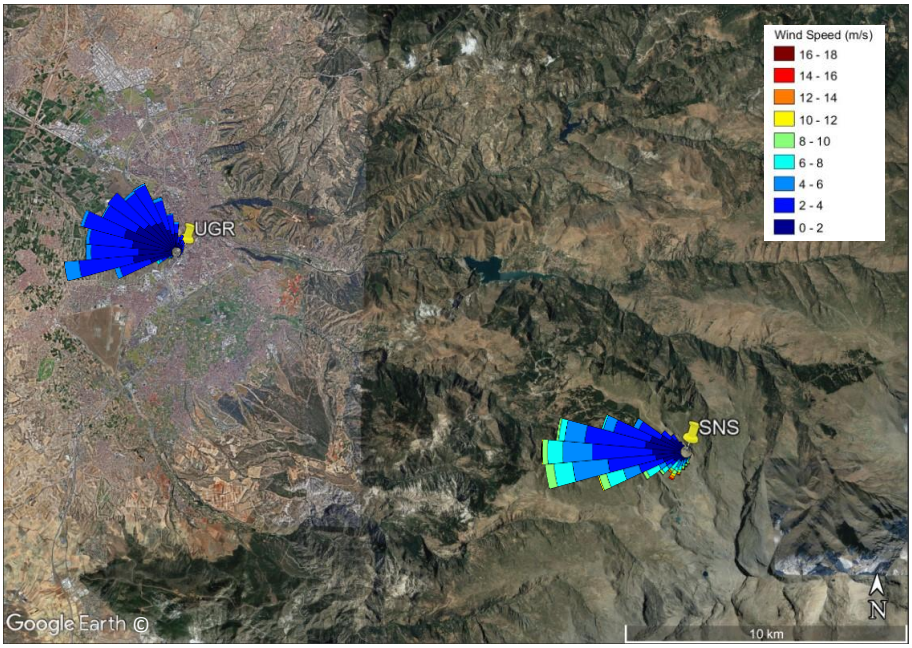

Figure S4 - Mean wind roses at SNS and UGR stations during the NPF event hours (from 10:00-15:00 during event days).

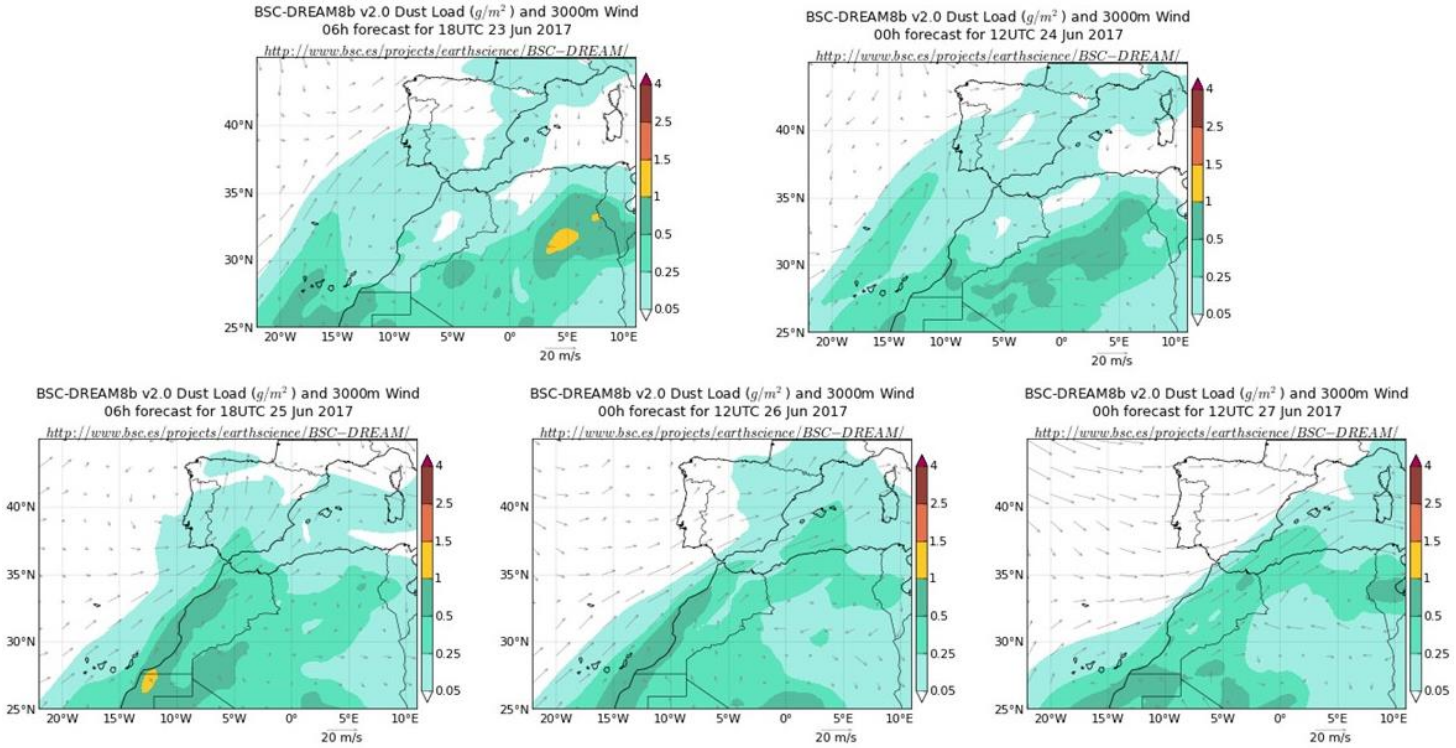

Figure S5 - Evolution of modelled dust load (g·m^{-2}) for the period 23 to 27 June 2017.

List of symbols and acronyms

a.g.l.	Above ground level
a.s.l.	Above sea level
ACI	Aerosol-Cloud Interactions
ACTRIS	Aerosol, Clouds and Trace gases InfraStructure network
AE33	Multiwavelength absorption photometer manufactured by Magee Scientific
AGORA	Andalusian Global ObseRvatory of the Atmosphere
AMICUS	Aerosol MIcrophysical and Chemical properties at Urban atmoSphere
APS	Aerodynamic Particle Sizer
ARI	Aerosol-Radiation Interactions
BB	Biomass Burning
BC	Black Carbon
CoagS	Coagulation Sink
CPC	Condensation Particle Counter
CS	Condensation Sink
DMA	Differential Mobility Analyzer
EC	Eddy covariance
FF	Fossil Fuel

F_N	Vertical aerosol fluxes
FT	Free troposphere
GFAT	Atmospheric Physics Group
GR	Growth Rate
GR^{SA}	Growth rate due to sulfuric acid
HOM	Highly Oxygenated Molecule
IFAPA	Andalusian Institute of Agricultural and Fisheries Research and Training
IISTA- CEAMA	Andalusian Institute for Earth System Research
IN	Ice forming nuclei
IPCC	Intergovernmental Panel on Climate Change
J	Formation Rate
N, N_{Tot}	Total particle number concentration
N_1	Primary aerosol particle number concentration
N_2	Secondary aerosol particle number concentration
$N_{D_{P_1}-D_{P_2}}$	Particle number concentration with diameters from D_{p_1} to D_{p_2}
N_{D_p}	Particle number concentration with diameters less than D_p
NFAN	NOAA Federated Aerosol Network
NPF	New Particle Formation
OC	Organic carbon
P	Probability parameter
PBL	Planetary Boundary Layer
PM_{D_p}	Particulate matter with diameters less than D_p
r	Pearson correlation coefficient
RH	Relative humidity
SARGAN	in-Situ AeRosol GAW Network

SLOPE II	Sierra Nevada Lidar AerOsol Profiling Experiment II
SMPS	Scanning Mobility Particle Sizer
SNS	Sierra Nevada high-altitude remote station
UCPC	Ultrafine Condensation Particle Counter
UFP	Ultrafine particles
UGR	Granada urban station
VOCs	Volatile Organic Compounds
α_{ap}	Aerosol absorption Ångström exponent
α_{ap}^{bb}	Biomass Burning aerosol absorption Ångström exponent
α_{ap}^{ff}	Fossil Fuel aerosol absorption Ångström exponent
w	Vertical wind speed
ω_0	Aerosol single scattering albedo
λ	Wavelength

List of figures

List of tables

/References

Aalto, P., Hämeri, K., Paatero, P., Kulmala, M., Bellander, T., Berglind, N., et al. (2005). Aerosol particle number concentration measurements in five european cities using tsi-3022 condensation particle counter over a three-year period during health effects of air pollution on susceptible subpopulations. *Journal of the Air and Waste Management Association*, *55*(8), 1064–1076. https://doi.org/10.1080/10473289.2005.10464702

del Águila, A., Sorribas, M., Lyamani, H., Titos, G., Olmo, F. J., Arruda-Moreira, G., et al. (2018). Sources and physicochemical characteristics of submicron aerosols during three intensive campaigns in Granada (Spain). *Atmospheric Research*, *213*, 398–410. https://doi.org/10.1016/j.atmosres.2018.06.004

Aitken, J. A. (1897). On some nuclei of cloudy condensation. *Transactions of the Royal Society*, XXXIX.

Alonso-Blanco, E., Gómez-Moreno, F. J., Artíñano, B., Iglesias-Samitier, S., Juncal-Bello, V., Piñeiro-Iglesias, M., et al. (2018). Temporal and spatial variability of atmospheric particle number size distributions across Spain. *Atmospheric Environment*, *190*, 146–160. https://doi.org/10.1016/j.atmosenv.2018.06.046

Alves, C., Vicente, A., Nunes, T., Gonçalves, C., Fernandes, A. P., Mirante, F., et al. (2011). Summer 2009 wildfires in Portugal: Emission of trace gases and aerosol composition. *Atmospheric Environment*, *45*(3), 641–649. https://doi.org/10.1016/j.atmosenv.2010.10.031

Amato, F., Alastuey, A., Karanasiou, A., Lucarelli, F., Nava, S., Calzolai, G., et al. (2016). AIRUSE-LIFE+: A harmonized PM speciation and source apportionment in five southern European cities. *Atmospheric Chemistry and Physics*, *16*(5), 3289–3309. https://doi.org/10.5194/acp-16-3289-2016

Andrews, E., Sheridan, P. J., Ogren, J. A., Hageman, D., Jefferson, A., Wendell, J., et al. (2019).

Overview of the NOAA/ESRL federated aerosol network. *Bulletin of the American Meteorological Society*, *100*(1), 123–135. https://doi.org/10.1175/BAMS-D-17-0175.1

Ansmann, A., Bösenberg, J., Chiakovsky, A., Comerón, A., Eckhardt, S., Eixmann, R., et al. (2003). Long-range transport of Saharan dust to northern Europe: The 11-16 October 2001 outbreak observed with EARLINET. *Journal of Geophysical Research: Atmospheres*, *108*(24). https://doi.org/10.1029/2003jd003757

Arnold, F. (1982). Ion nucleation - A potential source for stratospheric aerosols. *Nature*, *299*(5879), 134–137. https://doi.org/10.1038/299134a0

de Arruda Moreira, G., Guerrero-Rascado, J. L., Bravo-Aranda, J. A., Benavent-Oltra, J. A., Ortiz-Amezcua, P., Róman, R., et al. (2018). Study of the planetary boundary layer by microwave radiometer, elastic lidar and Doppler lidar estimations in Southern Iberian Peninsula. *Atmospheric Research*. https://doi.org/10.1016/j.atmosres.2018.06.007

Aubinet, M., Grelle, A., Ibrom, A., Rannik, Ü., Moncrieff, J., Foken, T., et al. (1999). Estimates of the Annual Net Carbon and Water Exchange of Forests: The EUROFLUX Methodology. *Advances in Ecological Research*, *30*(C), 113–175. https://doi.org/10.1016/S0065-2504(08)60018-5

Aubinet, Marc, Vesala, T., & Dario, P. (Eds.). (2012). *Eddy Covariance: A Practical Guide to Measurement and Data Analysis*. *Eddy Covariance*. Springer Netherlands. https://doi.org/10.1007/978-94-007-2351-1

Beddows, D. C.S., Harrison, R. M., Green, D. C., & Fuller, G. W. (2015). Receptor modelling of both particle composition and size distribution from a background site in London, UK. *Atmospheric Chemistry and Physics*. https://doi.org/10.5194/acp-15-10107-2015

Beddows, David C.S., Dall'Osto, M., & Harrison, R. M. (2009). Cluster analysis of rural, urban, and curbside atmospheric particle size data. *Environmental Science and Technology*, *43*(13), 4694–4700. https://doi.org/10.1021/es803121t

Benavent-Oltra, J. A., Román, R., Casquero-Vera, J. A., Pérez-Ramírez, D., Lyamani, H., Ortiz-Amezcua, P., et al. (2019). Different strategies to retrieve aerosol properties at night-time with the GRASP algorithm. *Atmospheric Chemistry and Physics*, *19*(22), 14149–14171. https://doi.org/10.5194/acp-19-14149-2019

Beres, N. D., Lapuerta, M., Cereceda-Balic, F., & Moosmüller, H. (2020). Snow surface albedo

sensitivity to black carbon: Radiative transfer modelling. *Atmosphere*, *11*(10). https://doi.org/10.3390/atmos11101077

Bianchi, F., Praplan, A. P., Sarnela, N., Dommen, J., Kürten, A., Ortega, I. K., et al. (2014). Insight into acid-base nucleation experiments by comparison of the chemical composition of positive, negative, and neutral clusters. *Environmental Science and Technology*, *48*(23), 13675–13684. https://doi.org/10.1021/es502380b

Bianchi, F., Garmash, O., He, X., Yan, C., Iyer, S., Rosendahl, I., et al. (2017). The role of highly oxygenated molecules (HOMs) in determining the composition of ambient ions in the boreal forest. *Atmospheric Chemistry and Physics*, *17*(22), 13819–13831. https://doi.org/10.5194/acp-17-13819-2017

Bianchi, F., Kurtén, T., Riva, M., Mohr, C., Rissanen, M. P., Roldin, P., et al. (2019). Highly Oxygenated Organic Molecules (HOM) from Gas-Phase Autoxidation Involving Peroxy Radicals: A Key Contributor to Atmospheric Aerosol. *Chemical Reviews*. https://doi.org/10.1021/acs.chemrev.8b00395

Birmili, W., Weinhold, K., Rasch, F., Sonntag, A., Sun, J., Merkel, M., et al. (2016). Long-term observations of tropospheric particle number size distributions and equivalent black carbon mass concentrations in the German Ultrafine Aerosol Network (GUAN). *Earth System Science Data*, *8*(2), 355–382. https://doi.org/10.5194/essd-8-355-2016

Bond, T. C., Doherty, S. J., Fahey, D. W., Forster, P. M., Berntsen, T., Deangelo, B. J., et al. (2013). Bounding the role of black carbon in the climate system: A scientific assessment. *Journal of Geophysical Research Atmospheres*, *118*(11), 5380–5552. https://doi.org/10.1002/jgrd.50171

Borrás, E. (2013). *Caracterización de material particulado atmosférico generado en reactores fotoquímicos y procedente de muestras ambientales*. Universitat Politècnica de València, Spain. Retrieved from https://dialnet.unirioja.es/servlet/tesis?codigo=83384

Boulon, J., Sellegri, K., Venzac, H., Picard, D., Weingartner, E., Wehrle, G., et al. (2010). New particle formation and ultrafine charged aerosol climatology at a high altitude site in the Alps (Jungfraujoch, 3580 m a.s.l., Switzerland). *Atmospheric Chemistry and Physics*. https://doi.org/10.5194/acp-10-9333-2010

Boulon, J., Sellegri, K., Hervo, M., Picard, D., Pichon, J. M., Fréville, P., & Laj, P. (2011). Investigation of nucleation events vertical extent: A long term study at two different altitude

sites. *Atmospheric Chemistry and Physics*, *11*(12), 5625–5639. https://doi.org/10.5194/acp-11-5625-2011

Brines, M., Dall'Osto, M., Beddows, D. C. S., Harrison, R. M., Gómez-Moreno, F., Núñez, L., et al. (2015). Traffic and nucleation events as main sources of ultrafine particles in high-insolation developed world cities. *Atmospheric Chemistry and Physics*, *15*(10), 5929–5945. https://doi.org/10.5194/acp-15-5929-2015

Buseck, P. R., & Adachi, K. (2008). Nanoparticles in the atmosphere. *Elements*, *4*(6), 389–394. https://doi.org/10.2113/gselements.4.6.389

Cai, J., Chu, B., Yao, L., Yan, C., Heikkinen, L. M., Zheng, F., et al. (2020). Size-segregated particle number and mass concentrations from different emission sources in urban Beijing. *Atmospheric Chemistry and Physics*, *20*(21), 12721–12740. https://doi.org/10.5194/acp-20-12721-2020

Carnerero, C., Pérez, N., Reche, C., Ealo, M., Titos, G., Lee, H. K., et al. (2018). Vertical and horizontal distribution of regional new particle formation events in Madrid. *Atmospheric Chemistry and Physics*, *18*(22), 16601–16618. https://doi.org/10.5194/acp-18-16601-2018

Casquero-Vera, J. A., Lyamani, H., Titos, G., Borrás, E., Olmo, F. J., & Alados-Arboledas, L. (2019). Impact of primary NO2 emissions at different urban sites exceeding the European NO2 standard limit. *Science of the Total Environment*. https://doi.org/10.1016/j.scitotenv.2018.07.360

Casquero-Vera, J.A., Lyamani, H., Titos, G., Minguillón, M. C., Dada, L., Alastuey, A., et al. (2021). Quantifying traffic, biomass burning and secondary source contributions to atmospheric particle number concentrations at urban and suburban sites. *Science of the Total Environment*, *768*. https://doi.org/10.1016/j.scitotenv.2021.145282

Casquero-Vera, J. A., Lyamani, H., Dada, L., Hakala, S., Paasonen, P., Román, R., et al. (2020). New particle formation at urban and high-altitude remote sites in the south-eastern Iberian Peninsula. *Atmospheric Chemistry and Physics Discussions*, 1–32. https://doi.org/10.5194/acp-2020-394

Cassee, F., Morawska, L., Peters, A., Wierzbicka, A., Buonanno, G., Cyrys, J., et al. (2019). White Paper Ambient ultrafine particles evidence for policy makers.

Cassee, F. R., Morawska, L., Peters, A., Wierzbicka, A., Buonanno, G., Cyrys, J., et al. (2019).

Ambient ultrafine particles: evidence for policy makers [White paper], 1–23. Retrieved from https://efca.net/files/WHITE PAPER-UFP evidence for policy makers (25 OCT).pdf%0Ahttps://lup.lub.lu.se/record/3b718eb2-6b88-4223-a1d5-eb0b05de4b56

Cazorla, A., Casquero-Vera, J. A., Román, R., Luis Guerrero-Rascado, J., Toledano, C., Cachorro, V. E., et al. (2017). Near-real-time processing of a ceilometer network assisted with sun-photometer data: Monitoring a dust outbreak over the Iberian Peninsula. *Atmospheric Chemistry and Physics*, *17*(19), 11861–11876. https://doi.org/10.5194/acp-17-11861-2017

Chan, T. W., Meloche, E., Kubsh, J., & Brezny, R. (2014). Black carbon emissions in gasoline exhaust and a reduction alternative with a gasoline particulate filter. *Environmental Science and Technology*, *48*(10), 6027–6034. https://doi.org/10.1021/es501791b

Cherian, R., Quaas, J., Salzmann, M., & Tomassini, L. (2017). Black carbon indirect radiative effects in a climate model. *Tellus, Series B: Chemical and Physical Meteorology*, *69*(1). https://doi.org/10.1080/16000889.2017.1369342

Chu, B., Matti Kerminen, V., Bianchi, F., Yan, C., Petäjä, T., & Kulmala, M. (2019). Atmospheric new particle formation in China. *Atmospheric Chemistry and Physics*, *19*(1), 115–138. https://doi.org/10.5194/acp-19-115-2019

Collaud Coen, M., Weingartner, E., Apituley, A., Ceburnis, D., Fierz-Schmidhauser, R., Flentje, H., et al. (2010). Minimizing light absorption measurement artifacts of the Aethalometer: Evaluation of five correction algorithms. *Atmospheric Measurement Techniques*, *3*(2), 457–474. https://doi.org/10.5194/amt-3-457-2010

Conte, M., Donateo, A., & Contini, D. (2018). Characterisation of particle size distributions and corresponding size-segregated turbulent fluxes simultaneously with CO2 exchange in an urban area. *Science of the Total Environment*, *622–623*, 1067–1078. https://doi.org/10.1016/j.scitotenv.2017.12.040

Conte, M., Contini, D., & Held, A. (2021). Multiresolution decomposition and wavelet analysis of urban aerosol fluxes in Italy and Austria. *Atmospheric Research*, *248*. https://doi.org/10.1016/j.atmosres.2020.105267

Contini, D., Donateo, A., Elefante, C., & Grasso, F. M. (2012). Analysis of particles and carbon dioxide concentrations and fluxes in an urban area: Correlation with traffic rate and local micrometeorology. *Atmospheric Environment*, *46*, 25–35.

https://doi.org/10.1016/j.atmosenv.2011.10.039

Costabile, F., Alas, H., Aufderheide, M., Avino, P., Amato, F., Argentini, S., et al. (2017). First results of the "Carbonaceous Aerosol in Rome and Environs (CARE)" Experiment: Beyond current standards for PM10. *Atmosphere*, *8*(12). https://doi.org/10.3390/atmos8120249

Dada, L., Paasonen, P., Nieminen, T., Buenrostro Mazon, S., Kontkanen, J., Peräkylä, O., et al. (2017). Long-term analysis of clear-sky new particle formation events and nonevents in Hyytiälä. *Atmospheric Chemistry and Physics*, *17*(10), 6227–6241. https://doi.org/10.5194/acp-17-6227-2017

Dal Maso, M., Kulmala, M., Riipinen, I., Wagner, R., Hussein, T., Aalto, P. P., & Lehtinen, K. E. J. (2005). Formation and growth of fresh atmospheric aerosols: Eight years of aerosol size distribution data from SMEAR II, Hyytiälä, Finland. *Boreal Environment Research*, *10*(5), 323–336.

Denby, B., Karl, M., Laupsa, H., Johansson, C., Pohjola, M., Karppinen, A., et al. (2010). Procena lokalne emisije čestica sagorevanjem drveta u dva nordijska grada kombinovanjem posmatranja vazduha sa modelima prijema i rasprostiranja. *Chemical Industry and Chemical Engineering Quarterly*, *16*(3), 237–241. https://doi.org/10.2298/CICEQ091214019D

Deventer, M. J., Griessbaum, F., & Klemm, O. (2013). Size-resolved flux measurement of sub-micrometer particles over an urban area. *Meteorologische Zeitschrift*, *22*(6), 729–737. https://doi.org/10.1127/0941-2948/2013/0441

Dinoi, A., Cesari, D., Marinoni, A., Bonasoni, P., Riccio, A., Chianese, E., et al. (2017). Inter-comparison of carbon content in PM2.5 and PM10 collected at five measurement sites in Southern Italy. *Atmosphere*, *8*(12). https://doi.org/10.3390/atmos8120243

Donateo, A., Conte, M., Grasso, F. M., & Contini, D. (2019). Seasonal and diurnal behaviour of size segregated particles fluxes in a suburban area. *Atmospheric Environment*, *219*. https://doi.org/10.1016/j.atmosenv.2019.117052

Dorsey, J. R., Nemitz, E., Gallagher, M. W., Fowler, D., Williams, P. I., Bower, K. N., & Beswick, K. M. (2002). Direct measurements and parameterisation of aerosol flux, concentration and emission velocity above a city. *Atmospheric Environment*, *36*(5), 791–800. https://doi.org/10.1016/S1352-2310(01)00526-X

Drinovec, L., Močnik, G., Zotter, P., Prévôt, A. S. H., Ruckstuhl, C., Coz, E., et al. (2015). The "dual-

spot" Aethalometer: An improved measurement of aerosol black carbon with real-time loading compensation. *Atmospheric Measurement Techniques*, *8*(5), 1965–1979. https://doi.org/10.5194/amt-8-1965-2015

Dupart, Y., King, S. M., Nekat, B., Nowak, A., Wiedensohler, A., Herrmann, H., et al. (2012). Mineral dust photochemistry induces nucleation events in the presence of SO2. *Proceedings of the National Academy of Sciences of the United States of America*, *109*(51), 20842–20847. https://doi.org/10.1073/pnas.1212297109

Ealo, M., Alastuey, A., Ripoll, A., Pérez, N., Minguillón, M. C., Querol, X., & Pandolfi, M. (2016). Detection of Saharan dust and biomass burning events using near-real-time intensive aerosol optical properties in the north-western Mediterranean. *Atmospheric Chemistry and Physics*, *16*(19), 12567–12586. https://doi.org/10.5194/acp-16-12567-2016

EEA (2019). *Air quality in Europe — 2019 report*. European Environment Agency. https://www.eea.europa.eu/publications/air-quality-in-europe-2019

Ehn, M., Thornton, J. A., Kleist, E., Sipilä, M., Junninen, H., Pullinen, I., et al. (2014). A large source of low-volatility secondary organic aerosol. *Nature*, *506*(7489), 476–479. https://doi.org/10.1038/nature13032

Fan, J., Rosenfeld, D., Zhang, Y., Giangrande, S. E., Li, Z., Machado, L. A. T., et al. (2018). Substantial convection and precipitation enhancements by ultrafine aerosol particles. *Science*, *359*(6374), 411–418. https://doi.org/10.1126/science.aan8461

Favez, O., Cachier, H., Sciare, J., Sarda-Estève, R., & Martinon, L. (2009). Evidence for a significant contribution of wood burning aerosols to PM2.5 during the winter season in Paris, France. *Atmospheric Environment*, *43*(22–23), 3640–3644. https://doi.org/10.1016/j.atmosenv.2009.04.035

Fernández-Camacho, R., Rodríguez, S., De La Rosa, J., Sánchez De La Campa, A. M., Viana, M., Alastuey, A., & Querol, X. (2010). Ultrafine particle formation in the inland sea breeze airflow in Southwest Europe. *Atmospheric Chemistry and Physics*, *10*(19), 9615–9630. https://doi.org/10.5194/acp-10-9615-2010

Fialho, P., Hansen, A. D. A., & Honrath, R. E. (2005). Absorption coefficients by aerosols in remote areas: A new approach to decouple dust and black carbon absorption coefficients using seven-wavelength Aethalometer data. *Journal of Aerosol Science*, *36*(2), 267–282.

https://doi.org/10.1016/j.jaerosci.2004.09.004

Fuchs, N. A. (1963). On the stationary charge distribution on aerosol particles in a bipolar ionic atmosphere. *Geofisica Pura e Applicata*, *56*(1), 185–193. https://doi.org/10.1007/BF01993343

Fuchs, N. A., & Sutugin, A. G. (1971). High-Dispersed Aerosols. In *Topics in Current Aerosol Research* (p. 1). https://doi.org/10.1016/b978-0-08-016674-2.50006-6

Fuller, G. W., Tremper, A. H., Baker, T. D., Yttri, K. E., & Butterfield, D. (2014). Contribution of wood burning to PM10 in London. *Atmospheric Environment*, *87*, 87–94. https://doi.org/10.1016/j.atmosenv.2013.12.037

García, M. I., Rodríguez, S., González, Y., & García, R. D. (2014). Climatology of new particle formation at Izaña mountain GAW observatory in the subtropical North Atlantic. *Atmospheric Chemistry and Physics*, *14*(8), 3865–3881. https://doi.org/10.5194/acp-14-3865-2014

Gieré, R., & Querol, X. (2010). Solid particulate matter in the atmosphere. *Elements*, *6*(4), 215–222. https://doi.org/10.2113/gselements.6.4.215

Gómez-Moreno, F. J., Pujadas, M., Plaza, J., Rodríguez-Maroto, J. J., Martínez-Lozano, P., & Artíñano, B. (2011). Influence of seasonal factors on the atmospheric particle number concentration and size distribution in Madrid. *Atmospheric Environment*, *45*(18), 3169–3180. https://doi.org/10.1016/j.atmosenv.2011.02.041

Grimmond, C. S. B., & Oke, T. R. (1999). Aerodynamic properties of urban areas derived from analysis of surface form. *Journal of Applied Meteorology*, *38*(9), 1262–1292. https://doi.org/10.1175/1520-0450(1999)038<1262:APOUAD>2.0.CO;2

Hama, S. M.L., Cordell, R. L., & Monks, P. S. (2017). Quantifying primary and secondary source contributions to ultrafine particles in the UK urban background. *Atmospheric Environment*, *166*, 62–78. https://doi.org/10.1016/j.atmosenv.2017.07.013

Hama, Sarkawt M.L., Cordell, R. L., Kos, G. P. A., Weijers, E. P., & Monks, P. S. (2017). Sub-micron particle number size distribution characteristics at two urban locations in Leicester. *Atmospheric Research*, *194*, 1–16. https://doi.org/10.1016/j.atmosres.2017.04.021

Hamilton, R. S., & Mansfield, T. A. (1991). Airborne particulate elemental carbon: Its sources, transport and contribution to dark smoke and soiling. *Atmospheric Environment Part A, General Topics*, *25*(3–4), 715–723. https://doi.org/10.1016/0960-1686(91)90070-N

Harrison, R. M., Dall'Osto, M., Beddows, D. C. S., Thorpe, A. J., Bloss, W. J., Allan, J. D., et al. (2012). Atmospheric chemistry and physics in the atmosphere of a developed megacity (London): An overview of the REPARTEE experiment and its conclusions. *Atmospheric Chemistry and Physics*. https://doi.org/10.5194/acp-12-3065-2012

Helin, A., Niemi, J. V., Virkkula, A., Pirjola, L., Teinilä, K., Backman, J., et al. (2018). Characteristics and source apportionment of black carbon in the Helsinki metropolitan area, Finland. *Atmospheric Environment*, *190*, 87–98. https://doi.org/10.1016/j.atmosenv.2018.07.022

Herich, H., Hueglin, C., & Buchmann, B. (2011). A 2.5 year's source apportionment study of black carbon from wood burning and fossil fuel combustion at urban and rural sites in Switzerland. *Atmospheric Measurement Techniques*, *4*(7), 1409–1420. https://doi.org/10.5194/amt-4-1409-2011

Hime, N. J., Marks, G. B., & Cowie, C. T. (2018). A comparison of the health effects of ambient particulate matter air pollution from five emission sources. *International Journal of Environmental Research and Public Health*. https://doi.org/10.3390/ijerph15061206

Hirsikko, A., Bergman, T., Laakso, L., Dal Maso, M., Riipinen, I., Hõrrak, U., & Kulmala, M. (2007). Identification and classification of the formation of intermediate ions measured in boreal forest. *Atmospheric Chemistry and Physics*, *7*(1), 201–210. https://doi.org/10.5194/acp-7-201-2007

Hofman, J., Staelens, J., Cordell, R., Stroobants, C., Zikova, N., Hama, S. M. L., et al. (2016). Ultrafine particles in four European urban environments: Results from a new continuous long-term monitoring network. *Atmospheric Environment*, *136*, 68–81. https://doi.org/10.1016/j.atmosenv.2016.04.010

Horst, T. W. (1997). A simple formula for attenuation of eddy fluxes measured with first-order-response scalar sensors. *Boundary-Layer Meteorology*, *82*(2), 219–233. https://doi.org/10.1023/A:1000229130034

Horvath, H. (2000, October 1). Aerosol - An introduction. *Journal of Environmental Radioactivity*. Elsevier. https://doi.org/10.1016/S0265-931X(00)00041-2

Hussein, T., Dal Maso, M., Petäjä, T., Koponen, I. K., Paatero, P., Aalto, P. P., et al. (2005). Evaluation of an automatic algorithm for fitting the particle number size distributions. *Boreal Environment Research*, *10*(5), 337–355.

IPCC (2013). *Climate Change 2013: The Physical Science Basis.* Contribution of Working Group I to the Fifth Assessment Report of the Intergovernmental Panel on Climate Change. Edited by T.F. Stocker, D. Qin, G.-K. Plattner, M. Tignor, S.K. Allen, J. Boschung, A. Nauels, Y. Xia, V. Bex, P.M. Midgley. Cambridge, UK.

Janssen, N. A., Gerlofs-Nijland, M. E., Lanki, T., Salonen, R. O., Cassee, F., Hoek, G., et al. (2012). Health effects of black carbon. *World Health …*. Retrieved from http://www.euro.who.int/en/health-topics/environment-and-health/air-quality/publications/2012/health-effects-of-black-carbon

Janssen, N. A. H., Hoek, G., Simic-Lawson, M., Fischer, P., van Bree, L., Brink, H. Ten, et al. (2011). Black carbon as an additional indicator of the adverse health effects of airborne particles compared with pm10 and pm2.5. *Environmental Health Perspectives*. https://doi.org/10.1289/ehp.1003369

Järvi, L., Rannik, Ü., Mammarella, I., Sogachev, A., Aalto, P. P., Keronen, P., et al. (2009). Annual particle flux observations over a heterogeneous urban area. *Atmospheric Chemistry and Physics*, *9*(20), 7847–7856. https://doi.org/10.5194/acp-9-7847-2009

Kalogridis, A. C., Vratolis, S., Liakakou, E., Gerasopoulos, E., Mihalopoulos, N., & Eleftheriadis, K. (2018). Assessment of wood burning versus fossil fuel contribution to wintertime black carbon and carbon monoxide concentrations in Athens, Greece. *Atmospheric Chemistry and Physics*, *18*(14), 10219–10236. https://doi.org/10.5194/acp-18-10219-2018

Kerminen, V. M., Chen, X., Vakkari, V., Petäjä, T., Kulmala, M., & Bianchi, F. (2018). Atmospheric new particle formation and growth: Review of field observations. *Environmental Research Letters*. https://doi.org/10.1088/1748-9326/aadf3c

Kirchstetter, T. W., Novakov, T., & Hobbs, P. V. (2004). Evidence that the spectral dependence of light absorption by aerosols is affected by organic carbon. *Journal of Geophysical Research D: Atmospheres*, *109*(21). https://doi.org/10.1029/2004JD004999

Kljun, N., Calanca, P., Rotach, M. W., & Schmid, H. P. (2004). A simple parameterisation for flux footprint predictions. *Boundary-Layer Meteorology*, *112*(3), 503–523. https://doi.org/10.1023/B:BOUN.0000030653.71031.96

Kontkanen, J. (2016). *on the Formation and Growth of Sub-3 Nm Atmospheric Particles and Molecular Clusters*. University of Helsinki. Retrieved from

https://helda.helsinki.fi/handle/10138/168770

Kulmala, M., Dal Maso, M., Mäkelä, J. M., Pirjola, L., Väkevä, M., Aalto, P., et al. (2001). On the formation, growth and composition of nucleation mode particles. *Tellus, Series B: Chemical and Physical Meteorology*, *53*(4), 479–490. https://doi.org/10.3402/tellusb.v53i4.16622

Kulmala, M., Vehkamäki, H., Petäjä, T., Dal Maso, M., Lauri, A., Kerminen, V. M., et al. (2004). Formation and growth rates of ultrafine atmospheric particles: A review of observations. *Journal of Aerosol Science*, *35*(2), 143–176. https://doi.org/10.1016/j.jaerosci.2003.10.003

Kulmala, M., Petäjä, T., Ehn, M., Thornton, J., Sipilä, M., Worsnop, D. R., & Kerminen, V.-M. (2014). Chemistry of Atmospheric Nucleation: On the Recent Advances on Precursor Characterization and Atmospheric Cluster Composition in Connection with Atmospheric New Particle Formation. *Annual Review of Physical Chemistry*, *65*(1), 21–37. https://doi.org/10.1146/annurev-physchem-040412-110014

Kulmala, M., Kerminen, V. M., Petäjä, T., Ding, A. J., & Wang, L. (2017). Atmospheric gas-to-particle conversion: Why NPF events are observed in megacities? *Faraday Discussions*. https://doi.org/10.1039/c6fd00257a

Kulmala, M., & Kerminen, V. M. (2008). On the formation and growth of atmospheric nanoparticles. *Atmospheric Research*, *90*(2–4), 132–150. https://doi.org/10.1016/j.atmosres.2008.01.005

Kulmala, M., Petäjä, T., Nieminen, T., Sipilä, M., Manninen, H. E., Lehtipalo, K., et al. (2012). Measurement of the nucleation of atmospheric aerosol particles. *Nature Protocols*, *7*(9), 1651–1667. https://doi.org/10.1038/nprot.2012.091

Kulmala, M., Kontkanen, J., Junninen, H., Lehtipalo, K., Manninen, H. E., Nieminen, T., et al. (2013). Direct observations of atmospheric aerosol nucleation. *Science*, *339*(6122), 943–946. https://doi.org/10.1126/science.1227385

Kulmala, M., Luoma, K., Virkkula, A., Petäjä, T., Paasonen, P., Kerminen, V. M., et al. (2016). On the mode-segregated aerosol particle number concentration load: Contributions of primary and secondary particles in Hyytiälä and Nanjing. *Boreal Environment Research*, *21*(3–4), 319–331.

Kurppa, M., Nordbo, A., Haapanala, S., & Järvi, L. (2015). Effect of seasonal variability and land use on particle number and CO2 exchange in Helsinki, Finland. *Urban Climate*, *13*, 94–109. https://doi.org/10.1016/j.uclim.2015.07.006

Kurtén, T., Noppel, M., Vehkamäki, H., Salonen, M., & Kulmala, M. (2007). Quantum chemical studies of hydrate formation of H2so 4 and HSO4-. *Boreal Environment Research*, *12*(3), 431–453.

Lähde, T., Rönkkö, T., Virtanen, A., Schuck, T. J., Pirjola, L., Hämeri, K., et al. (2009). Heavy duty diesel engine exhaust aerosol particle and ion measurements. *Environmental Science and Technology*, *43*(1), 163–168. https://doi.org/10.1021/es801690h

Laj, P., Bigi, A., Rose, C., Andrews, E., Lund Myhre, C., Collaud Coen, M., et al. (2020). A global analysis of climate-relevant aerosol properties retrieved from the network of Global Atmosphere Watch (GAW) near-surface observatories. *Atmospheric Measurement Techniques*, *13*(8), 4353–4392. https://doi.org/10.5194/amt-13-4353-2020

Leaitch, W. R., Korolev, A., Aliabadi, A. A., Burkart, J., Willis, M. D., Abbatt, J. P. D., et al. (2016). Effects of 20-100nm particles on liquid clouds in the clean summertime Arctic. *Atmospheric Chemistry and Physics*. https://doi.org/10.5194/acp-16-11107-2016

Lehtipalo, K., Rondo, L., Kontkanen, J., Schobesberger, S., Jokinen, T., Sarnela, N., et al. (2016). The effect of acid-base clustering and ions on the growth of atmospheric nano-particles. *Nature Communications*, *7*. https://doi.org/10.1038/ncomms11594

Leng, C., Zhang, Q., Tao, J., Zhang, H., Zhang, D., Xu, C., et al. (2014). Impacts of new particle formation on aerosol Cloud Condensation Nuclei (CCN) activity in Shanghai: Case study. *Atmospheric Chemistry and Physics*. https://doi.org/10.5194/acp-14-11353-2014

Lenschow, D. H., Lothon, M., Mayor, S. D., Sullivan, P. P., & Canut, G. (2012). A Comparison of Higher-Order Vertical Velocity Moments in the Convective Boundary Layer from Lidar with In Situ Measurements and Large-Eddy Simulation. *Boundary-Layer Meteorology*, *143*(1), 107–123. https://doi.org/10.1007/s10546-011-9615-3

Liakakou, E., Stavroulas, I., Kaskaoutis, D. G., Grivas, G., Paraskevopoulou, D., Dumka, U. C., et al. (2020). Long-term variability, source apportionment and spectral properties of black carbon at an urban background site in Athens, Greece. *Atmospheric Environment*, *222*, 117137. https://doi.org/10.1016/j.atmosenv.2019.117137

Liou, K. N. (1980). *Applications of radiative transfer to remote sensing of the atmosphere*. *International Geophysics* (Vol. 26). https://doi.org/10.1016/S0074-6142(08)60682-8

Liu, D., Taylor, J. W., Crosier, J., Marsden, N., Bower, K. N., Lloyd, G., et al. (2018). Aircraft and

ground measurements of dust aerosols over the west African coast in summer 2015 during ICE-D and AER-D. *Atmospheric Chemistry and Physics*, *18*(5), 3817–3838. https://doi.org/10.5194/acp-18-3817-2018

Lv, G., Sui, X., Chen, J., Jayaratne, R., & Mellouki, A. (2018). Investigation of new particle formation at the summit of Mt. Tai, China. *Atmospheric Chemistry and Physics*, *18*(3), 2243–2258. https://doi.org/10.5194/acp-18-2243-2018

Lyamani, H., Olmo, F. J., Alcántara, A., & Alados-Arboledas, L. (2006). Atmospheric aerosols during the 2003 heat wave in southeastern Spain I: Spectral optical depth. *Atmospheric Environment*, *40*(33), 6453–6464. https://doi.org/10.1016/j.atmosenv.2006.04.048

Lyamani, H., Olmo, F. J., & Alados-Arboledas, L. (2010). Physical and optical properties of aerosols over an urban location in Spain: Seasonal and diurnal variability. *Atmospheric Chemistry and Physics*, *10*(1), 239–254. https://doi.org/10.5194/acp-10-239-2010

Lyamani, H., Olmo, F. J., Foyo, I., & Alados-Arboledas, L. (2011). Black carbon aerosols over an urban area in south-eastern Spain: Changes detected after the 2008 economic crisis. *Atmospheric Environment*, *45*(35), 6423–6432. https://doi.org/10.1016/j.atmosenv.2011.07.063

Lyamani, H., Fernández-Gálvez, J., Pérez-Ramírez, D., Valenzuela, A., Antón, M., Alados, I., et al. (2012). Aerosol properties over two urban sites in South Spain during an extended stagnation episode in winter season. *Atmospheric Environment*, *62*, 424–432. https://doi.org/10.1016/j.atmosenv.2012.08.050

Mandija, F., Guerrero-Rascado, J. L., Lyamani, H., Granados-Muñoz, M. J., & Alados-Arboledas, L. (2016). Synergic estimation of columnar integrated aerosol properties and their vertical resolved profiles in respect to the scenarios of dust intrusions over Granada. *Atmospheric Environment*, *145*, 439–454. https://doi.org/10.1016/j.atmosenv.2016.09.045

Mandija, F., Sicard, M., Comerón, A., Alados-Arboledas, L., Guerrero-Rascado, J. L., Bravo-Aranda, J. A., et al. (2017). Origin and pathways of the mineral dust transport to two Spanish EARLINET sites: Effect on the observed columnar and range-resolved dust optical properties. *Atmospheric Research*, *187*, 69–83. https://doi.org/10.1016/j.atmosres.2016.12.002

Manninen, H. E., Nieminen, T., Asmi, E., Gagné, S., Häkkinen, S., Lehtipalo, K., et al. (2010). EUCAARI ion spectrometer measurements at 12 European sites-analysis of new particle

formation events. *Atmospheric Chemistry and Physics*, *10*(16), 7907–7927. https://doi.org/10.5194/acp-10-7907-2010

Mårtensson, E. M., Nilsson, E. D., Buzorius, G., & Johansson, C. (2006). Eddy covariance measurements and parameterisation of traffic related particle emissions in an urban environment. *Atmospheric Chemistry and Physics*, *6*(3), 769–785. https://doi.org/10.5194/acp-6-769-2006

Martin, C. L., Longley, I. D., Dorsey, J. R., Thomas, R. M., Gallagher, M. W., & Nemitz, E. (2009). Ultrafine particle fluxes above four major European cities. *Atmospheric Environment*, *43*(31), 4714–4721. https://doi.org/10.1016/j.atmosenv.2008.10.009

Mauder, M., & Foken, T. (2011). *Documentation and Instruction Manual of the Eddy-Covariance Software Package TK3*. *Arbeitsergebnisse* (Vol. 26). Retrieved from http://nbn-resolving.de/urn/resolver.pl?urn:nbn:de:bvb:703-opus-8665%5Cnhttp://opus4.kobv.de/opus4-ubbayreuth/frontdoor/index/index/docId/681

Merikanto, J., Spracklen, D. V., Mann, G. W., Pickering, S. J., & Carslaw, K. S. (2009). Impact of nucleation on global CCN. *Atmospheric Chemistry and Physics*, *9*(21), 8601–8616. https://doi.org/10.5194/acp-9-8601-2009

Miller, R. L., & Tegen, I. (1998). Climate response to soil dust aerosols. *Journal of Climate*. https://doi.org/10.1175/1520-0442(1998)011<3247:CRTSDA>2.0.CO;2

Minguillón, M. C., Ripoll, A., Pérez, N., Prévôt, A. S. H., Canonaco, F., Querol, X., & Alastuey, A. (2015). Chemical characterization of submicron regional background aerosols in the western Mediterranean using an Aerosol Chemical Speciation Monitor. *Atmospheric Chemistry and Physics*, *15*(11), 6379–6391. https://doi.org/10.5194/acp-15-6379-2015

Mohr, C., Thornton, J. A., Heitto, A., Lopez-Hilfiker, F. D., Lutz, A., Riipinen, I., et al. (2019). Molecular identification of organic vapors driving atmospheric nanoparticle growth. *Nature Communications*, *10*(1). https://doi.org/10.1038/s41467-019-12473-2

Morawska, L., Ristovski, Z., Jayaratne, E. R., Keogh, D. U., & Ling, X. (2008). Ambient nano and ultrafine particles from motor vehicle emissions: Characteristics, ambient processing and implications on human exposure. *Atmospheric Environment*. https://doi.org/10.1016/j.atmosenv.2008.07.050

Moreira, G. de A., Guerrero-Rascado, J. L., Bravo-Aranda, J. A., Foyo-Moreno, I., Cazorla, A.,

Alados, I., et al. (2020). Study of the planetary boundary layer height in an urban environment using a combination of microwave radiometer and ceilometer. *Atmospheric Research*, *240*. https://doi.org/10.1016/j.atmosres.2020.104932

Németh, Z., Rosati, B., Zíková, N., Salma, I., Bozó, L., Dameto de España, C., et al. (2018). Comparison of atmospheric new particle formation events in three Central European cities. *Atmospheric Environment*, *178*, 191–197. https://doi.org/10.1016/j.atmosenv.2018.01.035

Ng, N. L., Herndon, S. C., Trimborn, A., Canagaratna, M. R., Croteau, P. L., Onasch, T. B., et al. (2011). An Aerosol Chemical Speciation Monitor (ACSM) for routine monitoring of the composition and mass concentrations of ambient aerosol. *Aerosol Science and Technology*, *45*(7), 780–794. https://doi.org/10.1080/02786826.2011.560211

Nie, W., Ding, A., Wang, T., Kerminen, V. M., George, C., Xue, L., et al. (2014). Polluted dust promotes new particle formation and growth. *Scientific Reports*, *4*(1), 6634. https://doi.org/10.1038/srep06634

Nieminen, T., Lehtinen, K. E. J., & Kulmala, M. (2010). Sub-10 nm particle growth by vapor condensation-effects of vapor molecule size and particle thermal speed. *Atmospheric Chemistry and Physics*, *10*(20), 9773–9779. https://doi.org/10.5194/acp-10-9773-2010

Nieminen, T., Kerminen, V. M., Petäjä, T., Aalto, P. P., Arshinov, M., Asmi, E., et al. (2018). Global analysis of continental boundary layer new particle formation based on long-term measurements. *Atmospheric Chemistry and Physics*, *18*(19), 14737–14756. https://doi.org/10.5194/acp-18-14737-2018

Oke, T.R. (1987). *Boundary Layer Climates*, 2nd. edn., Routledge, London.

Olivares, G., Johansson, C., Ström, J., & Hansson, H. C. (2007). The role of ambient temperature for particle number concentrations in a street canyon. *Atmospheric Environment*, *41*(10), 2145–2155. https://doi.org/10.1016/j.atmosenv.2006.10.068

Ortiz-Amezcua, P. (2019). Atmospheric profiling based on Aerosol and Doppler lidar. Retrieved from http://hdl.handle.net/10481/57771

Pakkanen, T. A., Kerminen, V. M., Ojanen, C. H., Hillamo, R. E., Aarnio, P., & Koskentalo, T. (2000). Atmospheric black carbon in Helsinki. *Atmospheric Environment*, *34*(9), 1497–1506. https://doi.org/10.1016/S1352-2310(99)00344-1

Pandolfi, M., Gonzalez-Castanedo, Y., Alastuey, A., de la Rosa, J. D., Mantilla, E., de la Campa, A. S., et al. (2011). Source apportionment of PM10 and PM2.5 at multiple sites in the strait of Gibraltar by PMF: Impact of shipping emissions. *Environmental Science and Pollution Research*, *18*(2), 260–269. https://doi.org/10.1007/s11356-010-0373-4

Pandolfi, M., Alados-Arboledas, L., Alastuey, A., Andrade, M., Angelov, C., Artiñano, B., et al. (2018). A European aerosol phenomenology - 6: Scattering properties of atmospheric aerosol particles from 28 ACTRIS sites. *Atmospheric Chemistry and Physics*, *18*(11), 7877–7911. https://doi.org/10.5194/acp-18-7877-2018

Patrón, D., Lyamani, H., Titos, G., Casquero-Vera, J. A., Cardell, C., Močnik, G., et al. (2017). Monumental heritage exposure to urban black carbon pollution. *Atmospheric Environment*, *170*, 22–32. https://doi.org/10.1016/j.atmosenv.2017.09.030

Pérez, N., Pey, J., Cusack, M., Reche, C., Querol, X., Alastuey, A., & Viana, M. (2010). Variability of particle number, black carbon, and PM10, PM 2.5, and PM1 Levels and Speciation: Influence of road traffic emissions on urban air quality. In *Aerosol Science and Technology* (Vol. 44, pp. 487–499). https://doi.org/10.1080/02786821003758286

Petäjä, T., Mauldin, R. L., Kosciuch, E., McGrath, J., Nieminen, T., Paasonen, P., et al. (2009). Sulfuric acid and OH concentrations in a boreal forest site. *Atmospheric Chemistry and Physics*, *9*(19), 7435–7448. https://doi.org/10.5194/acp-9-7435-2009

Pey, J., Alastuey, A., Querol, X., & Rodríguez, S. (2010). Monitoring of sources and atmospheric processes controlling air quality in an urban Mediterranean environment. *Atmospheric Environment*, *44*(38), 4879–4890. https://doi.org/10.1016/j.atmosenv.2010.08.034

Pirjola, L., Kulmala, M., Wilck, M., Bischoff, A., Stratmann, F., & Otto, E. (1999). Formation of sulphuric acid aerosols and cloud condensation nuclei: An expression for significant nucleation and model comparison. *Journal of Aerosol Science*, *30*(8), 1079–1094. https://doi.org/10.1016/S0021-8502(98)00776-9

Putaud, J. P., Van Dingenen, R., Alastuey, A., Bauer, H., Birmili, W., Cyrys, J., et al. (2010). A European aerosol phenomenology - 3: Physical and chemical characteristics of particulate matter from 60 rural, urban, and kerbside sites across Europe. *Atmospheric Environment*, *44*(10), 1308–1320. https://doi.org/10.1016/j.atmosenv.2009.12.011

Querol, X., Alastuey, A., Rodriguez, S., Plana, F., Ruiz, C. R., Cots, N., et al. (2001). PM10 and

PM2.5 source apportionment in the Barcelona Metropolitan area, Catalonia, Spain. *Atmospheric Environment*, *35*(36), 6407–6419. https://doi.org/10.1016/S1352-2310(01)00361-2

Rannik, Ü., Sogachev, A., Foken, T., Göckede, M., Kljun, N., Leclerc, M. Y., & Vesala, T. (2012). Footprint Analysis. In *Eddy Covariance* (pp. 211–261). Springer Netherlands. https://doi.org/10.1007/978-94-007-2351-1_8

Reche, C., Querol, X., Alastuey, A., Viana, M., Pey, J., Moreno, T., et al. (2011). New considerations for PM, Black Carbon and particle number concentration for air quality monitoring across different European cities. *Atmospheric Chemistry and Physics*, *11*(13), 6207–6227. https://doi.org/10.5194/acp-11-6207-2011

Rejano, F., Titos, G., Casquero-Vera, J. A., Lyamani, H., Andrews, E., Sheridan, P., et al. (2021). Activation properties of aerosol particles as cloud condensation nuclei at urban and high-altitude remote sites in southern Europe. *Science of the Total Environment*, *762*. https://doi.org/10.1016/j.scitotenv.2020.143100

Ripamonti, G., Järvi, L., Mølgaard, B., Hussein, T., Nordbo, A., & Hämeri, K. (2013). The effect of local sources on aerosol particle number size distribution, concentrations and fluxes in Helsinki, Finland. *Tellus, Series B: Chemical and Physical Meteorology*, *65*(1). https://doi.org/10.3402/tellusb.v65i0.19786

Rivas, I., Beddows, D. C. S., Amato, F., Green, D. C., Järvi, L., Hueglin, C., et al. (2020). Source apportionment of particle number size distribution in urban background and traffic stations in four European cities. *Environment International*. https://doi.org/10.1016/j.envint.2019.105345

Rodríguez, S., & Cuevas, E. (2007). The contributions of "minimum primary emissions" and "new particle formation enhancements" to the particle number concentration in urban air. *Journal of Aerosol Science*, *38*(12), 1207–1219. https://doi.org/10.1016/j.jaerosci.2007.09.001

Rönkkö, T., Kuuluvainen, H., Karjalainen, P., Keskinen, J., Hillamo, R., Niemi, J. V., et al. (2017). Traffic is a major source of atmospheric nanocluster aerosol. *Proceedings of the National Academy of Sciences of the United States of America*, *114*(29), 7549–7554. https://doi.org/10.1073/pnas.1700830114

Rose, C., Sellegri, K., Freney, E., Dupuy, R., Colomb, A., Pichon, J. M., et al. (2015). Airborne measurements of new particle formation in the free troposphere above the Mediterranean Sea

during the HYMEX campaign. *Atmospheric Chemistry and Physics*, *15*(17), 10203–10218. https://doi.org/10.5194/acp-15-10203-2015

Rose, C., Sellegri, K., Velarde, F., Moreno, I., Ramonet, M., Weinhold, K., et al. (2015). Frequent nucleation events at the high altitude station of Chacaltaya (5240m a.s.l.), Bolivia. *Atmospheric Environment*, *102*, 18–29. https://doi.org/10.1016/j.atmosenv.2014.11.015

Rose, C., Sellegri, K., Moreno, I., Velarde, F., Ramonet, M., Weinhold, K., et al. (2017). CCN production by new particle formation in the free troposphere. *Atmospheric Chemistry and Physics*, *17*(2), 1529–1541. https://doi.org/10.5194/acp-17-1529-2017

Rose, C., Zha, Q., Dada, L., Yan, C., Lehtipalo, K., Junninen, H., et al. (2018). Observations of biogenic ion-induced cluster formation in the atmosphere. *Science Advances*, *4*(4). https://doi.org/10.1126/sciadv.aar5218

Rose, C., Foucart, B., Picard, D., Colomb, A., Metzger, J. M., Tulet, P., & Sellegri, K. (2019). New particle formation in the volcanic eruption plume of the Piton de la Fournaise: Specific features from a long-term dataset. *Atmospheric Chemistry and Physics*, *19*(20), 13243–13265. https://doi.org/10.5194/acp-19-13243-2019

Rose, C., Collaud Coen, M., Andrews, E., Lin, Y., Bossert, I., Lund Myhre, C., et al. (2021). Seasonality of the particle number concentration and size distribution: a global analysis retrieved from the network of Global Atmosphere Watch (GAW) near-surface observatories. *Atmospheric Chemistry and Physics*, 1–69. https://doi.org/10.5194/acp-2020-1311

Russell, P. B., Bergstrom, R. W., Shinozuka, Y., Clarke, A. D., Decarlo, P. F., Jimenez, J. L., et al. (2010). Absorption Angstrom Exponent in AERONET and related data as an indicator of aerosol composition. *Atmospheric Chemistry and Physics*, *10*(3), 1155–1169. https://doi.org/10.5194/acp-10-1155-2010

Salma, I., Borsós, T., Németh, Z., Weidinger, T., Aalto, P., & Kulmala, M. (2014). Comparative study of ultrafine atmospheric aerosol within a city. *Atmospheric Environment*, *92*, 154–161. https://doi.org/10.1016/j.atmosenv.2014.04.020

Sandradewi, J., Prévôt, A. S. H., Szidat, S., Perron, N., Alfarra, M. R., Lanz, V. A., et al. (2008). Using aerosol light abosrption measurements for the quantitative determination of wood burning and traffic emission contribution to particulate matter. *Environmental Science and Technology*, *42*(9), 3316–3323. https://doi.org/10.1021/es702253m

Schmidt, A., & Klemm, O. (2008). Direct determination of highly size-resolved turbulent particle fluxes with the disjunct eddy covariance method and a 12 stage electrical low pressure impactor. *Atmospheric Chemistry and Physics*, *8*(24), 7405–7417. https://doi.org/10.5194/acp-8-7405-2008

Schobesberger, S., Junninen, H., Bianchi, F., Lönn, G., Ehn, M., Lehtipalo, K., et al. (2013). Molecular understanding of atmospheric particle formation from sulfuric acid and large oxidized organic molecules. *Proceedings of the National Academy of Sciences of the United States of America*, *110*(43), 17223–17228. https://doi.org/10.1073/pnas.1306973110

Seinfeld, J.H. and Pandis, S.N. (2016). *Atmospheric Chemistry and Physics: From Air Pollution to Climate Change*, 3rd Edition, John Wiley & Sons, Hoboken, New Jersey.

Sellegri, K., Rose, C., Marinoni, A., Lupi, A., Wiedensohler, A., Andrade, M., et al. (2019). New particle formation: A review of ground-based observations at mountain research stations. *Atmosphere*, *10*(9). https://doi.org/10.3390/atmos10090493

Shindell, D., Kuylenstierna, J. C. I., Vignati, E., Van Dingenen, R., Amann, M., Klimont, Z., et al. (2012). Simultaneously mitigating near-term climate change and improving human health and food security. *Science*, *335*(6065), 183–189. https://doi.org/10.1126/science.1210026

Singh, V., Ravindra, K., Sahu, L., & Sokhi, R. (2018). Trends of atmospheric black carbon concentration over United Kingdom. *Atmospheric Environment*, *178*, 148–157. https://doi.org/10.1016/j.atmosenv.2018.01.030

Sorribas, M., Adame, J. A., Olmo, F. J., Vilaplana, J. M., Gil-Ojeda, M., & Alados-Arboledas, L. (2015). A long-term study of new particle formation in a coastal environment: Meteorology, gas phase and solar radiation implications. *Science of the Total Environment*, *511*, 723–737. https://doi.org/10.1016/j.scitotenv.2014.12.011

Stull, R. B. (1988). *An Introduction to Boundary Layer Meteorology*, Springer, New York.

Tao, J., Zhang, L., Cao, J., & Zhang, R. (2017). A review of current knowledge concerning PM2. 5 chemical composition, aerosol optical properties and their relationships across China. *Atmospheric Chemistry and Physics*. https://doi.org/10.5194/acp-17-9485-2017

Tegen, I., & Schepanski, K. (2009). The global distribution of mineral dust. *IOP Conference Series: Earth and Environmental Science*, *7*, 012001. https://doi.org/10.1088/1755-1307/7/1/012001

Titos, G., Lyamani, H., Pandolfi, M., Alastuey, A., & Alados-Arboledas, L. (2014). Identification of fine (PM1) and coarse (PM10-1) sources of particulate matter in an urban environment. *Atmospheric Environment*, *89*, 593–602. https://doi.org/10.1016/j.atmosenv.2014.03.001

Titos, G., Lyamani, H., Drinovec, L., Olmo, F. J., Močnik, G., & Alados-Arboledas, L. (2015). Evaluation of the impact of transportation changes on air quality. *Atmospheric Environment*, *114*, 19–31. https://doi.org/10.1016/j.atmosenv.2015.05.027

Titos, G., del Águila, A., Cazorla, A., Lyamani, H., Casquero-Vera, J. A., Colombi, C., et al. (2017). Spatial and temporal variability of carbonaceous aerosols: Assessing the impact of biomass burning in the urban environment. *Science of the Total Environment*, *578*, 613–625. https://doi.org/10.1016/j.scitotenv.2016.11.007

Tröstl, J., Chuang, W. K., Gordon, H., Heinritzi, M., Yan, C., Molteni, U., et al. (2016). The role of low-volatility organic compounds in initial particle growth in the atmosphere. *Nature*, *533*(7604), 527–531. https://doi.org/10.1038/nature18271

Tuovinen, S., Kontkanen, J., Jiang, J., & Kulmala, M. (2020). Investigating the effectiveness of condensation sink based on heterogeneous nucleation theory. *Journal of Aerosol Science*, *149*. https://doi.org/10.1016/j.jaerosci.2020.105613

Valenzuela, A., Olmo, F. J., Lyamani, H., Antón, M., Quirantes, A., & Alados-Arboledas, L. (2012a). Aerosol radiative forcing during African desert dust events (2005-2010) over Southeastern Spain. *Atmospheric Chemistry and Physics*. https://doi.org/10.5194/acp-12-10331-2012

Valenzuela, A., Olmo, F. J., Lyamani, H., Antón, M., Quirantes, A., & Alados-Arboledas, L. (2012b). Classification of aerosol radiative properties during African desert dust intrusions over southeastern Spain by sector origins and cluster analysis. *Journal of Geophysical Research Atmospheres*. https://doi.org/10.1029/2011JD016885

Valenzuela, A., Olmo, F. J., Lyamani, H., Antón, M., Titos, G., Cazorla, A., & Alados-Arboledas, L. (2015). Aerosol scattering and absorption Angström exponents as indicators of dust and dust-free days over Granada (Spain). *Atmospheric Research*, *154*, 1–13. https://doi.org/10.1016/j.atmosres.2014.10.015

Venzac, H., Sellegri, K., Villani, P., Picard, D., & Laj, P. (2009). Seasonal variation of aerosol size distributions in the free troposphere and residual layer at the puy de Dôme station, France. *Atmospheric Chemistry and Physics*, *9*(4), 1465–1478. https://doi.org/10.5194/acp-9-1465-2009

Venzac, H., Sellegri, K., Laj, P., Villani, P., Bonasoni, P., Marinoni, A., et al. (2008). High frequency new particle formation in the Himalayas. *Proceedings of the National Academy of Sciences of the United States of America*, *105*(41), 15666–15671. https://doi.org/10.1073/pnas.0801355105

Vickers, D., & Mahrt, L. (1997). Fetch limited drag coefficients. *Boundary-Layer Meteorology*, *85*(1), 53–79. https://doi.org/10.1023/A:1000472623187

Vinet, L., & Zhedanov, A. (2011). A "missing" family of classical orthogonal polynomials. In *Journal of Physics A: Mathematical and Theoretical* (Vol. 44). https://doi.org/10.1088/1751-8113/44/8/085201

Vogt, M., Nilsson, E. D., Ahlm, L., Mårtensson, E. M., & Johansson, C. (2011). Seasonal diurnal cycles of 0.25-2.5 μm aerosol fluxes over urban Stockholm, Sweden. *Tellus, Series B: Chemical and Physical Meteorology*, *63*(5), 935–951. https://doi.org/10.1111/j.1600-0889.2011.00551.x

Wang, F., Cernuschi, S., Ozgen, S., Ripamonti, G., Vecchi, R., Valli, G., & Lonati, G. (2016). UFP and BC at a mid-sized city in Po valley, Italy: Size-resolved partitioning between primary and newly formed particles. *Atmospheric Environment*, *142*, 120–131. https://doi.org/10.1016/j.atmosenv.2016.07.030

Weingartner, E., Nyeki, S., & Baltensperger, U. (1999). Seasonal and diurnal variation of aerosol size distributions (10 < D < 750 nm) at a high-alpine site (Jungfraujoch 3580 m asl). *Journal of Geophysical Research Atmospheres*, *104*(D21), 26809–26820. https://doi.org/10.1029/1999JD900170

WHO. (2013). *Review of evidence on health aspects of air pollution – REVIHAAP Project Technical Report*. Retrieved from http://www.euro.who.int/pubrequest

Wiedensohler, A. (1988). An approximation of the bipolar charge distribution for particles in the submicron size range. *Journal of Aerosol Science*, *19*(3), 387–389. https://doi.org/10.1016/0021-8502(88)90278-9

Wiedensohler, A., Wiesner, A., Weinhold, K., Birmili, W., Hermann, M., Merkel, M., et al. (2018). Mobility particle size spectrometers: Calibration procedures and measurement uncertainties. *Aerosol Science and Technology*, *52*(2), 146–164. https://doi.org/10.1080/02786826.2017.1387229

Yao, L., Garmash, O., Bianchi, F., Zheng, J., Yan, C., Kontkanen, J., et al. (2018). Atmospheric new particle formation from sulfuric acid and amines in a Chinese megacity. *Science*, *361*(6399), 278–281. https://doi.org/10.1126/science.aao4839

Yli-Juuti, T., Nieminen, T., Hirsikko, A., Aalto, P. P., Asmi, E., Hõrrak, U., et al. (2011). Growth rates of nucleation mode particles in Hyytiälä during 2003-2009: Variation with particle size, season, data analysis method and ambient conditions. *Atmospheric Chemistry and Physics*, *11*(24), 12865–12886. https://doi.org/10.5194/acp-11-12865-2011

Yus-Díez, J., Bernardoni, V., Močnik, G., Alastuey, A., Ciniglia, D., Ivančič, M., et al. (2021). Determination of the multiple-scattering correction factor and its cross-sensitivity to scattering and wavelength dependence for different AE33 Aethalometer filter tapes: A multi-instrumental approach. *Atmos. Meas. Tech. Discuss.*, *2021*, 1–30. https://doi.org/10.5194/amt-2021-46

Zhang, R., Khalizov, A., Wang, L., Hu, M., & Xu, W. (2012). Nucleation and growth of nanoparticles in the atmosphere. *Chemical Reviews*. https://doi.org/10.1021/cr2001756